DD&T

Drug Discoveries & Therapeutics

IRCA
BSSA

IACMHR

www.ddtjournal.com

DD&T
Drug Discoveries & Therapeutics

Drug Discoveries & Therapeutics is one of a series of peer-reviewed journals of the International Research and Cooperation Association for Bio & Socio-Sciences Advancement (IRCA-BSSA) Group and is published bimonthly by the International Advancement Center for Medicine & Health Research Co., Ltd. (IACMHR Co., Ltd.) and supported by the IRCA-BSSA and Shandong University China-Japan Cooperation Center for Drug Discovery & Screening (SDU-DDSC).

Drug Discoveries & Therapeutics publishes contributions in all fields of pharmaceutical and therapeutic research such as medicinal chemistry, pharmacology, pharmaceutical analysis, pharmaceutics, pharmaceutical administration, and experimental and clinical studies of effects, mechanisms, or uses of various treatments. Studies in drug-related fields such as biology, biochemistry, physiology, microbiology, and immunology are also within the scope of this journal.

Drug Discoveries & Therapeutics publishes Original Articles, Brief Reports, Reviews, Policy Forum articles, Case Reports, News, and Letters on all aspects of the field of pharmaceutical research. All contributions should seek to promote international collaboration in pharmaceutical science.

Editorial Board

CONTENTS   *Volume 6, Number 5, 2012*

CONTENTS   (*Continued*)

Case Report

Letter

Guide for Authors

Copyright

Mini-Review

Topoisomerase IIα, rather than IIβ, is a promising target in development of anti-cancer drugs

Wang Chen[1], Jin Qiu[1,2], Yuemao Shen[1,*]

[1] *School of Pharmaceutical Sciences, Shandong University, Ji'nan, Shandong, China;*
[2] *School of Pharmaceutical Sciences, Shandong University of Traditional Chinese Medicine, Ji'nan, Shandong, China.*

ABSTRACT: DNA topoisomerase II (TOP2) is a well-known anticancer target. Its inhibitors are among the most effective anticancer drugs currently in clinical use. TOP2-targeting agents fall into two major classes of "Topo poisons" and "Topo inhibitors" based on their mechanisms of action. Mammalian cells possess two genetically distinct TOP2 isoforms, TOP2α and TOP2β, that are differentially regulated and play different roles in living cells. Compared to TOP2β, TOP2α may be an efficacious and safe chemotherapeutic target for cancer treatment. This review discusses the advantage of targeting TOP2α over TOP2β and action of various agents on TOP2α.

Keywords: Topoisomerase IIα, topoisomerase IIβ, therapeutic target, inhibitors, cancer therapy

1. Introduction

Cancer has become one of the leading causes of death in many countries such as China and Japan that are witnessing the aging of society. Screening for effective anticancer agents is an important part of oncotherapy. Alkylating agents have numerous drawbacks such as greater toxicity and less selectivity. In contrast, anticancer reagents that target topoisomerases are more selective, so they restrain the DNA replication of tumor cells in the proliferative phase. Among topoisomerases, DNA topoisomerase II (TOP2) is a well-known anticancer target. Agents that target TOP2 are among the most effective anticancer drugs currently available for the treatment of human cancers. Nevertheless, TOP2-based chemotherapy remains associated with incidences of life-threatening toxic side effects, *e.g.* drug-induced secondary malignancies (*1*). Intriguingly, previous

studies suggested that suppressing TOP2β, a subtype of TOP2, was responsible for the development of secondary malignancy associated with etoposide treatment (*1*). However, etoposide and doxorubicin may have potent anti-cancer activity because they target another subtype of TOP2, *i.e.* TOP2α (*2*). Hence, agents specifically targeting TOP2α may potentially be efficacious and safe chemotherapeutic drugs with a reduced risk of treatment related to secondary malignancies (*2*). The current paper discusses the advantage of targeting TOP2α over TOP2β and the therapeutic effects of various agents on TOP2α.

2. DNA topoisomerase

DNA topoisomerases are enzymes that regulate the overwinding or underwinding of DNA and are required for the survival of all organisms. They play an important role in regulating cellular processes such as replication, transcription, and chromosomal segregation by altering DNA topology. The main families of mammalian DNA topoisomerases are topoisomerase I (TOP1) and topoisomerase II (TOP2). Most type I DNA topoisomerases modify DNA topology in an ATP-independent fashion by creating single strand breaks in DNA whereas type II DNA topoisomerases do so in an ATP-dependent fashion by creating double strand breaks in DNA (*3*). That said, the classification of the topoisomerase family is less unambiguous. There are some similarities between the families, both in functions and amino acid sequences. For example, TOPVI β subunit (Spo11) shares GHKL sequence motifs with type IIA topoisomerases, indicating the evolutionary relationship between these enzymes (*4*).

2.1. *Activity of topoisomerases and its role in cancer pathology*

Despite sequence homology and functional motifs, the mechanisms of action of TOP1 and TOP2 differ. TOP1, the so-called ω protein from *Escherichia coli*, was the first DNA topoisomerase and was discovered by James Wang in 1971 (*5*). TOP1 is an enzyme that relaxes supercoiled DNA through a cycle of cleavage and

---

Address correspondence to:
Dr. Yuemao Shen, School of Pharmaceutical Sciences, Shandong University, No. 44, Wenhuaxi Road, Ji'nan 250012, Shandong, China.
E-mail: yshen@sdu.edu.cn

religation steps involving the active site residue Tyr723 (*6*). This residue attacks the phosphodiester backbone, breaking the single strand and forming a covalent 'cleavage complex' in which the unbroken strand undergoes 'controlled rotation' and relaxes the DNA. After relaxation, the scissile strand is religated and the enzyme is released (*7*). TOP2 is a ubiquitous ribozyme that alters the instantaneous cleavage of double-stranded DNA and the chromosomal topological structure, facilitating subsequent double-strand break (DSB) religation (*2,8*). These enzymes are involved in many aspects of DNA metabolism, including DNA replication, transcription, repair, and chromosome condensation/ segregation (*2,9*).

Because of the high level of TOP2 expression in cancer cells, TOP2 represents an important target for cancer chemotherapy (*10*). Several widely prescribed anticancer drugs induce TOP2-mediated chromosome DNA breakage and death of cancer cells by increasing the population of TOP2 cleavage complex (*11*). There are two major classes of TOP2, TOP2α and TOP2β, in mammalian cells, and they share catalytic mechanisms and have a high degree of amino acid similarity (~70% identity at the amino acid level) (*12,13*). Despite their similar structural features and biological properties, the two isoforms are differentially regulated and are involved in different cellular processes.

2.2. *Advantage of targeting TOP2α over TOP2β in the development of anti-cancer drugs*

TOP2α is essential for cell growth and is typically expressed at high levels in rapidly growing cancer cells. Its expression is cell cycle-regulated, peaking in G2/ M, whereas TOP2β is expressed in quiescent cells in virtually all tissues throughout the whole cell cycle and is dispensable for cell survival (*14*). The drawbacks of targeting TOP2β include the induction of cardiotoxicity and the potential development of secondary malignancies. Etoposide (**1**), teniposide (**2**), and doxorubicin (**3**) all target both isoforms of TOP2 and are among the most effective anticancer drugs in clinical use; however, these drugs often cause serious side effects, such as secondary malignancies (Table 1). These facts, together with the evidence that specific inhibition of TOP2α resulted in significant anti-tumor action (*1*), suggest that TOP2α-targeted therapy may be a valuable approach for cancer chemotherapy.

Podophyllotoxin is a well-known naturally occurring antitumor lignan lactone isolated from the genus *Podophyllum*. The semisynthetic podophyllotoxin derivative etoposide (VP-16) is in clinical use as antineoplastic agent because of its ability to inhibit TOP2 (*15*). Studies indicated that VP-16-induced carcinogenesis involves mainly the β isoform rather than the α isoform of TOP2. In a mouse skin carcinogenesis model, the incidence of VP-16-induced melanomas in the skin of 7, 12-dimethylbenz[*a*] anthracene-treated mice was found to be significantly higher in *TOP2β(+)* than in skin-specific *TOP2β*-knockout mice (*1*). Furthermore, VP-16-induced DNA sequence rearrangements and DSB were found to be TOP2β-dependent and preventable by co-treatment with a proteasome inhibitor, suggesting the importance of proteasomal degradation of the TOP2β-DNA cleavage complexes in VP-16-induced DNA sequence rearrangements. The anticancer activity of VP-16 on transformed cells expressing both TOP2 isozymes was, however, found to be primarily TOP2β-dependent. These results indicate the importance of developing TOP2α-specific anticancer drugs for effective chemotherapy without causing the development of treatment-related secondary malignancies (*1*).

Anthracyclines such as doxorubicin (adriamycin, **3**) and daunomycin (**4**) are TOP2-targeting drugs and are some of the most effective anticancer drugs in clinical use. However, doxorubicin-based chemotherapy could result in, among other toxic side effects, life-threatening cardiotoxicity (*17-20*). Doxorubicin is known to potentially cause damage to the heart in some individuals. In addition, other anthracyclines (like epirubicin and mitoxantrone) may also cause heart damage. Doxorubicin induced less DNA damage in *TOP2β(-/-)* mouse embryonic fibroblasts (MEF) than in *TOP2β(+/+)* MEFs, and the damage was reduced by the proteasome inhibitors bortezomib and MG132. These findings suggest the specific involvement of proteasome and TOP2β in doxorubicin-induced DNA damage. This supposition is compatible with a model in which proteasome processing of doxorubicin-induced TOP2β-DNA covalent complexes exposed TOP2β-concealed DNA DSB (*21*).

Mitoxantrone (**5**) is a synthetic antibiotic widely used as a chemotherapeutic drug for the treatment of solid tumors, leukemia, and lymphoma (*22,23*). It was approved by the US Food and Drug Administration (FDA) in 2000 for the treatment of neurologic disability and/or reduction of the frequency of clinical relapses in patients with secondary progressive, progressive relapsing, or worsening relapsing-remitting multiple sclerosis. Numerous studies on the interaction of mitoxantrone and DNA have been undertaken and all indicate that the drug functions by intercalating into DNA double strands (*24,25*). It has often been referred to as a TOP2 poison, but mitoxantrone also belongs to the class of TOP2 inhibitors (*26,27*). Mitoxantrone is not a specific TOP2α poison (or inhibitor) and it has marked myelosuppression, heart damage, and hepatotoxicity due to its inhibition of TOP2β.

Although the mechanisms of these side effects have not been fully studied, there might be a considerable benefit to developing TOP2-targeting drugs that are specific for the TOP2α isoform.

3. TOP2α-targeting agents

TOP2 is known to play important roles in cell cycle events, such as DNA replication, chromosome

Table 1. Structure, origin and activity of TOP2 targeting agents

Compound	Origin	Chemical structure	Target	Mechanism and activity (IC$_{50}$)	References
Etoposide (**1**) (VP-16)	*Sinopodophyllum emodi* (Wall.)		TOP2α,β	Topo poison (2.6 ± 0.8 μM)	(*19*)
Teniposide (**2**) (VM-26)	Semisynthesis		TOP2α,β	Topo poison	(*19*)
Doxorubicin (**3**) (Adriamycin)	Semisynthesis		TOP2α,β	Topo poison (0.1 – 65 μM)	(*20-24*)
Daunomycin (**4**)	*Streptomyces peucetius*		TOP2α,β	Topo poison (9.4 – 100μM)	(*20-24*)
Mitoxantrone (**5**)	Semisynthesis		TOP2α,β	Topo poison	(*32,33*)
Amsacrine (**6**)	Synthesis		TOP2α,β	Topo poison (0.2 – 2.0μM)	(*38*)
NK314 (**7**)	Synthesis		TOP2α	Topo poison (5.3 – 12.9 μM)	(*25*)
Tricitrinol B (**8**)	*Penicillium citrinum*		TOP2α	Topo poison (1 – 10 μM)	(*26*)
Dp44mT (**9**)	Synthesis		TOP2α	Topo poison (0.1 μM)	(*27,28*)
Bimolane (**10**)	Synthesis		TOP2α	Topo inhibitor	(*29,30*)
MST-16 (**11**)	Synthesis		TOP2α	Topo inhibitor	(*29,30*)
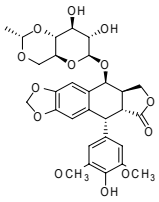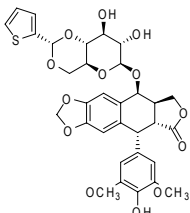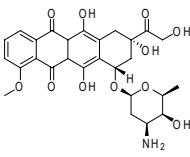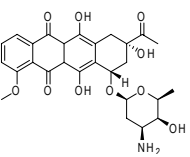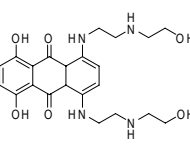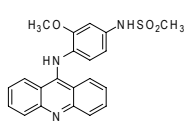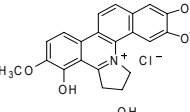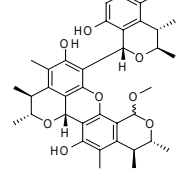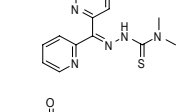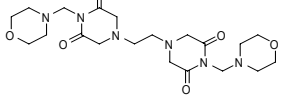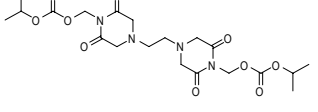
Continued

Dexrazoxane (**12**) (ICRF-187)	Synthesis		TOP2α	Topo inhibitor	(*29,30*)
Daurinol (**13**)	*Haplophyllum dauricum*		TOP2α	Topo inhibitor	(*48*)
Echinoside A (**14**)	*Holothuria nobilis* Selenka		TOP2α	Topo inhibitor (2.39 μM)	(*41*)
Wedelolactone (**15**)	*Wedelia calandulaceae*		TOP2α	Topo inhibitor (10 – 20 μM)	(*42*)
TSC (**16**)	Synthesis		TOP2α	Topo inhibitor (0.3 – 1.6 μM)	(*43*)
Flavone (**17**)	*Gardenia carinata* (Rubiaceae)		TOP2α	Undetermined (3.4 μM)	(*48*)
Flavone (**18**)	*Gardenia carinata* (Rubiaceae)		TOP2α	Undetermined	(*48*)
Garcinone E (**19**)	*Garcinia mangostana* L.		TOP2α	Undetermined (0.5 – 5.4 μM)	(*49,50*)
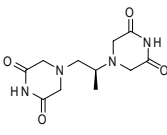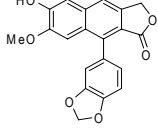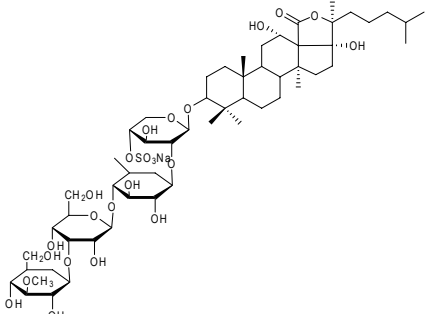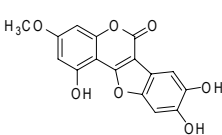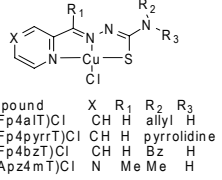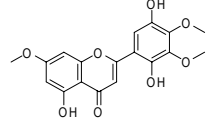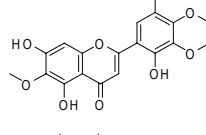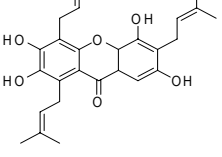
For TSC (**16**):

```
compound         X    R₁  R₂  R₃
Cu(Fp4aIT)Cl     CH   H   allyl     H
Cu(Fp4pyrrT)Cl   CH   H   pyrrolidine
Cu(Fp4bzT)Cl     CH   H   Bz   H
Cu(Apz4mT)Cl     N    Me  Me   H
```

condensation/decondensation, and sister chromatid segregation (*9*). TOP2-targeting agents, involving etoposide, doxorubicin, and mitoxantrone, are the most effective and most widely used anti-cancer drugs in cancer chemotherapy (Table 1) (28). Distinct from "TOP2 inhibitors", these agents are referred to as "TOP2 poisons". TOP2 poisons convert the essential enzyme into a highly cytotoxic DNA-damaging agent through the formation of 'cleavage complex'. There, a TOP2-linked DNA strand-passing intermediate is stabilized, allowing the generation of double strand breaks (*29*).

TOP2 poisons come in two types, intercalating and non-intercalating agents. Intercalators may interact with DNA through covalent binding, electrostatic binding, or intercalating (*30*). When agents of an appropriate size and chemical structure fit themselves between base pairs of DNA, intercalation occurs. These agents are mainly polycyclic, aromatic, and planar. Non-intercalating agents may lead to protein-drug interactions involving TOP2 poisons and trapped TOP2 covalent complexes because they do not interact strongly with DNA. "TOP2 inhibitors" interrupt the binding of TOP2 and DNA by

binding enzymes to inhibit TOP2 catalytic activity but do not generate increases in the levels of TOP2 covalent complexes (Table 1). In cell culture experiments, TOP2 inhibitors antagonize the toxicity of TOP2 poisons, indicating that TOP2 inhibitors act by separate mechanisms (*31*). These agents may competitively or non-competitively inhibit TOP2 ATPase activity or trap TOP2 and thus interrupt the binding of TOP2 and DNA. These drugs encompass a diverse group of natural and synthetic compounds that are commonly used to treat a variety of human malignancies (*32-34*).

3.1. TOP2α poisons

Di-2-pyridylketone-4,4-dimethyl-3-thiosemicarbazone (Dp44mT, **6**), an iron chelator, is presumed to have selective antitumor activity *in vitro* and *in vivo* (*35*). In previous studies, Dp44mT alone was capable of inducing apoptosis in neuroepithelioma, melanoma, and breast cancer cells in contrast to healthy fibroblasts. It also had activity in VP-16-resistant clones of MCF-7 breast tumor and KB3-1 epidermoid carcinoma cells. Short-term studies with low-dose Dp44mT inhibited lung, melanoma, and neuroepithelioma tumor growth in nude mice without systemic iron depletion, changes in organ weights, or differences in serum biochemical parameters, in contrast to triapine. Dp44mT inhibits TOP2α activity at low concentrations (*36*) that are 10- to 100-fold lower than those used to show TOP2 inhibition by ICRF-187 (*21*). Dp44mT is able to induce the formation of stable cellular TOP2α-DNA complexes, indicative of TOP2α poisoning in cancer cells.

NK314 (**7**) is a novel synthetic benzo[c]phenanthridine alkaloid that has strong antitumor activity. The compound was previously reported to stabilize TOP2 cleavage complexes and induce rapid DSBs, causing G2 arrest in tumor cells. Subsequently, NK314 was found to be an α isoform-specific TOP2 poison in living mammalian cells that induces TOP2-DNA complexes and chromosomal DSBs in a TOP2α-dependent manner (*37*). NK-314 can also inhibit DNA-dependent protein kinase (DNA-PK) and induce ataxia telangiectasia, mutated (ATM), contributing to cell survival (*38*). This perhaps is the reason why NK314 had an antitumor activity on etoposide and doxorubicin-resistant cell lines.

Tricitrinol B (**8**), a citrinin trimer derivative, was extracted from a volcano ash isolate of the fungus Penicillium citrinum HGY1-5 (*39*). It had comprehensive cytotoxicity in 17 tumor cell lines (IC$_{50}$: 1-10 μM) and was equally cytotoxic toward two multidrug-resistant cell lines overexpressing Pgp compared to the parental cell lines. Tricitrinol B induced cell cycle arrest in the G2/M phase and apoptosis by inducing DNA fragmentation and caspase activation. Molecular modeling and topoisomerase-mediated DNA relaxation experiments suggested that it is an intercalating TOP2α poison. It

inhibited TOP2α isomer activity by interfering with the TOP2α-mediated poststrand-passage cleavage/religation equilibrium in comparison to the prestrand-passage cleavage/religation equilibrium and increased the amount of broken DNA in cells.

Amsacrine (**9**) is a chemotherapy drug that is usually given in combination with other chemotherapy drugs to treat types of adult and childhood leukemia (*40*). Its major and minor groove proportions can be altered because its planar fused ring system can intercalate into the DNA of tumor cells. Amsacrine inhibits DNA replication and transcription by reducing the association between the affected DNA and DNA polymerase, RNA polymerase, and transcription factors. Like the better-known agent etoposide, amsacrine also inhibits topoisomerases (*41*). That said, intercalation of the molecule in the structurally similar *o*-amsacrine is insufficient to trap TOP2 as a covalent complex on DNA because of the different position of the methoxy substituent group on the anilino-ring. This precludes TOP2 poisons despite amsacrine's intercalative behavior (*42*).

3.2. TOP2α inhibitors

Bisdioxopiperazines (Biz) such as ICRF-154 (**10**), MST-16 (**11**), and ICRF-187 (**12**) both non-competitively inhibit TOP2 ATPase activity (*43*) and trap the TOP2 structure as a closed clamp. Biz have been the most commonly used specific catalytic inhibitors of type II topoisomerases in mammalian cells (*44*). They are catalytic noncleavable complex-forming inhibitors of DNA TOP2 that do not produce protein-linked DNA strand breaks. Biz have been widely used as a cardioprotectant against anthracycline-induced cardiomyopathy (*31,45*). Their mechanism of cardioprotection is through anthracycline-induced generation of reactive oxygen species (*46*). Biz could lead to degradation of TOP2β, a toxic source of anthracycline.

Wedelolactone (**13**), a coumestan isolated in 1956, is one of the active polyphenolic compounds in extracts of *Wedelia calandulaceae* and *Eclipta prostrata*. Wedelolactone has been found to have a wide range of biological effects. Wedelolactone was previously thought to attenuate the NF-κB transcription factor and/or androgen receptor activity and orthotopic growth of prostate cancer in nude mice. However, wedelolactone was cytotoxic to breast cancer MDA-MB-231 cells at concentrations that did not inhibit NF-κB activity. Wedelolactone induced S and G2/M phase cell cycle arrest and led to DNA damage signaling (*47*). Wedelolactone was found to inhibit DNA relaxation and TOP2α-mediated decatenation. Inhibition of growth and promotion of apoptosis by wedelolactone did not result from deregulation of NF-κB but were more likely attributable to its ability to bind dsDNA, inhibit TOP2α, and block DNA synthesis.

Daurinol (**14**), a novel arylnaphthalene lignan isolated from the ethnopharmacological plant *Haplophyllum dauricum*, has potent catalytic inhibition of human TOP2α and induces S phase cell cycle arrest through the enhanced expression of cyclins E and A and by activation of the ATM/Chk/Cdc25A pathway in HCT116 cells (*48*). Unlike etoposide, daurinol did not cause DNA damage or nuclear enlargement *in vitro*. It has potential antitumor action in mice, with fewer side effects than etoposide, although it has same chemical structure backbone as etoposide.

Echinoside A (**15**), isolated from the sea cucumber *Holothuria nobilis* Selenka, has potent anticancer activity. It is a new nonintercalative TOP2α inhibitor because of its inhibition of the noncovalent binding of TOP2α to DNA rather than the ATPase activity of TOP2. Echinoside A interferes with the binding of TOP2 to DNA, thus impairing the prestrand passage cleavage/religation equilibrium. In addition, echinoside A results in TOP2α-dependent DNA DSBs. These facts make echinoside A the first marine-derived triterpene glycoside TOP2α inhibitor (*49*). Echinoside A reduces the noncovalent binding of TOP2 to DNA. Echinoside imitates DNA action and competitively inhibits the binding of the enzyme to DNA. This concept may lead to novel strategies for designing new TOP2 inhibitors, and more importantly, echinoside A can be used to implement such a strategy.

Thiosemicarbazone (CuII(thiosemicarbazonato)Cl complexes, TSC, **16**), condensed heterocyclic carboxaldehyde moieties, have been found to have marked antibacterial, antiviral, antifungal, and, most intriguingly, antineoplastic activity (*50*). Recent studies indicated that the thiosemicarbazones and their metal complexes had the ability to inhibit TOP2α These studies both reinforced the significant potential of metal-thiosemicarbazonato complexes in cancer research and they also expanded the array of potential biochemical targets for those molecules (*51-54*). *R*-Heterocyclic thiosemicarbazones and their Cu(II) complexes are capable of *in vivo* and *in vitro* inhibition of TOP2α at an IC_{50} below that of the widely employed TOP2α poison etoposide (VP-16). Given the great potential of TSCs and their metal complexes in the development of chemotherapeutic agents and the importance of TOP2α in many forms of cancer, they may be a promising avenue for study (*51-53*).

3.3. *TOP2α inhibitors with undetermined mechanisms*

Two novel flavones, 5,2',5'-trihydroxy-7,3',4'-trimethoxyflavone (**17**), and 5,7,2',5'-tetrahydroxy-6,3',4'-trimethoxyflavone (**18**), were isolated from the leaves and twigs of Gardenia carinata (Rubiaceae). Flavone **16** had cytotoxic activity against P-388 and MCF-7 cell lines, while **17** acted only on the P-388 cell line. All active compounds were found to inhibit DNA TOP2α activity, which may be responsible for the observed cytotoxicity

(*55*). Active compounds were evaluated in terms of their DNA TOP2α inhibition in a relaxation assay. All compounds had similar inhibition of the TOP2α enzyme at a low concentration. This indicates that all of the tested compounds effectively inhibited the relaxation activity of TOP2α like the positive control etoposide did at the same concentration. This inhibitory activity may be responsible for their observed cytotoxicity.

Xanthones (for example, garcinone E, **19**) are hetero-tricyclic planar compounds originally isolated as secondary metabolites from plants and microorganisms (*56*). Xanthones have a diverse biological profile including antihypertensive, anticonvulsant, anti-thrombotic, anticholinesterase, and anti-cancer activity. This activity depends on differing structures modified by substituents on the xanthone ring. Recently, epoxide ring-opened xanthone derivatives were synthesized and tested for their topoisomerase inhibitory activity and cytotoxicity. Most of the compounds had TOP2α-specific inhibitory activity (*57*).

3.4. *Prospects for development of TOP2α-targeting agents in the future*

Classifying all of these TOP2α-targeting compounds would be difficult due to their various chemical structures, origins, and mechanisms. Additionally, drugs in clinical use have several flaws (*e.g.* drug resistance, myelosuppression, cardiotoxicity, hepatotoxicity, and poor water solubility) that need to be remedied. Nowadays, Biz is a promising TOP2α inhibitor that could be developed into a drug (*31,44,45*). Natural products are still the main source of TOP2α-targeting agents since more effective novel etoposide-related natural products continue to be isolated (*48,58*). Podophyllotoxin derivatives might be a safer anticancer drug, but the majority of TOP II-targeting compounds are (semi)synthetic products, so the design and synthesis of podophyllotoxin derivatives may have good prospects.

4. Conclusion and perspectives

TOP2-targeting agents encompass a diverse group of natural and synthetic compounds that are commonly used to treat a variety of human malignancies (*32-34*). Although TOP2 is the cytotoxic target of the drugs, the relative contributions of TOP2α and TOP2β to the chemotherapeutic effects of these agents have yet to be elucidated. Until now, no truly 'isoform-specific' agents have been identified. However, some drugs appear to favor one isoform or the other. TOP2α-favoring drugs may be a valuable novel approach for cancer treatment, so more active compounds targeting TOP2α need to be sought. The discussion herein should contribute to the development of more potent and effective TOP2α inhibitors and an enhanced understanding of their mechanisms of action.

References

1. Azarova AM, Lyu YL, Lin CP, Tsai YC, Lau JY, Wang JC, Liu LF. Roles of DNA topoisomerase II isozymes in chemotherapy and secondary malignancies. Proc Natl Acad Sci U S A. 2007; 104:11014-11019.

2. Toyoda E, Kagaya S, Cowell IG, Kurosawa A, Kamoshita K, Nishikawa K, Iiizumi S, Koyama H, Austin CA, Adachi N. NK314, a topoisomerase II inhibitor that specifically targets the α isoform. J Biol Chem. 2008; M803936200.

3. Schoeffler AJ, Berger JM. DNA topoisomerases: Harnessing and constraining energy to govern chromosome topology. Q Rev Biophys. 2008; 41:41-101.

4. Corbett KD, Berger JM. Structure of the topoisomerase VI-B subunit: Implications for type II topoisomerase mechanism and evolution. EMBO J. 2003; 22:151-163.

5. Wang JC. Interaction between DNA and an *Escherichia coli* protein omega. J Mol Biol. 1971; 55:523-533.

6. Tesauro C, Fiorani P, D'Annessa I, Chillemi G, Turchi G, Desideri A. Erybraedin C, a natural compound from the plant Bituminaria bituminosa, inhibits both the cleavage and religation activities of human topoisomerase I. Biochem J. 2010; 425:531-539.

7. Peterson KE, Cinelli MA, Morrell AE, Mehta A, Dexheimer TS, Agama K, Antony S, Pommier Y, Cushman M. Alcohol-, diol-, and carbohydrate-substituted indenoisoquinolines as topoisomerase I inhibitors: Investigating the relationships involving stereochemistry, hydrogen bonding, and biological activity. J Med Chem. 2011; 54:4937-4953.

8. Dong KC, Berger JM. Structural basis for gate-DNA recognition and bending by type IIA topoisomerases. Nature. 2007; 450:1201-1205.

9. Wang JC. Cellular roles of DNA topoisomerases: A molecular perspective. Nat Rev Mol Cell Biol. 2002; 3:430-440.

10. Li TK, Liu LF. Tumor cell death induced by topoisomerase-targeting drugs. Annu Rev Pharmacol Toxicol. 2001; 41:53-77.

11. Wu CC, Li TK, Farh L, Lin LY, Lin TS, Yu YJ, Yen TJ, Chiang CW, Chan NL. Structural basis of type II topoisomerase inhibition by the anticancer drug etoposide. Science. 2011; 333:459-462.

12. Austin CA, Sng JH, Patel S, Fisher LM. Novel HeLa topoisomerase II is the II β isoform: Complete coding sequence and homology with other type II topoisomerases. Biochim Biophys Acta. 1993; 1172:283-291.

13. Jenkins JR, Ayton P, Jones T, Davies SL, Simmons DL, Harris AL, Sheer D, Hickson ID. Isolation of cDNA clones encoding the β isozyme of human DNA topoisomerase II and localisation of the gene to chromosome 3p24. Nucleic Acids Res. 1992; 20:5587-5592.

14. Woessner RD, Mattern MR, Mirabelli CK, Johnson RK, Drake FH. Proliferation- and cell cycle-dependent differences in expression of the 170 kilodalton and 180 kilodalton forms of topoisomerase II in NIH-3T3 cells. Cell Growth Differ. 1991; 2:209-214.

15. Meresse P, Dechaux E, Monneret C, Bertounesque E. Etoposide: Discovery and medicinal chemistry. Curr Med Chem. 2004; 11:2443-2466.

16. Long BH. Mechanisms of action of teniposide (VM-26) and comparison with etoposide (VP-16). Semin Oncol. 1992; 19:3-19.

17. De Beer EL, Bottone AE, Voest EE. Doxorubicin and mechanical performance of cardiac trabeculae after acute and chronic treatment: A review. Eur J Pharmacol. 2001; 415:1-11.

18. Wallace KB. Doxorubicin-induced cardiac mitochondrionopathy. Pharmacol Toxicol. 2003; 93:105-115.

19. Zucchi R, Danesi R. Cardiac toxicity of antineoplastic anthracyclines. Curr Med Chem Anticancer Agents. 2003; 3:151-171.

20. Xu X, Persson HL, Richardson DR. Molecular pharmacology of the interaction of anthracyclines with iron. Mol Pharmacol. 2005; 68:261-271.

21. Lyu YL, Kerrigan JE, Lin CP, Azarova AM, Tsai YC, Ban Y, Liu LF. Topoisomerase II mediated DNA double-strand breaks: Implications in doxorubicin cardiotoxicity and prevention by dexrazoxane. Cancer Res. 2007; 67:8839-8846.

22. Holmes FA, Yap HY, Esparza L, Buzdar AU, Hortobagyi GN, Blumenschein GR. Mitoxantrone, cyclophosphamide, and 5-fluorouracil in the treatment of hormonally unresponsive metastatic breast cancer. Semin Oncol. 1984; 11:28-31.

23. Velasquez WS, Lew D, Grogan TM, Spiridonidis CH, Balcerzak SP, Dakhil SR, Miller TP, Lanier KS, Chapman RA, Fisher RI. Combination of fludarabine and mitoxantrone in untreated stages III and IV low-grade lymphoma: S9501. J Clin Oncol. 2003; 21:1996-2010.

24. Lown JW, Morgan AR, Yen SF, Wang YH, Wilson WD. Characteristics of the binding of the anticancer agents mitoxantrone and ametantrone and related structures to deoxyribonucleic acids. Biochemistry. 1985; 24:4028-4035.

25. Krishnamoorthy CR, Yen SF, Smith JC, Lown JW, Wilson WD. Stopped-flow kinetic analysis of the interaction of anthraquinone anticancer drugs with calf thymus DNA, poly[d(G-C)].poly[d(G-C)], and poly[d(A-T)].poly[d(A-T)]. Biochemistry. 1986; 25:5933-5940.

26. Fortune JM, Osheroff N. Topoisomerase II as a target for anticancer drugs: When enzymes stop being nice. Prog Nucleic Acid Res Mol Biol. 2000; 64:221-253.

27. Giles GI, Sharma RP. Topoisomerase enzymes as therapeutic targets for cancer chemotherapy. Med Chem. 2005; 1:383-394.

28. Osheroff N. Effect of antineoplastic agents on the DNA cleavage/religation reaction of eukaryotic topoisomerase II: inhibition of DNA religation by etoposide. Biochemistry. 1989; 28:6157-6160.

29. Nitiss JL, Wang JC. Mechanisms of cell killing by drugs that trap covalent complexes between DNA topoisomerases and DNA. Mol Pharmacol. 1996; 50:1095-1102.

30. Richards AD, Rodger A. Synthetic metallomolecules as agents for the control of DNA structure. Chem Soc Rev. 2007; 36:471-483.

31. Speyer JL, Green MD, Kramer E, Rey M, Sanger J, Ward C, Dubin N, Ferrans V, Stecy P, Zeleniuch-Jacquotte A. Protective effect of the bispiperazinedione ICRF-187 against doxorubicin-induced cardiac toxicity in women with advanced breast cancer. N Engl J Med. 1988; 319:745-752.

32. McClendon AK, Osheroff N. DNA topoisomerase II, genotoxicity, and cancer. Mutat Res. 2007; 623:83-97.

33. Bender RP, Osheroff N. DNA Topoisomerases as targets for the chemotherapeutic treatment of cancer. In: Cancer Drug Discovery and Development. Checkpoint Responses in Cancer Therapy (Dai W, ed.). Humana Press, New York, NY, USA, 2008; pp. 57-91.

34. Martincic D, Hande KR. Topoisomerase II inhibitors. Cancer Chemother Biol Response Modif. 2005; 22:101-121.

35. Whitnall M, Howard J, Ponka P, Richardson DR. A class of iron chelators with a wide spectrum of potent antitumor activity that overcomes resistance to chemotherapeutics. Proc Natl Acad Sci U S A. 2006; 103:14901-14906.

36. Yuan J, Lovejoy DB, Richardson DR. Novel di-2-pyridyl-derived iron chelators with marked and selective antitumor activity: *In vitro* and *in vivo* assessment. Proc Natl Acad Sci U S A. 2006; 103:14901-14906.

37. Toyoda E, Kagaya S, Cowell IG, Kurosawa A, Kamoshita K, Nishikawa K, Iiizumi S, Koyama H, Austin CA, Adachi N. NK314, a topoisomerase II inhibitor that specifically targets the isoform. Blood. 2004; 104:1450-1458.

38. Guo L, Liu X, Jiang Y, Nishikawa K, Plunkett W. DNA dependent protein kinase and ataxia telangiectasia mutated (ATM) promote cell survival in response to NK314, a topoisomerase IIα inhibitor. Mol Pharmacol. 2011; 80:321-327.

39. Du L, Liu HC, Fu W, Li DH, Pan QM, Zhu TJ, Geng MY, Gu QQ. Unprecedented citrinin trimer tricitinol B functions as a novel topoisomerase IIα inhibitor. J Med Chem. 2011; 54:5796-5810.

40. Horstmann MA, Hassenpflug WA, zur Stadt U, Escherich G, Janka G, Kabisch H. Amsacrine combined with etoposide and high-dose methylprednisolone as salvage therapy in acute lymphoblastic leukemia in children. Haematologica. 2005; 90:1701-1703.

41. Wadkins RM, Graves DE. Thermodynamics of the interactions of *m*-AMSA and *o*-AMSA with nucleic acids: Influence of ionic strength and DNA base composition. Nucleic Acids Res. 1989; 17:9933-9946.

42. Nitiss JL. Targeting DNA topoisomerase II in cancer chemotherapy. Nat Rev Cancer. 2009; 9:338-350.

43. Roca J, Ishida R, Berger JM, Andoh T, Wang JC. Antitumor bisdioxopiperazines inhibit yeast DNA topoisomerase II by trapping the enzyme in the form of a closed protein clamp. Proc Natl Acad Sci U S A. 1994; 91:1781-1785.

44. Andoh T, Ishida R. Catalytic inhibitors of DNA topoisomerase II. Biochim Biophys Acta. 1998; 1400:155-171.

45. Shan K, Lincoff AM, Young JB. Anthracycline-induced cardiotoxicity. Ann Intern Med. 1996; 125:47-58.

46. Menna P, Salvatorelli E, Minotti G. Cardiotoxicity of antitumor drugs. Chem Res Toxicol. 2008; 21:978-989.

47. Benes P, Knopfova L, Trcka F, Nemajerova A, Pinheiro D, Soucek K, Fojta M, Smarda J. Inhibition of topoisomerase IIα: Novel function of wedelolactone. Cancer Lett. 2011; 303:29-38.

48. Kang K, Oh SH, Yun JH, Jho EH, Kang JH, Batsuren D, Tunsag J, Park KH, Kim M, Nho CW. A novel topoisomerase inhibitor, daurinol, suppresses growth of HCT116 cells with low hematological toxicity compared to etoposide. Neoplasia. 2011; 13:1043-1057.

49. Li M, Miao ZH, Chen Z, Chen Q, Gui M, Lin LP, Sun P, Yi YH, Ding J. Echinoside A, a new marine-derived anticancer saponin, targets topoisomerase II by unique interference with its DNA binding and catalytic cycle. Ann Oncol. 2009; 21:597-607.

50. Yu Y, Kalinowski DS, Kovacevic Z, Siafakas AR, Jansson PJ, Stefani C, Lovejoy DB, Sharpe PC, Bernhardt PV, Richardson DR. Thiosemicarbazones from the old to new: iron chelators that are more than just ribonucleotide reductase inhibitors. J Med Chem. 2009; 52:5271-5294.

51. Miller MC, 3rd, Bastow KF, Stineman CN, Vance JR, Song SC, West DX, Hall IH. The cytotoxicity of 2-formyl and 2-acetyl-(6-picolyl)-4N-substituted thiosemicarbazones and their copper(II) complexes. Arch Pharm (Weinheim). 1998; 331:121-127.

52. Miller MC, 3rd, Stineman CN, Vance JR, West DX, Hall IH. The cytotoxicity of copper(II) complexes of 2-acetylpyridyl-4N-substituted thiosemicarbazones. Anticancer Res. 1998; 18:4131-4139.

53. Miller MC, Stineman CN, Vance JR, West DX, Hall IH. Multiple mechanisms for cytotoxicity induced by copper(II) complexes of 2-acetylpyrazine-N-substituted thiosemicarbazones. Applied Organometallic Chemistry. 1999; 13:9-19.

54. Zeglis BM, Divilov V, Lewis JS. Role of metalation in the topoisomerase IIα inhibition and antiproliferation activity of a series of α-heterocyclic-N4-substituted thiosemicarbazones and their Cu(II) complexes. J Med Chem. 2011; 54:2391-2398.

55. Kongkum N, Tuchinda P, Pohmakotr M, Reutrakul V, Piyachaturawat P, Jariyawat S, Suksen K, Yoosook C, Kasisit J, Napaswad C. DNA topoisomerase IIα inhibitory and anti-HIV-1 flavones from leaves and twigs of Gardenia carinata. Fitoterapia. 2011; 83:368-372.

56. Pinto MMM, Sousa ME, Nascimento MSJ. Xanthone derivatives: New insights in biological activities. Curr Med Chem. 2005; 12:2517-2538.

57. Jun KY, Lee EY, Jung MJ, Lee OH, Lee ES, Choo HYP, Na Y, Kwon Y. Synthesis, biological evaluation, and molecular docking study of 3-(3'-heteroatom substituted-2'-hydroxy-1'-propyloxy) xanthone analogues as novel topoisomerase IIα catalytic inhibitor. Eur J Med Chem. 2011; 46:1964-1971.

58. Liu Y, Zhao C, Li H, Yu M, Gao J, Wang L, Zhai Y. Cytotoxicity and apoptosis induced by a new podophyllotoxin glucoside in human hepatoma (HepG2) cells. Can J Physiol Pharmacol. 2010; 88:472-479.

Brief Report

A new boronic acid-based fluorescent sensor for L-dihydroxy-phenylalanine

Zhongyu Wu[1], Xinying Yang[1], Wenfang Xu[1], Binghe Wang[1,2], Hao Fang[1,*]

[1] *Department of Medicinal Chemistry, Key Laboratory of Chemical Biology (Ministry of Education), School of Pharmacy, Shandong University, Ji'nan, China;*
[2] *Department of Chemistry and Center for Biotechnology and Drug Design, Georgia State University, Atlanta, GA, USA.*

ABSTRACT: Catecholamines, such as dopamine and L-dihydroxyphenylalanine (L-DOPA), are associated with different physiological functions and diseases. In our recent studies, a novel water-soluble boronic acid compound 3c was identified as a selective fluorescent sensor for L-DOPA. This compound not only has the ability to interact with dopamine and catechol, but also has no fluorescence intensity change for L-DOPA precursors *in vivo*, such as L-tyrosine.

Keywords: Boronic acid, fluorescent chemosensor, L-DOPA, dopamine

1. Introduction

As a series of endogenous bioactive substances *in vivo*, catecholamine derivatives are generated from L-dihydroxyphenylalanine (L-DOPA) which is converted from L-tyrosine. L-DOPA can be degraded to dopamine by DOPA decarboxylase in the body and then following conversion can release norepinephrine and epinephrine. It is well known that dopamine, norepinephine, and epinephrine exhibit various physiological effects, such as increasing heart rate and blood pressure. In addition, dopamine and its precursor L-DOPA are involved in many diseases including parkinsonism, hypertension, and schizophrenia (*1-8*). For example, significant depletion of dopamine was found in brains of Parkinson's disease victims. Administration of L-DOPA could supply the dopamine *in vivo* and offset its deficient effect (*9,10*). For this reason, it is of great interest for scientists to develop various analytical methodology to detect catecholamine derivatives, such as spectrophotometry,

gas chromatography, radioimmunoassay, voltammetric determination, potentiometry, chemiluminescense, and flow injection analysis (FIA) (*11*). Currently, the commonly used simultaneous determination of L-DOPA and dopamine are done using high-performance liquid chromatography (HPLC) (*12,13*). Other methods using nuclear magnetic resonance (NMR) spectroscopy (*14*) and capillary electrophoresis (CE) (*15*) have also been reported.

Recently, some selective fluorometric methods for dopamine have been reported (*16*). In 2004, Akkaya reported a selective fluorescent chemosensor for L-DOPA using a Lucifer yellow scaffold to link a phenyl boronic acid structure. The phenyl boronic acid was used to recognize the catechol moiety in the structure of L-DOPA (*17*). However, this fluorescent sensor did not give a binding constant for other catecholamine derivatives, such as dopamine and catechol. Recently, our group reported compound **1** is a selective fluorescent chemosensor for catechol derivatives (*18*). However, this compound did not show selectivity for catechol derivatives, especially for dopamine and L-DOPA. According to our previous results, amidation of the carboxyl group in compound **1** didn't influence its binding affinity for catechol derivatives. In our on-going study, binding affinity and selectivity could be improved by introducing a second binding site and this strategy has also been successfully used to develop other selective chemosensors for dopamine (*16,19*). This paper describes our recent work focus on introducing a carboxylic acid as a second binding site with different linker, which could help us develop selective fluorescent chemosensor for L-DOPA.

2. Materials and Methods

2.1. *General methods*

Solvents were reagent grade and were purified and dried using standard methods when necessary. All melting points were determined on a micromelting point apparatus (and are uncorrected). ^{1}H-NMR and ^{13}C-NMR spectra were obtained on a Bruker

---

Address correspondence to:
Dr. Fang Hao, Department of Medicinal Chemistry, Key Laboratory of Chemical Biology (Ministry of Education), School of Pharmacy, Shandong University, 44 West Wenhua Rd., Ji'nan 250012, China.
E-mail: haofangcn@sdu.edu.cn

Avance-300 instrument in the indicated solvent. Chemical shifts are expressed in delta (δ) units with TMS as internal reference. ESI-MS were determined on an API 4000 spectrometer. All reactions were monitored using TLC on 0.25 mm silica gel plates (60GF-254) and visualized with UV light. Flash column chromatography was performed on a column packed with silica gel 60 (200-300 mesh). Concentration of the reaction solutions involved use of a rotary evaporator at reduced pressure.

2.2. General procedure for the preparation of title compounds (3a-3c)

Compound **1** was refluxed with thionyl chloride to generate the corresponding acyl chloride and then reacted with different ω-aminoalkanoic acid methylesters to yield **2a-2c**. The hydrolysis of methylester will give target compound **3a-3c** (Scheme 1).

2.3. Binding study

Different concentration of analytes (0.10 mM to 1.0 mM) were added to the solution of the target compound (**3a-3c**) at a concentration of 3.0×10^{-5} M in phosphate buffer at pH 7.4. The fluorescent intensity was recorded by a THERMO-LABSYSTEMS VARIOSKAN FLASH Multimode Spectral Scanning Microplate Reader. The apparent association constant (Ka) was calculated according to the Benesi-Hildebrand equation.

3. Results

3.1. Fluorescent intensity changes and associate constants

The fluorescence intensity of three target compounds decreased significantly after addition of catechol and catecholamine derivatives. For example, the fluorescence intensity decreased almost 65% after addition of 1 mM L-DOPA (Figure 1). According to the apparent association constants (Ka) of three target compounds (Table 1), L-DOPA showed a two-fold greater affinity than catechol and dopamine for compound **3c**. For compound **3a** and **3b**, the association constants for catechol, dopamine, and L-DOPA are almost the same, which suggests that these two compounds have no selectivity for catecholamine derivatives.

These results indicate that the length of the linker of the target compound has a significant influence on the binding affinity and selectivity for L-DOPA. For example, compounds with the linker of one or three methylene units (compound **3a** and **3b**) have no selectivity for catechol and catecholamine derivatives. While when the linker was extended to five methylene units, such as compound **3c**, the binding affinity and selectivity for L-DOPA could be increased.

3.2. Selectivity of compound 3c interacting with analytes

Considering that the origin of L-DOPA is related
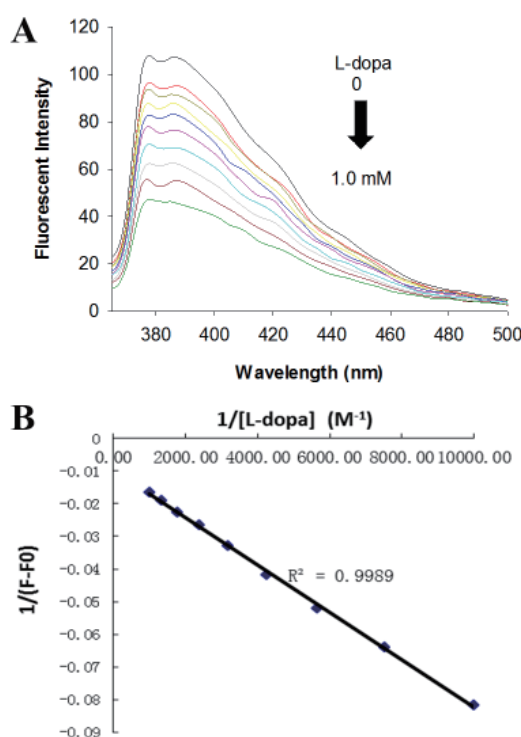
Figure 1. Fluorescent spectral changes of compound 3c (3×10^{-5} M) upon addition of various concentrations of catechol in 0.1 M phosphate buffer at pH 7.4, λ_{ex} = 337 nm, λ_{em}= 385 nm. (A) Fluorescence spectra of **3c** upon addition of catechol; **(B)** Relative fluorescent intensity changes *vs.* concentration of catechol.

Scheme 1. Synthetic scheme, reagents, and conditions. (a) $SOCl_2$, reflux; **(b)** NH_2-R-$COOCH_3$; **(c)** NaOH; **(d)** HCl.

Table 1. Apparent association constants (Ka) of chemosensors (3×10^{-5} M in 0.1 M phosphate buffer, pH 7.4) with catechol, dopamine, and L-DOPA

Chemosensors	Catechol	Dopamine	L-DOPA
3a	780	674	730
3b	837	890	770
3c	680	791	1405
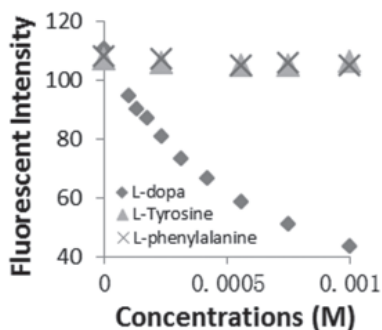
Figure 2. Fluorescense changes *versus* concentration of various analytes whose structures are related to L-DOPA (L-DOPA, L-tyrosine and L-phenylalaine) added to 3c (3 × 10^{-5} M) in phosphate buffer (0.1 M, pH 7.4), λ_{ex} = 337 nm, λ_{em} = 382 nm.

to L-tyrosine and L-phenylalanine *in vivo*, apparent association constants of **3c** interacting with L-tyrosine and L-phenylalanine were also tested. The results showed that fluorescence intensity had no change after adding them to the buffer of **3c** (Figure 2). The possible reason is that the catechol moiety does not exist in the structure of L-tyrosine and L-phenylalanine, which leads to missing the crucial interaction with phenylboronic acid in compound **3c** which is maybe due to the missing catechol moiety.

4. Discussion

L-DOPA has a similar structure to dopamine and possesses an important role in the treatment of parkinsonism. Until now, few chemosensors have been reported to have good selectivity for L-DOPA in the literature. As we know, phenylboronic acid has the unique property to bind to 1,2- or 1,3-diols in aqueous solution. A stronger binding interaction can easily occur for an adjacent rigid *cis* diol in the structure of catechol or carbohydrate. Therefore, boronic acids have been investigated as chemosensors for catechol and carbohydrate in the recent two decades (*16,19,20*). Compound **1** is a new water-soluble fluorescent sensor for carbohydrate and catechol (*18*). This compound shows decreasing fluorescence intensity after addition of catechol and enhancing fluorescence intensity after addition of carbohydrate. This different fluorescence changing properties are no doubt very useful to develop selective chemosensor for catechol derivatives without interference of carbohydrate. In our recent studies, compound **3c** was identified as a novel chemosensor for L-DOPA by coupling with an alkanoic acid with five methylene units. This result indicated that carboxylic acid could be used as the second binding site to interact with the amino group in L-DOPA, which could be helpful to improve binding affinity and selectivity for the chemosensor **3c**. On the other hand, the linker also showed a crucial role in constructing a selective chemosensor. Therefore, further studies could focus on

introducing long alaphatic chains or rigid rings as linkers to develop a better chemosensor for catecholamine derivatives.

In conclusion, compound **3c** was found to be a new water-soluble fluorescent chemosensor for L-DOPA under physiological conditions compared with sugars and some phenol derivatives. This demonstrates that structural modifications on carboxyl groups will be helpful for developing new selective chemosensors for bioactive catechol derivatives in the future.

References

1. Gorina AS, Kolesnichenko LS, Mikhnovich VI. Catecholamines and their metabolites in children with Asperger and Kanner syndromes. Biomed Khim. 2011; 57:562-570.
2. Hamdy NM, El-Wakeel L, Suwailem SM. Involvement of depressive catecholamines as thrombosis risk/inflammatory markers in non-smoker, non-obese congestive heart failure, linked to increased epidermal growth factor-receptor (EGF-R) production. Indian J Clin Biochem. 2011; 26:140-145.
3. Riva R, Mork PJ, Westgaard RH, Johansen TO, Lundberg U. Catecholamines and heart rate in female fibromyalgia patients. J Psychosom Res. 2012; 72:51-57.
4. Vuda M, Brander L, Schroder R, Jakob SM, Takala J, Djafarzadeh S. Effects of catecholamines on hepatic and skeletal muscle mitochondrial respiration after prolonged exposure to faecal peritonitis in pigs. Innate Immun. 2012; 18:217-230.
5. Peterson G, Kumar A, Gart E, Narayanan S. Catecholamines increase conjugative gene transfer between enteric bacteria. Microb Pathog. 2011; 51:1-8.
6. Kotecha R, Toledo-Pereyra LH. The effect of catecholamines on hepatic artery vasospasm in small-for-size syndrome liver grafts. J Surg Res. 2012; 172:77-79.
7. Holloway EL, Polumbo RA, Harrison DC. Acute circulatory effects of dopamine in patients with pulmonary hypertension. Br Heart J. 1975; 37:482-485.
8. Lv H, Li A, Liu F, Ma H, Yao B. Effects of gastrodin on the dopamine system of Tourette's syndrome rat models. Biosci Trends. 2009; 3:58-62.
9. Cotzias GC, Papavasiliou PS, Gellene R. Modification of Parkinsonism-chronic treatment with L-dopa. N Engl J Med. 1969; 280:337-345.
10. Paisán-Ruiz C, Guevara R, Federoff M, Hanagasi H, Sina F, Elahi E, Schneider SA, Schwingenschuh P, Bajaj N, Emre M. Early-onset L-dopa-responsive parkinsonism with pyramidal signs due to ATP13A2, PLA2G6, FBXO7 and spatacsin mutations. Mov Disord. 2010;

25:1791-1800.

11. Pistonesi M, Centurion ME, Fernandez Band BS, Damiani PC, Olivieri AC. Simultaneous determination of levodopa and benserazide by stopped-flow injection analysis and three-way multivariate calibration of kinetic-spectrophotometric data. J Pharm Biomed Anal. 2004; 36:541-547.

12. Sagar KA, Smyth MR. Simultaneous determination of levodopa, carbidopa and their metabolites in human plasma and urine samples using LC-EC. J Pharm Biomed Anal. 2000; 22:613-624.

13. Karimi M, Carl JL, Loftin S, Perlmutter JS. Modified high-performance liquid chromatography with electrochemical detection method for plasma measurement of levodopa, 3-O-methyldopa, dopamine, carbidopa and 3,4-dihydroxyphenyl acetic acid. J Chromatogr B Analyt Technol Biomed Life Sci. 2006; 836:120-123.

14. Talebpour Z, Haghgoo S, Shamsipur M. [1]H nuclear magnetic resonance spectroscopy analysis for simultaneous determination of levodopa, carbidopa and methyldopa in human serum and pharmaceutical formulations. Anal Chim Acta. 2004; 506:97-104.

15. Ha PT, Van Schepdael A, Hauta-Aho T, Roets E, Hoogmartens J. Simultaneous determination of dopa and carbidopa enantiomers by capillary zone electrophoresis. Electrophoresis. 2002; 23:3404-3409.

16. Seto D, Maki T, Soh N, Nakano K, Ishimatsu R, Imato T. A simple and selective fluorometric assay for dopamine using a calcein blue-Fe^{2+} complex fluorophore. Talanta. 2012; 94:36-43.

17. Coskun A, Akkaya EU. Three-point recognition and selective fluorescence sensing of L-DOPA. Org Lett. 2004; 6:3107-3109.

18. Wu Z, Li M, Fang H, Wang B. A new boronic acid based fluorescent reporter for catechol. Bioorg Med Chem Lett. 2012; 23:7179-7182.

19. Jin S, Li M, Zhu C, Tran V, Wang B. Computer-based *de novo* design, synthesis, and evaluation of boronic acid-based artificial receptors for selective recognition of dopamine. Chembiochem. 2008; 9:1431-1438.

20. Huang S, Jia M, Xie Y, Wang J, Xu W, Fang H. The progress of selective fluorescent chemosensors by boronic acid. Curr Med Chem. 2012; 19:2621-2637.

Appendix

Synthesis of compounds 3a-3c.

2-(2-(4-Boronophenyl)quinoline-2-carboxamido)butanoic acid (3a)

Compound **1** (0.28 g, 1.0 mmol) was refluxed in thionyl chloride (15 mL) for 2 h and the thionyl chloride was removed *in vacuo* to give the acyl chloride. Then using triethylamine (0.61 g, 6.0 mmol) as the acid neutralizer, the acyl chloride reacted with glycine methyl ester chloride (0.38 g, 3.0 mmol) in anhydrous methylene dichloride to yield amide **2a** (0.24 g). Crude product **2a** was dissovled in 15 mL methanol and 3.0 mL of 2N NaOH solution (6.0 mmol) was added. The mixture solution was stirred for 1 h until the reaction was completed. The methanol was removed the methanol *in vacuo* and filterd to give a yellow solid. The product was purified by chromtography (DCM:MeOH = 15/1) to give a light yellow power **3a** (0.18 g). Yield: 49%. ^{1}H-NMR (600 Mz, CD$_3$OD) δ 8.38 (m, 1H), 8.12-8.20 (m, 4H), 7.84 (m, 3H), 7.65 (m, 1H), 3.59 (s, 2H); ^{13}C-NMR (150 Mz, DMSO-d_6) δ 170.77, 167.82, 156.24, 148.79, 142.59, 139.87, 135.15 (2C), 130.76, 129.94, 127.70 (2C), 126.59, 125.58, 123.84, 117.31, 41.46; MS (ESI) m/z (%) 351 (M + 1, 100).

4-(2-(4-Boronophenyl)quinoline-4-carboxamido)butanoic acid (3b)

Yield: 56%. ^{1}H-NMR (600 Mz, CD$_3$OD) δ 8.40 (m, 1H), 8.15-8.20 (m, 4H), 7.84 (m, 3H), 7.70 (m, 1H), 3.10 (m, 2H), 2.06 (m, 2H); ^{13}C-NMR (150 Mz, DMSO-d_6) δ 170.77, 167.82, 156.24, 148.79, 142.59, 139.87, 135.15 (2C), 130.76, 129.94, 127.70 (2C), 126.59, 125.58, 123.84, 117.31, 40.42, 35.54, 23.40; MS (ESI) m/z (%) 379 (M + 1, 100).

6-(2-(4-Boronophenyl)quinoline-4-carboxamido)hexanoic acid (3c)

Yield: 52%. ^{1}H-NMR (600 Mz, CD$_3$OD) δ 8.36 (m, 1H), 8.12-8.20 (m, 4H), 7.84 (m, 3H), 7.65 (m, 1H), 3.06 (m, 2H), 2.05 (m, 2H), 1.30-1.50 (m, 6H); ^{13}C-NMR (150 Mz, DMSO-d_6) δ 170.77, 167.82, 156.24, 148.79, 142.59, 139.87, 135.15 (2C), 130.76, 129.94, 127.70 (2C), 126.59, 125.58, 123.84, 117.31, 41.42, 34.40, 30.54, 24.90, 26.40; MS (ESI) m/z (%) 407 (M + 1, 100).

Cloning and expression analysis of squalene synthase, a key enzyme involved in antifungal steroidal glycoalkaloids biosynthesis from *Solanum nigrum*

Yi Sun, Ying Zhao, Lei Wang, Hongxiang Lou, Aixia Cheng*

School of Pharmaceutical Sciences, Shandong University, Ji'nan, Shandong, China.

ABSTRACT: Steroidal glycoalkaloids (SGAs) are a family of nitrogenous secondary metabolites produced in solanaceous plants. In our present study, γ-solamargine and its aglycone solasodine from *Solanum nigrum* were found to inhibit hyphae formation of *Fusarium oxysporum*. As phytoalexins, the formation of SGAs was significantly increased in the plants when infected with the spore of *F. oxysporum*. In order to understand this inducible defense mechanism, the rate-limiting enzyme squalene synthase in the biosynthesis process of SGAs was investigated well. A full-length cDNA encoding squalene synthase was isolated from *S. nigrum* (the squalene synthase in *S. nigrum* was designated as SnSS). The full-length cDNA of SnSS was 1,765 bp and contained a 1,236 bp open reading frame (ORF) encoding a polypeptide of 411 amino acids. Bioinformatic analysis revealed that the deduced SnSS protein had a high similarity with other plant squalene synthases. Real-time RT-PCR analysis showed that SnSS was expressed constitutively in all tested tissues, with the highest expression in stems. After treatment with the spore of *F. oxysporum*, the mRNA level of SnSS was significantly increased in the infected plants in accordance with the change of SGAs.

Keywords: Fusarium oxysporum, Solanum nigrum, squalene synthase, steroidal glycoalkaloids

1. Introduction

Plants encounter many different pathogens during their lifetime, and are armed and ready to defend themselves with a combination of pre-formed and inducible defense mechanisms, including phytoalexin synthesis (*1,2*). Steroidal glycoalkaloids (SGAs) are secondary metabolites which exhibit antifungal activities in a wide range of plants including the Solanaceae. These secondary metabolites provide built-in chemical protection against pest and pathogen attack and can also influence induced defense responses. Increasing foliar SGA content to enhance plant resistance against pests has resulted in elevated levels of SGAs in the tubers, whereas reduction or abolishment of plant SGAs for the sake of food safety may weaken pathogen resistance (*3*). SGAs accumulation varies in different plant organs during development (*4*). In addition to anticancer and some other pharmacological significance (*5*), our present tests found SGA and its aglycone from *Solanum nigrum* inhibits hyphae formation of *Fusarium oxysporum*, which is a root-infecting fungal pathogen and responsible for vascular wilt in many different plant species (*6*). The switch between the yeast and hyphae form of the dimorphic fungus *F. oxysporum* is very necessary in its pathogenesis and the hyphae formation is a prerequisite to infect plants. As phytoalexins, the production of SGAs was significantly increased in the *S. nigrum* plants when infected with the spore of *F. oxysporum*, which means that fungus infection stimulates biosynthesis of SGAs and results in self-defense.

The biosynthesis of SGA is *via* the mevalonate/isoprenoid pathway. The enzyme 3-hydroxy-3-methylglutaryl coenzyme A reductase (HMGR) catalyzes the first step in SGAs biosynthesis. Downstream, squalene synthase, which is a membrane bound enzyme (*7*) that condenses two farnesyl diphosphate molecules into squalene catalyzes the next important step leading to sterols and SGAs. SGAs accumulation appears to be regulated at different steps in the biosynthetic pathway in response to environmental stress and development. High transcript levels of potato HMGR and squalene synthase encoding genes were shown to be associated with high SGA levels (*8*), implying that the regulation of SGA biosynthesis involves the committed step of the mevalonate pathway as well as later steps of SGA formation. It indicated that along with HMGR,

***Address correspondence to:*
Dr. Aixia Cheng, School of Pharmaceutical Sciences, Shandong University, No. 44 West Wenhua Road, Ji'nan, 250012, China.
E-mail: aixiacheng@sdu.edu.cn

squalene synthase is a potential site for the regulation of SGA production. Squalene synthase genes have been characterized in *Nicotiana tabacum* (*9*), *Panax ginseng* (*10*), *Glycyrrhiza glabra* (*11*), and other plants (*12-18*).

In order to gain new insights into the role of squalene synthase in the SGAs formation in *S. nigrum*, in this work, we report the antifungal activity of SGAs and the molecular characterization and expression analysis of SnSS in *S. nigrum* while infected.

2. Materials and Methods

2.1. *Plant material and fungal inoculation*

Plants of *S. nigrum* were cultivated in green house pots at 25°C with a 12 h light/12 h dark cycle. Plant materials, including root, stem, leaf, flower, premature fruit, and mature fruit were sampled and frozen immediately in liquid nitrogen, and stored at –80°C for RNA isolation.

The seeds of *S. nigrum* were surface sterilized using 5% sodium hypochlorite and cultured on 1/2 B5 medium at 25°C with a 12 h light/12 h dark cycle for 3 weeks for inoculation. *F. oxysporum* was donated by Dr. Huiying Zhang of school of life sciences of Shandong University. The pathogen was grown on PDA medium at 28°C. Sixty 3-week-old seedlings were inoculated with infectious *F. oxysporum* suspension (OD600 = 1.0) using a root-dip inoculation method. After inoculation, the cultured seedling of *S. nigrum* was cultured for another week. Samples were collected and frozen immediately in liquid nitrogen, and stored at –80°C for RNA isolation and compounds analysis.

2.2. *Effect of SGAs on the hyphal formation of F. oxysporum*

γ-Solamargine and its aglycone solasodine (Figure 1) were

Solasodine

γ-Solamargine

Figure 1. The structure of the two compounds.

isolated from *S. nigrum* and the structures were confirmed by NMR in our lab (*19*). *F. oxysporum* (1×10^5 cells/mL in RPMI1640 medium) was incubated with γ-solamargine or solasodine in 96-well flat-bottomed microtitration plates at 37°C without shaking. Hyphae induction for microscopic observation was carried out in 96-well flat bottom non-tissue culture-treated plastic plates. After the incubation, they were microscopically photographed. Each experimental condition was tested in triplicate on a given day and repeated on separate days.

2.3. *Liquid chromatography-mass spectrometry analysis of solasodine and γ-solamargine*

Lyophilized leaf and root tissue were immersed in a solution of ethanol-2 M HCl (4:1) for 24 h and ultrasonically extracted with 80% ethanol for 1 h. The extracts were centrifuged at 3,000 g for 60 min and the supernatant was removed and evaporated under vacuum. The dried residue was resuspended in 0.5 M HCl and extracted with CHCl$_3$ twice. The pH of the water phase was adjusted to 10.5 and then extracted with CHCl$_3$ three times and evaporated under vacuum. The dried residue was resuspended in 200 μL acetonitrile and analyzed using HPLC-DAD-MS.

HPLC-DAD-MS was performed using an Agilent 1100 series II LC system (Agilent Technologies) equipped with a photodiode array detector coupled to an API 4000 mass spectrometer (Applied Biosystems/MDS Sciex) equipped with an electrosprayionization source. A reverse-phase, Venusil XBP-C18 (5 μm, 2.1 × 50 mm) column (Agilent Technologies) was used for separations. The mobile phases consisted of solvent A (0.1% (v/v) CH$_3$COOH in water) and solvent B (acetonitrile), and separations were performed using a linear gradient of 25% to 65% B (v/v) over 70 min. The flow rate was 0.3 mL/min, and the temperature of the column was kept at 28°C. Positive-ion ESI was performed using an ion source voltage of 5.0 kV.

2.4. *Standard curve and related indicators*

The stock solution of the solasodine and γ-solamargine were prepared precisely (100 μg/mL) and diluted with methanol to 0.5, 1, 2.5, 10, 50, 200, 500, 1,000 ng/mL. A low, medium, and high concentration (1, 50, 800 ng/mL) was chosen to make the best quality control (QC). Concentration were tested for horizontal, analyte peak area for the vertical weighted ($W = 1/C^2$) least squares regression calculation.

The standard curves: y = 6690x – 183, $r = 0.9981$ (solasodine); y = 3500x + 110, $r = 0.9983$ (γ-solamargine) within the linear range of 0.5-1,000 ng/mL were obtained by a weight ($W = 1/C^2$) least squares regression calculation using compounds concentration as horizontal and peak area (MS, total ion) as vertical. The contents of solasodine and γ-solamargine were calculated according to the standard curves.
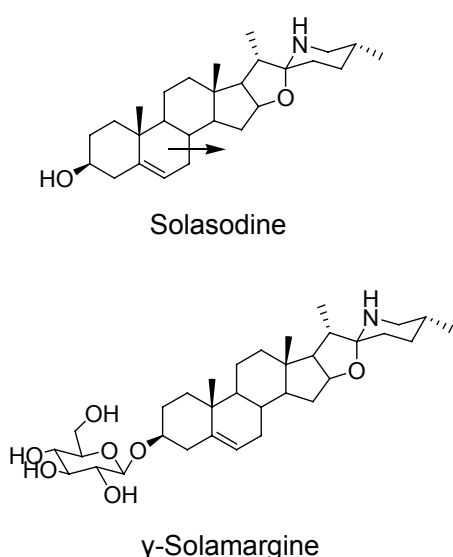
2.5. *RNA extraction and synthesis of the first-strand cDNA*

Samples of young leaves or other tissues were ground into fine powder and extracted using TRIzol reagent. The RNA pellets were washed with 70% ethanol. After a short drying at room temperature, the pellets were resuspended in diethylpyrocarbonate (DEPC)-treated water. Total RNA obtained was used as template for cDNA synthesis. cDNA was synthesized using a reverse transcription kit (TOYOBO, Japan) according to the manufacturer's instructions.

2.6. *5′ and 3′ rapid amplification of cDNA ends (RACE) and amplification of full-length cDNAs*

On the basis of highly conserved amino acid sequences from squalene synthases of several plants, two degenerate primers were synthesized for the PCR amplification of the corresponding *S. nigrum* cDNA. The forward (SnSSP1) and reverse (SnSSP2) primers were 5′-CC ATCGACGACTACGACGAGTAYTGYCAYTA-3′ and 5′-TGCCGATGGCCATGAYYTGNGGDAT-3′, respectively. D, N, and Y represent mixtures of nucleotides A/G/T, A/C/G/T, and C/T, respectively. Using the above-mentioned *S. nigrum* cDNA as a template, degenerate PCR was carried out under the following conditions: 35 cycles of 94°C for 1 min, 45°C for 1.5 min, and 72°C for 2 min. A single DNA fragment was recovered, cloned into the PMD-19T-vector (TaKaRa, Japan), and subjected to nucleotide sequencing. The 5′- and 3′- ends of the SnSS cDNA were obtained by RACE, using the SMART RACE cDNA amplification kit (Clontech) according to the manufacturer's instructions. For the 5′-RACE, the gene specific primers that were used in the 1st PCR, the 1st nested PCR amplifications were: 5′-GAAAGATGGCAGGATCACGCAA-3′ (SnSSGSP1) and 5′-GCCAGAACATACGACACTTAGG-3′ (SnSSGSP2), respectively. Those for 3′-RACE were 5′-GACCAGTTCCATCACGTTTCGAC-3′ (SnSSGSP3) and 5′-GCAAGGAGGTGGAAACAATCGA-3′ (SnSSGSP4), respectively. The 5′- and 3′- RACE products were subjected to direct sequencing of both strands, and a consensus open reading frame (ORF) sequence was obtained. Based on sequencing results of the 3′ and 5′ RACE products, the SnSS ORF was amplified using single-stranded cDNA templates and two gene specific primers, SnSSFLF: 5′-TTGTTGAGAAGAATGGGGAC-3′ and SnSSFLR: 5′-AGTTTGTGCTGTCTTCCCTG-3′.

2.7. *Expression patterns of SnSS*

PCR amplification was performed in an 8-tube strip format (Axygen, Union City, CA, USA) in triplicate. Each reaction contained 1 × SYBR Green PCR Master mix, 0.5 pmol/mL forward primer and reverse primer and 1 μL template cDNA in a final volume of 20 μL using a Mastercycler ep realplex apparatus (Eppendorf, Germany), with primers SnSSRT1 5′-GCCAGAACATACGACACT-3′ (P1), SnSSRT2: 5′-AAGGAGGTGGAAACAAT-3′ (P2). Elongation factor 1a (*EF-1a*) gene was also amplified as an internal control using EF1a-F (5′-ACCACTGGTGGTTTTGAAGC-3′) and EF1a-R (5′-ACGACCAACAGGGACAGTTC-3′) primers. The cycling profile included 35 cycles of 95°C for 30 s, 60°C for 30 s and 72°C for 45 s. Data acquisition and the analysis of real-time PCR assays were performed using the Mastercycler ep realplex. Each fluorescent reporter signal was measured against the internal reference dye signal to normalize for non-PCR-related fluorescence fluctuations between wells. The threshold cycle represented the refraction cycle number at which a positive amplification reaction was measured and set at ten times the standard deviation of the mean baseline emission calculated for amplification cycles 3-15. All samples were taken in triplicate independent experiments.

3. Results

3.1. *Effect of steroidal alkaloids on growth form of F. oxysporum*

F. oxysporum was cultured in RPMI 1640 medium. After 12 h incubation, *F. oxysporum* cells were photographed (Figure 2). The results showed that *F. oxysporum*
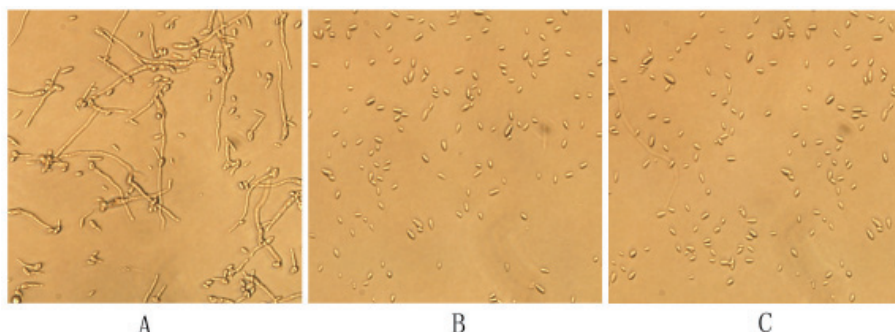
**Figure 2. Microscopic observation of *F. oxysporum* treated with two compounds.** *F. oxysporum* (1×10^5 cells/mL in RPMI 1640 medium) were incubated at 37°C for 6 h **(A)** and with 8 μg/mL solasodine **(B)**, 16 μg/mL γ-solamargine **(C)**.

suspended in RPMI 1640 medium grew in hyphal form. When solasodine and γ-solamargine were added to the medium, *F. oxysporum* grew in a yeast form. The ratio of hyphae formation was significantly inhibited by solasodine and γ-solamargine. These findings suggested that solasodine and γ-solamargine regulated the hyphae transformation of *F. oxysporum* cells.

3.2. *Isolation and sequence analysis of SnSS*

The full-length cDNA of SnSS was obtained through the RACE method. The SnSS cDNA contains an ORF encoding a protein of 411 amino acids. By aligning deduced sequences of SnSS with other squalene synthases from taxonomically diverse species, an SnSS amino acid sequence is 79.7, 95.8, 80.2, 79.7, 81.2, 74.6, 69.1% identical to those in *Glycyrrihiza glabra* (*11*), *Capsicum annuum* (*16*), *Panax ginseng* (*10*), S*olanum tuberosum* (*15*), *Euphorbia tirucalli* (*20*), *Arabidopsis thaliana* (*12,14,21*), *Oryza sativa* (*13*), respectively.

Six highly conserved peptide domains of 14-23 amino acids previously pointed out by Robinson (*22*) were also discernible within the SnSS amino acid sequence (Figure 3). Three domains (III, IV, and V) showed a highly conserved consensus sequence with other squalene synthase enzymes, while three domains (I, II, and VI) were much less conserved. Due to the high level of sequence identity shared with other squalene synthases reported so far, the SnSS cDNA might code for squalene synthase.

3.3. *F. oxysporum affects the biosynthesis of SGAs by regulating SnSS expression level*

The plants were kept in pots in a chamber at 25°C with light from fluorescent lights (12 h light/12 h dark). Plants (3-week-old) were inoculated and then the cultured seedling of *S. nigrum* was cultured for another week. The result indicated that the seedling inoculated with sterile water grew normally (Figures 4A and 4C) while the seedling inoculated with the spore suspension of *F. oxysporum* became small and yellow (Figures 4B and 4D). To investigate whether SnSS expression was positively correlated with the formation of SGAs, the concentration of solasodine and γ-solamargine and the expression level of SnSS were evaluated after inoculation of *F. oxysporum*. The concentration of solasodine and γ-solamargine increased in both leaves and roots after inoculation of *F. oxysporum* spores (Figure 4E). The solasodine concentration was 2.1- and 6-fold higher than the control in leaves and roots, respectively. The γ-solamargine concentration was 4.8- and 5.6-fold higher than the control in leaves and roots, respectively (Figure 4E). Real-time RT-PCR analysis was performed to determine transcription level of the *SnSS* gene in the solasodine and γ-solamargine biosynthetic pathway. The accumulation of SnSS

transcripts increased, which was 2.3- and 3-fold higher than the control in leaves and roots after *F. oxysporum* spores inoculation (Figure 4F).

3.4. *Tissue-specific and developmental expression of SnSS*

The expression pattern of genes in different tissues reflects the distribution of secondary metabolites (*23*). To further characterize the tissue specific expression of SnSS, transcripts of the gene were examined using real-time PCR. In 3-month-old plants, the *SnSS* gene had the highest steady-state level of transcripts in mature leaves, and a lower level in flowers and fruits (Figure 5). This result indicated that the synthesis of SGAs is mainly located in leaves and may help to fight against vascular related diseases occurring on the leaves.

4. Discussion

The root-infecting fungal pathogen *F. oxysporum* is responsible for vascular wilt in over 100 different plant species, including banana, cotton, grain legumes, oil palm, vegetables, and ornamental plants (*6*). *F. oxysporum* is a dimorphic fungus that can switch between yeast and hyphae growth modes. The infection process for *F. oxysporum* includes the germination of spores in the soil, the fungal hyphae penetrating root tips through wounds or at the point of lateral root formation, and advancing through to the root cortex intercellularly, and ultimately reaching the xylem vessels as reported in potatoes (*24,25*). From this point, the pathogen travels through the vascular tissues, mostly upward towards the stem. So hyphae formation is a prerequisite for *F. oxysporum* infection in plants. Our results indicate that steroidal alkaloids isolated from *S. nigrum* exhibited an excellent inhibition effect on *F. oxysporum* hyphae formation and plays important roles in plant defense.

It has been reported that biosynthesis of steroidal alkaloids is *via* the mevalonate pathway in which squalene synthase is a key rate-limiting enzyme. Squalene synthase is a membrane bound enzyme (*7*) that condenses two farnesyl diphosphate molecules into squalene. Squalene synthase is generally described as a crucial branch-point enzyme for synthesizing sterol and is intriguing as a potential regulatory-point carbon flux into sterol. There is also a positive correlation between the expression level of squalene synthase and the amount of triterpenes and sterol produced. Our results suggest that squalene synthase in *S. nigrum* is also a key rate-limiting enzyme in steroidal alkaloid biosynthesis. The content of solasodine and γ-solamargine and the expression of SnSS were increased after *F. oxysporum* infection, which indicated that solasodine and solamargine play an important role in resisting fungi infection in *S. nigrum*.

In conclusion, in the present investigation, we demonstrate that the steroidal alkaloids solasodine and γ-solamargine isolated from *S. nigrum* exhibited an excellent inhibition effect on *F. oxysporum* hyphae formation, which may play an important role in defense from *F. oxysporum* infection. Squalene synthase, a key enzyme in the SGAs biosynthesis, was molecularly cloned and the expression level was enhanced after *F. oxysporum* infection in accordance with the content of solasodine and γ-solamargine.
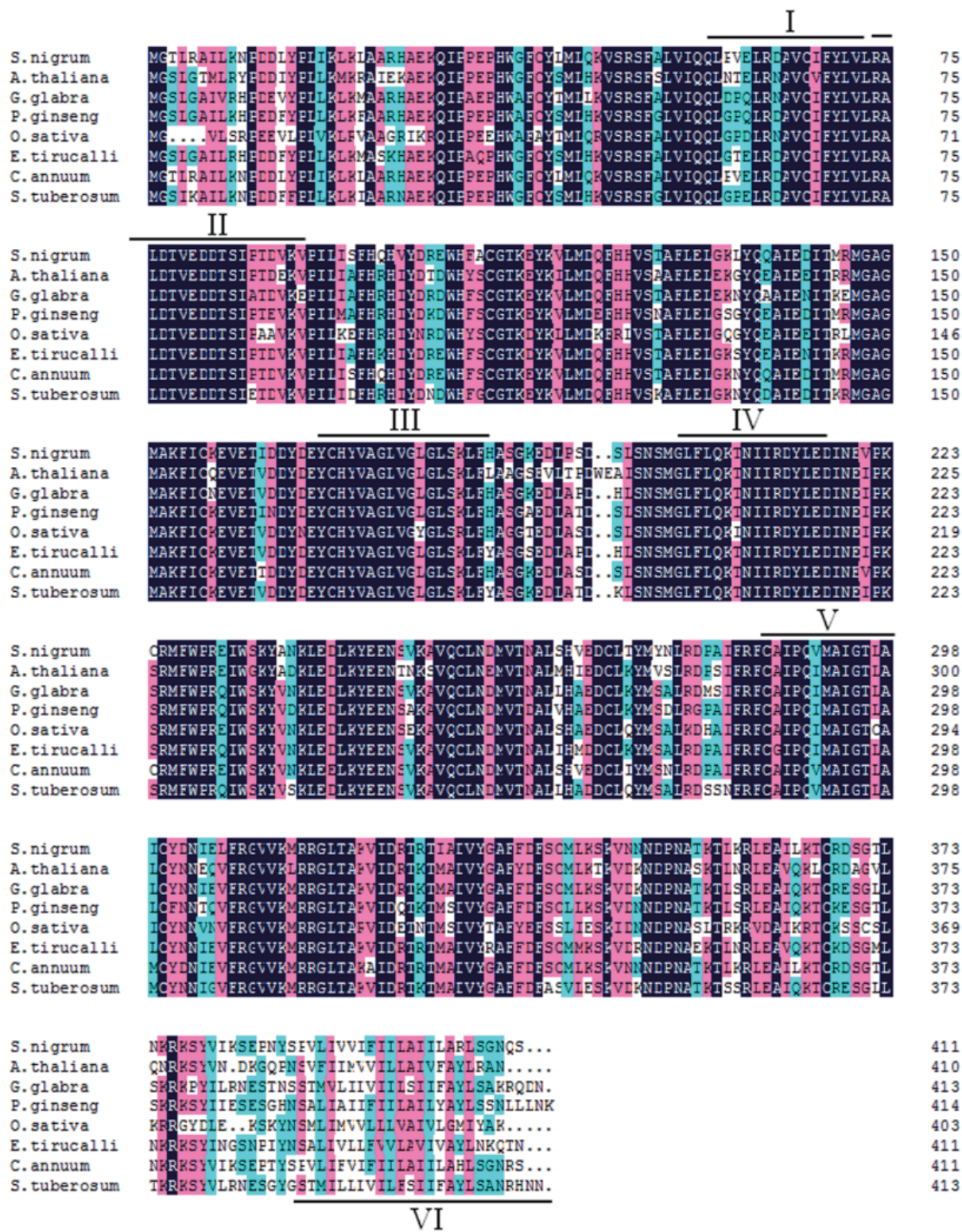
Figure 3. Multi-alignment of the deduced SnSS amino acid sequence with those of other plant squalene synthases. The DDBJ/GenBank/EMBL accession numbers of the retrieved sequences are AB433916 (*Euphorbia tirucalli*), D86409 (*Glycyrrhiza glabra*), AF124842 (*Capsicum annuum*), AB010148 (*Panax ginseng*), AB022599 (*Solanum tuberosum*), NM_119630 (*Arabidopsis thaliana*), and NM_001058160 (*Oryza sativa*).
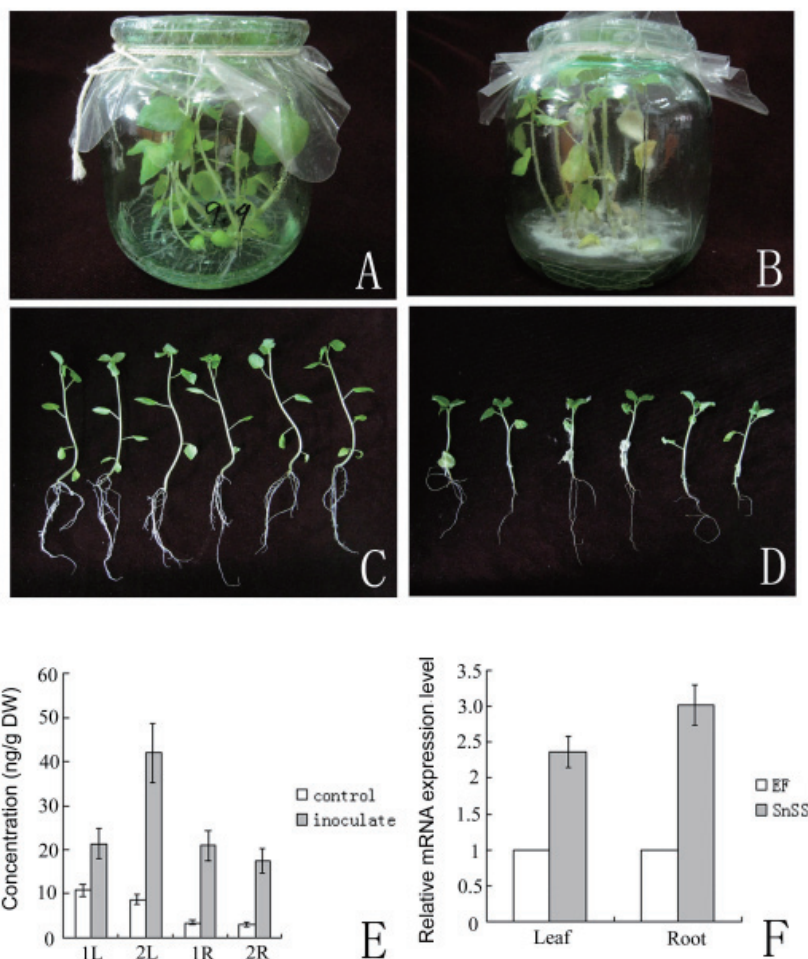
Figure 4. The plants were kept in pots in a chamber at 25°C with light from fluorescent lights (16 h light/8 h dark). 3-weeks old plants were inoculated with sterile water (**A** and **C**) or the spore suspension of *F. oxysporum* (**B** and **D**). Concentration of solasodine and γ-solamargine in leaves and roots of *S. nigrum* are shown in **E** and the changes of SnSS mRNA level after inoculation are shown in **F**. **1L**, **2L**, **1R**, **2R** means the content of compound 1 in leaf, compound 2 in leaf, compound 1 in root and compound 2 in root, respectively.
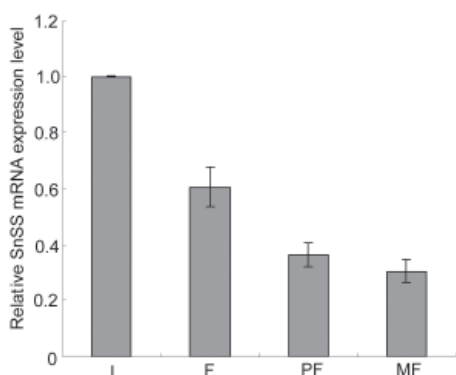
Figure 5. Real-time RT-PCR amplification of *SnSS*. PCR was performed using *S. nigrum SnSS*-specific primers and an equal amount of total RNA isolated from the leaves (**L**), the flower (**F**), premature fruits (**PF**) and mature fruits (**MF**). The elongation factor gene was amplified as a control.

References

1. Hammond-Kosack KE, Parker JE. Deciphering plant-pathogen communication: Fresh perspectives for molecular resistance breeding. Curr Opin Biotechnol. 2003; 14:177-193.
2. Thatcher LF, Anderson JP, Singh KB. Plant defence responses: What have we learnt from *Arabidopsis*? Funct Plant Biol. 2005; 32:1-19.
3. Sanford LL, Deahl KL, Sinden SL, Ladd TL. Glycoalkaloid contents in tubers from *Solanum tuberosum* populations selected for potato leafhopper resistance. Am potato J. 1992; 69:693-703.
4. Eltayeb EA, Al-Ansari AS, Roddick JG. Changes in the steroidal alkaloid solasodine during development of *Solanum nigrum* and *Solanum incanum*. Phytochem. 1997; 46:489-494.
5. Simons V, Morrissey JP, Latijnhouwers M, Csukai M, Cleaver A, Yarrow C, Osbourn A. Dual effects of plant steroidal alkaloids on *Saccharomyces cerevisiae*. Antimicrob Agents Chemother. 2006; 8:2732-2740.
6. Thatcher LF, Manners JM, Kazan K. *Fusarium oxysporum* hijacks COI1-mediated jasmonate signaling to promote disease development in Arabidopsis. Plant J.

2009; 58:927-939.

7. Popjak G, Agnew WS. Squalene synthetase. Mol Cell Biochem. 1979; 27:97-116.

8. Krits P, Fogelman E, Ginzberg I. Potato steroidal glycoalkaloid levels and the expression of key isoprenoid metabolic genes. Planta. 2007; 227:143-150.

9. Devarenne TP, Ghosh A, Chappell J. Regulation of squalene synthase, a key enzyme of sterol biosynthesis, in tobacco. Plant Physiol. 2002; 129:1095-1106.

10. Lee MH, Jeong JH, Seo JW, Shin CG, Kim YS, In JG, Yang DC, Yi JS, Choi YE. Enhanced triterpene and phytosterol biosynthesis in *Panax ginseng* overexpressing squalene synthase gene. Plant Cell Physiol. 2004; 45:976-984.

11. Hayashi H, Hirota A, Hiraoka N, Ikeshiro Y. Molecular cloning and characterization of two cDNAs for *Glycyrrhiza glabra* squalene synthase. Biol Pharm Bull. 1999; 22:947-950.

12. Nakashima T, Inoue T, Oka A, Nishino T, Osumi T, Hata S. Cloning, expression, and characterization of cDNAs encoding *Arabidopsis thaliana* squalene synthase. Proc Natl Acad Sci U S A. 1995; 92:2328-2332.

13. Hata S, Sanmiya K, Kouchi H, Matsuoka M, Yamamoto N, Izui K. cDNA cloning of squalene synthase genes from mono- and dicotyledonous plants, and expression of the gene in rice. Plant Cell Physiol. 1997; 38:1409-1413.

14. Kribii R, Arró M, del Arco A, González V, Balcells L, Delourme D, Ferrer A, Karst F, Boronat A. Cloning and characterization of the *Arabidopsis thaliana SQS1* gene encoding squalene synthase – involvement of the C-terminal region of the enzyme in the channeling of squalene through the sterol pathway. Eur J Biochem. 1997; 249:61-69.

15. Yoshioka H, Yamada N, Doke N. cDNA cloning of sesquiterpene cyclase and squalene synthase, and expression of the genes in potato tuber infected with *Phytophthora infestans*. Plant Cell Physiol. 1999; 40:993-998.

16. Lee JH, Yoon YH, Kim HY, Shin DH, Kim DU, Lee IJ, Kim KU. Cloning and expression of squalene synthase cDNA from hot pepper (*Capsicum annuum* L.). Mol Cells. 2002; 13:436-443.

17. Suzuki H, Achnine L, Xu R, Matsuda SPT, Dixon RA. A genomics approach to the early stages of triterpene saponin biosynthesis in *Medicago truncatula*. Plant J. 2002; 32:1033-1048.

18. Akamine S, Nakamori K, Chechetka SA, Banba M, Umehara Y, Kouchi H, Izui K, Hata S. cDNA cloning, mRNA expression, and mutational analysis of the squalene synthase gene of *Lotus japonicus*. Biochim Biophys Acta. 2003; 1626:97-101.

19. Zhao Y. Chemical constituents of two solanum species, microbial transformation and biological activities. 2010. PhD dissertation, Shandong University, Ji'nan, China.

20. Uchida H, Yamashita H, Kajikawa M, Ohyama K, Nakayachi O, Sugiyama R, Yamato KT, Muranaka T, Fukuzawa H, Takemura M, Ohyama K. Cloning and characterization of a squalene synthase gene from a petroleum plant, *Euphorbia tirucalli* L. Planta. 2009; 229:1243-1252.

21. Busquets A, Keim V, Closa M, del Arco A, Boronat A, Arró M, Ferrer A. *Arabidopsis thaliana* contains a single gene encoding squalene synthase. Plant Mol Biol. 2008; 67:25-36.

22. Robinson GW, Tsay YH, Kienzle BK, Smith-Monroy CA, Bishop RW. Conservation between human and fungal squalene synthetases: Similarities in structure, function, and regulation. Mol Cell Biol. 1993; 13:2706-2717.

23. Chen J, Xiao Y, Di P, Yu X, Chen S, Zhang L. Molecular cloning and characterization of a 2C-methyl-D: -erythritol 2,4-cyclodiphosphate synthase gene from *Cephalotaxus harringtonia*. Mol Biol Rep. 2009; 36:1749-1756.

24. Pietro DA, Madrid MP, Caracuel Z, Delgado-Jarana J, Roncero MI. *Fusarium oxysporum*: Exploring the molecular arsenal of a vascular wilt fungus. Mol Plant Pathol. 2003; 4:315-325.

25. Berrocal-Lobo M, Molina A. *Arabidopsis* defense response against *Fusarium oxysporum*. Trends Plant Sci. 2008; 13:145-150.

Original Article

Enhancement of anti-cholinesterase activity of *Zingiber cassumunar* essential oil using a microemulsion technique

Siriporn Okonogi*, Wantida Chaiyana

Department of Pharmaceutical Science, Faculty of Pharmacy, Chiang Mai University, Chiang Mai, Thailand.

ABSTRACT: The aim of the present study was to enhance the cholinesterase inhibitory activity of *Zingiber cassumunar* (ZC) oil using a microemulsion (ME) technique. Pseudoternary phase diagrams of the oil, water, and surfactant/co-surfactant mixture were constructed using a water titration method. Effects of co-surfactant, surfactant/co-surfactant ratio, ionic strength, and pH were examined by means of the microemulsion region which existed in the phase diagrams. The inhibition of acetylcholinesterase (AChE) and butyrylcholinesterase (BChE) were tested by Ellman's colorimetric assay. It was found that ZC oil possesses inhibitory activity against not only AChE but also BChE. Formulation of ZC oil as ME revealed that alkyl chain length and number of hydroxyl groups of co-surfactant exhibited a remarkable effect on the pseudoternary phase diagram. Longer alkyl chains and more hydroxyl groups gave smaller regions of MEs. Ionic strength also affected the ME region. However, the phase behavior was hardly influenced by pH. The suitable ZC oil ME was composed of Triton X-114 in combination with propylene glycol. The anti-cholinesterase activity of this ME was much higher than that of native ZC oil. It exhibited twenty times and twenty five times higher inhibitory activity against AChE and BChE, respectively. ZC oil loaded ME is an attractive formulation for further characterization and an *in vivo* study in an animal model with Alzheimer's disease.

Keywords: Alzheimer's disease, acetylcholinestrase, butyrylcholinesterase, phase diagram

1. Introduction

Alzheimer's disease (AD) is a devastating neurodegenerative disorder which is the most common of all brain degenerations (*1*). Patients with AD will generally present a gradual onset and a progressive sequential decline in cognitive, behavioral and motor functions which interfere with an individual's daily function and quality of life and eventually lead to an enormous burden on the country's health care system (*2-4*). Advances in preventing AD or delaying progression would have a huge global public health impact. However, there is still no specific biological marker to diagnose this disease. The definite diagnosis of AD is made upon histological verification, established by biopsy or at autopsy, of extracellular amyloid plaques and intracellular neurofibrillary tangles (*5*). Increased levels of acetylcholinesterase (AChE) and butyrylcholinesterase (BChE) have also been found in postmortem brain samples leading to the hypothesis that the cognitive decline in AD patients is related to progressive cholinergic degeneration (*6,7*). Various treatment strategies aimed at boosting cholinergic function, especially by the inhibition of synaptic acetylcholine degradation, has been an area of focus (*8*). Recently, a few synthetic medicines, *e.g.* tacrine, donepezil, and the natural product-based rivastigmine and galantamine have been used for treatment of cognitive dysfunction and memory loss associated with AD (*9,10*). Nevertheless, none of them can stop the disease and these compounds have been reported to have their own adverse effects including gastrointestinal disturbances and problems associated with bioavailability, which necessitates interest in finding better AChE inhibitors from natural resources and a better way to deliver these compounds.

The Zingiberaceae is among the plant families which are widely distributed throughout the tropics, particularly in Southeast Asia. Most members of this family are easily recognized by the characteristic aromatic leaves and fleshy rhizome when both of them are crushed (*11*). Several species of Zingiberaceae are used as spices, medicines and flavoring agents. *Zingiber cassumunar* Roxb. (ZC) is used in folklore remedies as a single plant or as a component of herbal recipes for the treatment

**Address correspondence to:*
Dr. Siriporn Okonogi, Department of Pharmaceutical Science, Faculty of Pharmacy, Chiang Mai University, Chiang Mai 50200, Thailand.
E-mail: sirioko@chiangmai.ac.th

of various conditions including inflammation, sprains, rheumatism, muscular pain, wounds, and asthma (*12*). It is also used as a mosquito repellant, an anti-dysenteric agent, a carminative, a mild laxative, and a cleansing solution for skin diseases (*13*). A number of pure compounds isolated from ZC have been shown to possess anti-inflammatory and antioxidant activity (*11,12*) which has become another focus of new treatment strategies against AD aside from anti-cholinesterase activity (*14-16*). Inflammation of the brain has been proposed to lead to neurological diseases, especially AD, since throughout the process of inflammation, the generation of neuronal cells of the adult brain is affected (*17*). Epidemiological studies point that the risk of AD is reduced among users of anti-inflammatory drugs (*18*). In the past decade, oxidative stress has also been described in the pathological changes that occur in AD (*19,20*). Nitric oxide (NO) is a diatomic free radical produced from L-arginine by constitutive and inducible nitric oxide synthase (cNOS and iNOS) in numerous mammalian cells and tissues (*21*). NO, superoxide (O_2^-) and their reaction product peroxynitrite ($ONOO^-$) may be generated in excess during the host response against infections and inflammatory conditions, contributing to some pathogenesis by promoting oxidative stress, tissue injury and even neurodegenerative disease (*22*). Since the reported antioxidant and anti-inflammation activity of ZC oil is associated with AD, investigation of the anti-cholinesterase activity of ZC oil would be an interesting aspect to confirm the possibility of using ZC oil in the treatment of AD. Moreover, incorporation of ZC oil in a novel topical formulation will also be fascinating because transdermal administration is the ideal therapeutic approach for chronic neurological disorders in elderly people since it provides sustained therapeutic plasma levels of drugs, is simple to use, and may reduce systemic adverse effects (*23*). ZC oil is a complex mixture of volatile components and its constituents can degrade during storage and lead to changes in biological activities. Therefore, incorporation of ZC oil into a suitable formulation would overcome its labile property as well as its hydrophobic property disadvantage. A microemulsion (ME) is a formulation used to incorporate ZC oil because it is an isotropic colloidal system that is formed spontaneously from appropriate combinations of oil, water, and surfactant/co-surfactant mixtures (*24*). ME is optically transparent since the internal phase droplet size ranges from 5 to 200 nm (*25,26*), which is below the wavelength of visible light. The physical appearance of the ME will be the same as the native oil. Therefore, this study aims to show the anti-cholinesterase activity of ZC oil and enhance its activity by loading the oil into a suitable ME system for topical application. The factors influencing the ME region in the pseudoternary phase diagram were also investigated to include surfactant type, co-surfactant type, surfactant/co-surfactant ratio, pH, and ionic strength of the aqueous phase. A suitable system was finally derived for the anti-cholinesterase activities.

2. Materials and Methods

2.1. *Plant materials*

Zingiber cassumunar Roxb. (Zingiberaceae) was collected from Chiang Mai, Thailand during January 2009. It was authenticated and voucher specimens were deposited in the Herbarium of the Faculty of Pharmacy, Chiang Mai University, Thailand.

2.2. *Chemicals and enzymes*

AChE (specific activity 425.94 U/mg) from *Electrophorus electricus*, BChE (specific activity 7.4 U/mg) from equine serum, 5,5'-dithiobis(2-nitrobenzoic acid) (DTNB), propylene glycol (PG), glycerin, polyethylene glycol 400 (PEG 400), and cetyl alcohol were from Sigma-Aldrich Chemicals (St. Louis, MO, USA). Acetylthiocholine iodide (ATCI) and butyrylthiocholine iodide (BTCI) were from Fluka (Steinheim, Germany). Octylphenoxy polyethoxy ethanol (Triton X-114) was from Acros Organics (New Jersey, USA). Ethanol, propan-1-ol and propan-2-ol were analytical grade from Merck (Darmstadt, Germany).

2.3. *Extraction of the essential oil*

The fresh rhizomes of ZC were cut into small pieces and subjected to hydro-distillation for 3 h by using a clevenger type apparatus for oil extraction. The extracted essential oils were collected and stored in a refrigerator and protected from light until further use.

2.4. *GC-MS analysis*

The essential oil was subjected to GC-MS in order to analyze the components existing in the oil. The GC-MS analysis was performed on an Agilent 6890 gas chromatography (Agilent Technologies, CA, USA) coupled to an electron impact (EI, 70 eV) HP 5973 mass selective detector (Hewlett Packard, CA, USA) and fitted with a fused silica capillary column (HP-5MS) supplied by Hewlett Packard, CA, USA (30.0 m × 250 mm, i.d. 0.25 mm film thickness). The analytical conditions were; carrier gas: helium (ca. 1.0 mL/min), injector temperature: 260°C, oven temperature: 3 min isothermal at 100°C (No peaks before 100°C after first injection), then at 3ºC/min to 188°C and then at 20°C/min to 280°C (3 min isothermal), and detector temperature: 280°C. The programmed-temperature Kováts retention indices (RI) were obtained by GC-MS analysis of an aliquot of the volatile oil spiked with an *n*-alkanes mixture containing each homologue from *n*-C11 to *n*-C27. Identification of the compounds was based on a comparison of their mass spectra database (WILEY&NIST) and spectroscopic data. The percentage amount of each component was calculated based on the total area of all peaks obtained from the oil. The data obtained were used as a standard for further batches of the oil.

2.5. *Cholinesterase activity determination*

Two types of cholinesterase enzymes, electric eel AChE and horse serum BChE, were used whereas ATCI and BTCI were used as substrates, respectively. The enzyme inhibitory action was done using Ellman's method (*27*). Briefly, 50 μL of 50 mM Tris-HCl buffer pH 8.0, 25 μL of 1.5 mM ATCI or BTCI, 125 μL of 3 mM DTNB and 25 μL of the extracted oils in Tris-HCl buffer containing 10% methanol were mixed accordingly. Then, 25 μL of 0.25 U/mL AChE or 0.91 U/mL BChE was added and the reaction was spectrophotometrically followed for 2 min at 415 nm with a microplate reader (Bio-Rad Laboratories Ltd., Tokyo, Japan). The Tris-HCl buffer containing 10% methanol was used as negative control for cholinesterase activity evaluation of ZC oil. In the case of inhibitory activity evaluation of the ME, 25 μL of ME containing 10% of the extracted oil was added instead of the extracted oil in Tris-HCl buffer with 10% methanol. The mixture containing 10% methanol, 30% PG, and 60% Triton X-114 was used as negative control in this case. The experiments were done in triplicate. The slope of the plot of absorbance *versus* time was taken as the enzymatic reaction rate. The enzyme inhibitory activity was calculated as *1 − (Vs/Vb)*, in which *Vs* is the mean reaction rate in the presence of a certain concentration of the oils and *Vb* is the mean reaction rate in the absence of the oils. IC_{50} values were statistically evaluated using the Graphpad/Prism program.

2.6. *Construction of phase diagrams*

Pseudoternary phase diagrams of the essential oils were constructed using a water titration method. The surfactant (Triton X-114) was mixed with a co-surfactant (ethanol, propan-1-ol, propan-2-ol, cetyl alcohol, glycerin, PG, or PEG 400) at a weight ratio of 2:1 to obtain the surfactant mixture (Smix). The essential oils and Smix were then mixed at various weight ratios (0:1, 1:9, 2:8, 3:7, 4:6, 5:5, 6:4, 7:3, 8:2, 9:1, and 1:0) and the resulting mixtures were subsequently titrated with water under moderate agitation at room temperature. The samples were classified as ME when they appeared visually as clear liquids. Instead of water, acetate buffers of pH 4.0 and 6.0 (composed of 0.1 M acetic acid and 0.1 M sodium acetate), phosphate buffers of pH 8.0 (composed of 0.2 M monosodium phosphate and 0.2 M disodium hydrogen phosphate) and solutions of 0.1, 0.5, and 1.0 M sodium chloride (NaCl) and magnesium chloride (MgCl₂) were also used to investigate the effect of pH and ionic strength on the phase diagrams, respectively. The different formulations were made in triplicate. The pseudoternary phase diagrams were drawn using the OriginPro 8 program.

3. Results and Discussion

3.1. *GC-MS of ZC oil*

The chemical compositions of ZC oil investigated by GC-MS are shown in Table 1. Fourteen components were identified accounting for 95.21% of the total yields. Terpinen-4-ol (67.06%) and γ-terpinene (13.26%) were major constituents. The results were in good agreement with previous reports (*14,28*).

3.2. *Cholinesterase inhibitory activity of ZC oil*

The dose response curves for anti-AChE and anti-BChE with ZC oil are shown in Figures 1 and 2, respectively. The calculated IC_{50} values show that ZC oil can be characterized as a moderate BChE inhibitor with IC_{50} of 0.355 ± 0.137 mg/mL and a weak AChE inhibitor with IC_{50} of 5.573 ± 0.176 mg/mL. Acetylcholine is a neurotransmitter released at the synaptic gap. The pathological features in central nervous system disorders are identified by neurotransmitter disturbances and are insufficient especially in cholinergic functions (*10*). Normally, acetylcholine is hydrolyzed by the cholinesterase enzyme. A greater amount of the enzyme leads to lower amount of aceylcholine found in the synaptic gap. Inhibition of cholinesterase therefore can restore the level of acetylcholine in the brain (*29*). AChE is lost up to nearly 85% in specific brain regions in AD patients, whereas the BChE level rises with disease progression (*30*). Distinctly, the imbalance in cholinesterase activity in the AD brain modifies the normally supportive role of BChE and represents the reason behind recent synthesis of new selective BChE inhibitors for mild to moderate forms of AD (*31*). Kim *et al.* (2006) have reported the memory enhancing effect of essential oil from *Abies koreana*, of which terpinen-4-ol was the major component, on scopolamine-induced amnesia in mice (*32*). Moreover, terpinen-4-ol has been reported for its inhibition of AChE activity (*33*).

Table 1. Chemical compositions of the essential oil of ZC

Retention time (min)	Compound	Peak area (%)
3.21	α-Terpinene	0.40
3.56	γ-Terpinene	13.26
3.68	*cis*-Sabinenehydrate	0.54
3.99	α-Terpinolene	3.04
4.16	*trans*-Linaool oxide	0.47
4.58	Neo-allo-ocimene	2.52
4.90	γ-Terpinene	1.76
5.93	Terpinen-4-ol	67.06
6.07	*p*-Cymen-8-ol	2.36
6.16	Dill ether	0.59
6.41	*cis*-Piperitol	1.03
10.42	δ-Elemene	0.31
16.44	Allo-ocimene	0.68
18.98	Caryophyllene oxide	1.19
	Total	95.21
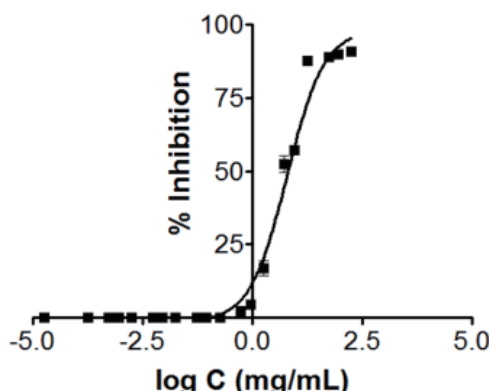
Figure 1. Dose response curves of ZC oil against AChE. AChE was added to the mixture of 50 mM Tris-HCl buffer pH 8.0, 1.5 mM ATCI, 3 mM DTNB, and the tested oil in Tris-HCl buffer containing 10% methanol. The reaction was spectrophotometrically determined at 415 nm by a microplate reader.
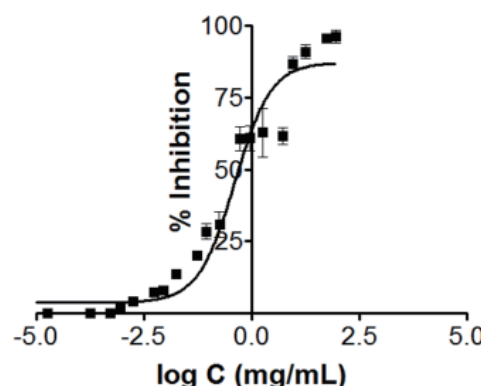

Figure 2. Dose response curves of ZC oil against BChE. BChE was added to the mixture of 50 mM Tris-HCl buffer pH 8.0, 1.5 mM ATCI, 3 mM DTNB, and the extracted oils in Tris-HCl buffer containing 10% methanol. The reaction was spectrophotometrically determined at 415 nm by a microplate reader.

Therefore, terpinen-4-ol is one of the possible affective agents that account for the anti-cholinesterase activity. However, a complex interaction between its various constituents, in which synergistic responses might be produced, resulted in the inhibitory activity of ZC oil (*34*).

3.3. *Influence of co-surfactant and surfactant/co-surfactant ratio on the phase diagrams*

ME is a clear, thermodynamically stable and optically isotropic system. ME forms spontaneously upon mixing a suitable proportion of oil, water, and surfactant either alone or in combination with a co-surfactant, thereby overcoming the need for any additional input of energy. Triton X-114, nonionic surfactant, was employed in this study since it shows low irritancy and low toxicity (*35*). The influence of co-surfactant type was studied since it can reduce surface tension and increase flexibility of the interface by partitioning themselves among the oil, water, and interface domains (*36*) which lead to the spontaneously formed ME (*37*). Since co-surfactant participates in a micelle and adjusts the polarity of water and oil, it thus affects the system of phase behavior and nature of the ME components (*38*). Therefore, the study of suitable co-surfactants would be appropriate. The phase behavior of the ZC oil/Triton X-114/co-surfactant/water system was represented in a pseudoternary phase diagram, in which ZC oil is one component, another one is water, and the third component is Smix, which is a mixture of Triton X-114 and co-surfactant. The ternary phase diagram was constructed adopting a simple titration method. Smix, in which the Triton X-114 and co-surfactant mass ratio was fixed, was first prepared by combining the required mass of Triton X-114 and co-surfactant. Then an appropriate quantity of ZC oil was introduced into the emulsifier and water was the titration component. The phase boundary was noted by observing

the transition from turbidity to transparency or from transparency to turbidity.

The effect of chain length of linear alcohols on the phase behavior of ME systems were investigated by using ethanol, *n*-propanol and cetyl alcohol. Figure 3 shows phase diagrams as well as percentage of ME region which occurred when various types of co-surfactant were mixed with Triton X-114. The results indicated that cetyl alcohol, the longest alkyl chain alcohol in this study, gave a very sparse ME region with Triton X-114. Moreover, the ME regions in the phase diagrams using ethanol were larger than that of *n*-propanol. These results were in accordance with the previous study of Alany *et al.* (*39*) which indicated that the ME region in the phase diagram was reduced upon increasing the chain length of alkane alcohols. Branch chained alcohols had no effect on the formation of the ME.

The effect of hydroxyl group numbers on the phase behavior was also considered. Isopropanol was selected as a representative of alkane mono-ol while PG and glycerin represented an alkane diol and triol, respectively. The results, as shown in Figure 3, indicate that glycerin was not a good co-surfactant and the ME region nearly disappeared with glycerin because of its highly hydrophilic property. On the other hand, PG and isopropanol were appropriate to form ME with Triton X-114 since they gave a larger ME area in the phase diagram. Moreover, PG showed a higher performance in ME formation when compared with PEG 400 because of its compact molecule (*35*). A likely explanation is that the complicated co-surfactant cannot form the ME properly if the structure of surfactant is complex (*39*). Therefore, PG was selected as a co-surfactant for further investigations because it gave a large ME region area in the phase diagram as well as its non-volatile properties. Figure 4 shows the effect of surfactant to co-surfactant ratio. The higher ratio of surfactant to co-surfactant gave a larger ME region in the phase diagram.
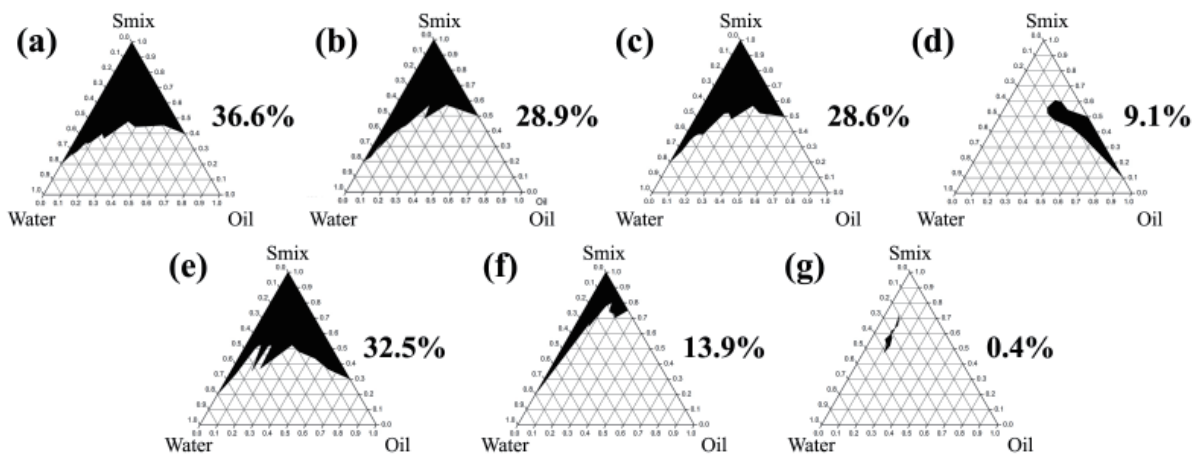
Figure 3. Pseudoternary phase diagrams of ZC oil ME showing the effect of co-surfactant types. The ZC oil ME comprises ZC oil/Triton X-114/co-surfactant/water with ethanol (**a**), propan-1-ol (**b**), propan-2-ol (**c**), cetyl alcohol (**d**), PG (**e**), PEG 400 (**f**), and glycerin (**g**) as a co-surfactant. The ratio of Triton X-114 to co-surfactant was 2:1. The dark area expressed by the number (%) represents the region of microemulsion.
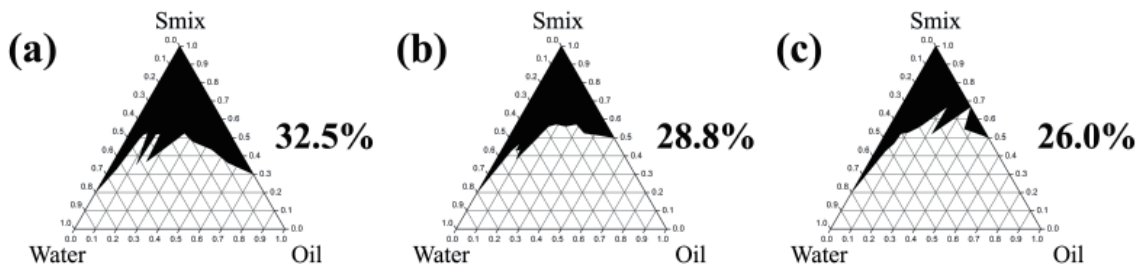
Figure 4. Pseudoternary phase diagrams of ZC oil ME showing the effect of surfactant to co-surfactant ratio. The ZC oil ME is comprised of ZC oil/Triton X-114/PG/water mixtures with a Triton X-114 to PG ratio of 2:1 (**a**), 1:1 (**b**), and 1:2 (**c**). The dark area expressed by the number (%) represents the region of microemulsion.

3.4. *Effect of ionic strength and pH on the phase diagrams*

Electrolyte was believed to have an effect on the region of MEs in the phase diagram because it affected the size of the emulsified droplets (*40*). Therefore, the effect of monovalent and divalent salts on the ZC oil ME system was investigated in the present study. Figure 5 exhibits the effect of electrolytes on the ZC oil ME system using Triton X-114 as a surfactant. NaCl was employed as a monovalent salt while $MgCl_2$ was employed as a divalent salt in this investigation. The results indicated that both electrolytes affected the ME regions. Moreover, $MgCl_2$ showed a stronger effect than NaCl. It was found that with higher concentration of salts, lower ME regions were obtained. This result was due to the salting effect of the divalent electrolyte (Mg^{2+}) that was higher than that of the monovalent electrolyte (Na^+) (*41*). In addition, the pH effects were also investigated and the results are shown in Figure 6. pH exhibited no effect on the ME region of the ZC oil system. Therefore, we concluded that the ME system comprised of ZC oil/Triton X-114/PG/water was hardly effected by variation of pH but could be affected by the ionic strength of the aqueous phase.

3.5. *Cholinesterase inhibitory activity of ZC oil/Triton X-114/PG/water*

The IC_{50} values of ZC oil/Triton X-114/PG/water system against AChE and BChE were compared with the native ZC oil alone. The results are shown in Table 2. It was found that ZC oil in the ME system possessed about twenty times higher inhibition of AChE and about twenty five times higher inhibition of BChE. This result could be due to the increase in solubility of the oil by the ME technique which were more compatible with the enzymes in the test medium.

4. Conclusion

ZC oil possesses inhibitory activity against not only AChE but also BChE. Formulation of ZC oil as ME revealed that alkyl chain length and number of hydroxyl groups of co-surfactants exhibited a remarkable effect on the pseudoternary phase diagram. Longer alkyl chains and more hydroxyl groups gave smaller regions of MEs. Ionic strength also affected the ME region. However, the phase behavior was hardly influenced by pH. The most
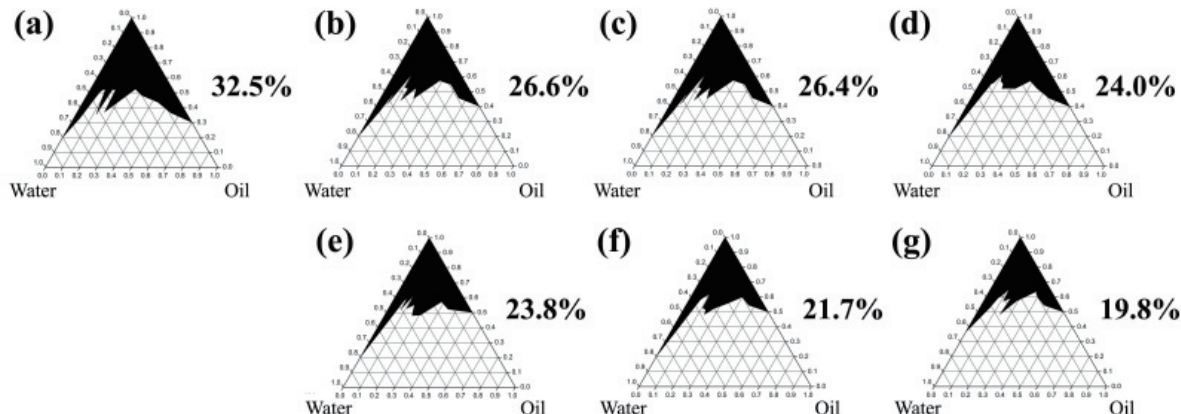
Figure 5. Pseudoternary phase diagrams of ZC oil ME showing the effect of ionic strength. The ZC oil ME using a 2:1 mixture of Triton X-114:PG as surfactant system contains an aqueous phase of water (**a**), 0.1 M NaCl (**b**), 0.5 M NaCl (**c**), 1.0 M NaCl (**d**), 0.1 M $MgCl_2$ (**e**), 0.5 M $MgCl_2$ (**f**) and 1.0 M $MgCl_2$ (**g**). The dark area expressed by the number (%) represents the microemulsion region.
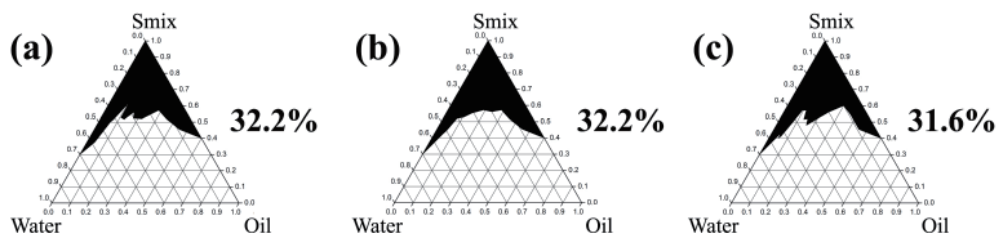
Figure 6. Pseudoternary phase diagrams of ZC oil ME showing the effect of pH. The ZC oil ME using a 2:1 mixture of Triton X-114:PG as surfactant system contains an aqueous phase of water pH 4.0 (**a**), 6.0 (**b**) and 8.0 (**c**). The dark area expressed by the number (%) represents the microemulsion region.

Table 2. IC_{50} of ME comprised of ZC oil against AChE and BChE

Formulations	IC_{50} (mg/mL)	
	AChE	BChE
ZC oil	5.573 ± 0.176	0.355 ± 0.137
ZC oil/ Triton X-114/PG/water	0.252 ± 0.096	0.014 ± 0.002

suitable ZC oil ME was composed of Triton X-114 in combination with PG. The anti-cholinesterase activity of this ME was much higher than that of native ZC oil. It exhibited twenty times and twenty five times higher inhibitory activity against AChE and BChE, respectively. A ZC oil loaded ME is an attractive formulation for further characterization and *in vivo* studies in animal models with AD.

Acknowledgements

References

1. Selkoe DJ. Alzheimer's disease is a synaptic failure. Science. 2002; 298:789-791.
2. Alloul K, Sauriol L, Kennedy W, Laurier C, Tessier G, Novosel S, Contandriopoulos A. Alzheimer's disease: A review of the disease, its epidemiology and economic impact. Arch Gerontol Geriatr Suppl. 1998; 27:189-221.
3. Brookmeyer R, Gray S, Kawas C. Projections of Alzheimer's disease in the United States and the public health impact of delaying disease onset. Am J Public Health. 1998; 88:1337-1342.
4. Brookmeyer R, Johnson E, Ziegler-Graham K, Arrighi HM. Forecasting the global burden of Alzheimer's disease. Alzheimers Dement. 2007; 3:186-191.
5. Szekely CA, Breitner JCS, Zandi PP. Prevention of Alzheimer's disease. Int Rev Psychiatr. 2007; 19:693-706.
6. Snyder SE, Gunupudi N, Sherman PS, Butch ER, Skaddan MB, Kilbourn MR, Koeppe RA, Kuhl DE. Radiolabeled Cholinesterase Substrates: *In vitro* methods for determining structure-activity relationships and identification of a positron emission tomography radiopharmaceutical for *in vivo* measurement of butyrylcholinesterase activity. J Cerebr Blood F Met. 2001; 21:132-143.
7. Auld DS, Kornecook TJ, Bastianetto S, Quirion R. Alzheimer's disease and the basal forebrain cholinergic system: Relations to [β]-amyloid peptides, cognition, and

treatment strategies. Prog Neurobiol. 2002; 68:209-245.

8. Van Beek AHEA, Claassen JAHR. The cerebrovascular role of the cholinergic neural system in Alzheimer's disease. Behav Brain Res. 2011; 221:537-542.

9. Farlow MR, Cummings JL. Effective pharmacologic management of Alzheimer's disease. Am J Med. 2007; 120:388-397.

10. Mukherjee PK, Kumar V, Mal M, Houghton PJ. Acetylcholinesterase inhibitors from plants. Phytomedicine. 2007; 14:289-300.

11. Habsah M, Amran M, Mackeen MM, Lajis NH, Kikuzaki H, Nakatani N, Rahman AA. Screening of *Zingiberaceae* extracts for antimicrobial and antioxidant activities. J Ethnopharmacol. 2000; 72:403-410.

12. Jeenapongsa R, Yoovathaworn K, Sriwatanakul KM, Pongprayoon U, Sriwatanakul K. Anti-inflammatory activity of (E)-1-(3, 4-dimethoxyphenyl) butadiene from *Zingiber cassumunar* Roxb. J Ethnopharmacol. 2003; 87:143-148.

13. Bhuiyan MNI, Chowdhury JU, Begum J. Volatile constituents of essential oils isolated from leaf and rhizome of *Zingiber cassumunar* Roxb. Bangladesh J Pharmacol. 2008; 3:69-75.

14. Hüll M, Fiebich BL, Schumann G, Lieb K, Bauer J. Anti-inflammatory substances-a new therapeutic option in Alzheimer's disease. Drug Discov Today. 1999; 4:275-282.

15. Eikelenboom P, Veerhuis R. The importance of inflammatory mechanisms for the development of Alzheimer's disease. Exp Gerontol. 1999; 34:453-461.

16. Sastre M, Klockgether T, Heneka MT. Contribution of inflammatory processes to Alzheimer's disease: Molecular mechanisms. Int J Dev Neurosci. 2006; 24:167-176.

17. Patel SA, Heinrich AC, Reddy BY, Rameshwar P. Inflammatory mediators: Parallels between cancer biology and stem cell therapy. J Inflamm Res. 2009; 2:13-19.

18. Anthony JC, Breitner JCS, Zandi PP, Meyer MR, Jurasova I, Norton MC, Stone SV. Reduced prevalence of AD in users of NSAIDs and H2 receptor antagonists: The cache county study. Neurology. 2000; 54:2066-2071.

19. Behl C. Alzheimer's disease and oxidative stress: Implications for novel therapeutic approaches. Prog Neurobiol. 1999; 57:301-323.

20. Markesbery WR. Oxidative stress hypothesis in Alzheimer's disease. Free Radic Biol Med. 1997; 23:134-147.

21. Liaudet L, Soriano FG, Szabó C. Biology of nitric oxide signaling. Crit Care Med. 2000; 28:N37-N52.

22. Loizzo MR, Menichini F, Conforti F, Tundis R, Bonesi M, Saab AM, Statti GA, Cindio B, Houghton PJ. Chemical analysis, antioxidant, anti-inflammatory and anti-cholinesterase activities of *Origanum ehrenbergii* Boiss and *Origanum syriacum* L. essential oils. Food Chem. 2009; 117:174-180.

23. Oertel W, Ross JS, Eggert K, Adler G. Rationale for transdermal drug administration in Alzheimer disease. Neurology. 2007; 69:S4-S9.

24. Moulik SP, Paul BK. Structure, dynamics and transport properties of microemulsions. Adv Colloid Interface Sci. 1998; 78:99-195.

25. García SF, Eliosa JG, Salas PA, Hernández-Garduza O, Ápam- Martínez D. Modeling of microemulsion phase diagrams from excess Gibbs energy models. Chem Eng J. 2001; 84:257-274.

26. Dixit SG, Mahadeshwar AR, Haram SK. Some aspects of

the role of surfactants in the formation of nanoparticles. Colloids Surf A. 1998; 133:69-75.

27. Ellman GL, Courtney KD. A new and rapid colorimetric determination of acetylcholinesterase activity. Biochem Pharmacol. 1961; 7:88-90.

28. Pithayanukul P, Tubprasert J, Wuthi-Udomlert M. *In Vitro* antimicrobial activity of *Zingiber cassumunar* (Plai) oil and a 5% Plai oil gel. Phytother Res. 2007; 21:164-169.

29. Howes MJR, Houghton PJ. Plants used in Chinese and Indian traditional medicine for improvement of memory and cognitive function. Pharmacol Biochem Behav. 2003; 75:513-527.

30. Perry EK, Tomlinson BE, Blessed G, Bergmann K, Gibson PH, Perry RH. Correlation of cholinergic abnormalities with senile plaques and mental test scores in senile dementia. Br Med J. 1978; 2:1457-1459.

31. Greig NH, Utsuki T, Wang Y, Ingram DK, Mamczar J, Rogers J, Yun QS, Holloway HW, Perry TA, Sambamurti K. P1-414 Selective butyrylcholinesterase inhibition elevates brain acetylcholine, augments learning and lowers amyloid-β peptide in rodents: A new treatment strategy for Alzheimer's disease. Neurobiol Aging. 2004; 25:S216.

32. Kim K, Bu Y, Jeong S, Lim J, Kwon Y, Cha DS, Kim J, Jeon S, Eun J, Jeon H. Memory-enhancing effect of a supercritical carbon dioxide fluid extract of the needles of *Abies koreana* on scopolamine-induced amnesia in mice. Biosci Biotechnol Biochem. 2006; 70:1821-1826.

33. Miyazawa M, Watanabe H, Kameoka H. Inhibition of acetylcholinesterase activity by monoterpenoids with a *p*-menthane skeleton. J Agri Food Chem. 1997; 45:677-679.

34. Savelev S, Okello E, Perry NSL, Wilkins RM, Perry EK. Synergistic and antagonistic interactions of anticholinesterase terpenoids in Salvia lavandulaefolia essential oil. Pharmacol Biochem Behav. 2003; 75:661-668.

35. Lawrence MJ, Rees GD. Microemulsion-based media as novel drug delivery systems. Adv Drug Deliv Rev. 2000; 45:89-121.

36. Palazzo G, Lopez F, Giustini M, Colafemmina G, Ceglie A. Role of the Cosurfactant in the CTAB/Water/n-Pentanol/n-Hexane Water-in-Oil Microemulsion. 1. Pentanol Effect on the Microstructure. J Phys Chem B. 2003; 107:1924-1931.

37. Zhang X, Zhuang W, Cui X, He H, Huang X. Preparation of BaMgAl (10) O (17): Eu (2+) and its phase behavior in microemulsion system. J Rare Earths (Engl Ed). 2006; 24:736-739.

38. Liu L, Tian S, Ning P. Phase behavior of TXs/toluene/water microemulsion systems for solubilization absorption of toluene. J Environ Sci. 2010; 22:271-276.

39. Alany RG, Rades T, Agatonovic-Kustrin S, Davies NM, Tucker IG. Effects of alcohols and diols on the phase behaviour of quaternary systems. Int J Pharm. 2000; 196:141-145.

40. Carlfors J, Blute I, Schmidt V. Lidocaine in microemulsion dermal delivery system. J Disper Sci Technol. 1991; 12:467-482.

41. Salabat A, Alinoori M. Salt effect on aqueous two-phase system composed of nonylphenyl ethoxylate non-ionic surfactant. Calphad. 2008; 32:611-614.

Original Article

Subcutaneous concentrations following topical iontophoretic delivery of diclofenac

Purna C. Kasha[1], Carter R. Anderson[2], Russ L. Morris[2], Walter L. Sembrowich[2], Ayyappa Chaturvedula[1], Ajay K. Banga[1,*]

[1] *Department of Pharmaceutical Sciences, College of Pharmacy and Health Sciences, Mercer University, Atlanta, GA, USA;*
[2] *Travanti Pharma Inc., Mendota Heights, MN, USA.*

ABSTRACT: A self-contained Wearable Electronic Disposable Drug Delivery (WEDD®) patch was used to demonstrate that diclofenac levels delivered by iontophoresis are greater than estimated minimal effective concentrations in local subcutaneous tissue and are also greater than either passive transdermal or intravenous delivery using hairless rats. *In vitro* iontophoretic delivery was evaluated to optimize donor cell formulation using Franz diffusion cells and 1000 NMWL Millipore ultrafiltration membrane. *In vivo* animal studies were done using patches powered with a 4-volt system, consisting of a 1-volt Zn anode and Ag/AgCl cathode with built in 3-volt lithium battery. Blood and microdialysis samples were collected at different time points after patch application. Current levels increased to 1.0 mA at 30 min, then fell to a steady state of ~ 0.4 mA. Both WEDD® and passive patches produced measurable levels of diclofenac in the subcutaneous tissue below the application site (C_{max} ± SE = 113.3 ± 61.7 ng/mL and 36.3 ± 15.9 ng/mL, respectively). The dose delivered in six hours was calculated to be 0.226 ± 0.072 mg and 0.430 ± 0.048 mg in passive and iontophoretic delivery, respectively. Diclofenac was not detected in the subcutaneous tissue after intravenous administration of 1.5 mg/kg diclofenac solution. The trend indicates that WEDD® can be used to successfully deliver diclofenac to subcutaneous tissue to concentrations higher when compared to either passive delivery or intravenous dosing of 1.5 mg/kg.

Keywords: NSAID, self-contained patches, WEDD®, cutaneous drug delivery, microdialysis, cyclic voltammetry

Address correspondence to:
Dr. Ajay K. Banga, College of Pharmacy and Health Sciences, 3001 Mercer University Drive, Mercer University, Atlanta, GA 30341, USA.
E-mail: banga_ak@mercer.edu

1. Introduction

Diclofenac is a potent and effective non-steroidal anti-inflammatory drug (NSAID), and is commercially available in the market as tablets, injections, and topical formulations for the treatment of rheumatoid arthritis, osteoarthritis, and non articular rheumatic conditions such as myositis and periarthritis (*1*). It was also approved for use in local treatment of actinic keratosis, a relatively common pre malignant skin lesion seen on areas of skin exposed to sun (*2,3*). Diclofenac is widely prescribed as an oral medication, but due to its gastrointestinal side effects such as gastric ulcers and gastrointestinal bleeding, extensive first pass metabolism (~ 50%), and short biological half-life, an alternative delivery approach is desirable. One such approach, iontophoretic delivery, can potentially provide deeper tissue penetration without compromising target tissue concentrations (*4*). Diclofenac potassium (pKa 4.0) has partition coefficient (*5*) of 13.4 at pH 7.4. The presence of salt forms in topical formulation with increased solubility (1% w/v in water), and their ability to dissociate and to form ion pairs offer pathways across skin either through hydrophilic pores or passive diffusion across lipid matrix (*6*). One aim of the present study is to demonstrate at least two times greater concentrations than the estimated minimally effective tissue concentration (MEC) in the subcutaneous tissue below the electrode, for a period of at least two consecutive hours when compared to passive delivery.

Iontophoresis is a technique where ions are transferred into the body using an applied electric field (*7*). This technique offers an advantage of delivering larger quantities of a given drug when compared to passive delivery (*8*). In a previous study by Hui *et al.*, transdermal iontophoresis was found to facilitate the direct penetration of diclofenac sodium to deeper tissue, as measured by radiolabeling techniques in extracted tissue samples (*8*). However, this study employed reusable tabletop power sources connected by wire to electrodes, which are cumbersome to use and commercially unacceptable. Additionally, the study also used relatively

high delivery current levels of 2-4 mA, which many patients would find uncomfortable to wear in a home setting. In addition, measurements were indirect, using radiolabeled diclofenac.

Microdialysis is a sampling technique used to measure tissue concentrations of drugs in pharmacokinetic and metabolism studies. The simultaneous estimation of the pharmacokinetics in skin and plasma helps in understanding the kinetic relationship between absorption at the two sites (*9*) and gives an understanding of drug permeation before entering the systemic circulation. Dermal absorption due to iontophoresis was previously investigated using microdialysis for the evaluation of dermal kinetics of various drugs including anoxacin, diclofenac, and acyclovir (*10-12*). Subcutaneous microdialysis has been reported in various pharmacokinetic studies to measure drug kinetics in extra cellular fluid (ECF). Subcutaneous tissue is homogenous in nature and the ECF is in constant equilibrium with the systemic circulation. The subcutaneous microdialysis technique is also considered to be easier than dermal microdialyisis (*13*). With dermal microdialysis, probe insertion and control over insertion depth are difficult, and the probe itself can increase skin thickness (*14,15*).

The present study had several objectives. In a first *in vitro* portion of the study, formulation of the donor electrode-pad was investigated as a means to improve delivery efficiency with an objective of optimizing the total delivery at lower and more acceptable current level. The *in vitro* portion of the study also served to evaluate the effect of potential formulation additives (such as hydrogels and anti-microbial compounds) on the iontophoretic delivery efficiency. Yet another objective of our *in vitro* studies was to evaluate the electrochemical stability of diclofenac under conditions of applied voltage, using cyclic voltammetry. In a second *in vivo* portion of this study, custom-designed Wearable Electronic Drug Delivery (WEDD®) patches were used to deliver diclofenac. Subcutaneous microdialysis (MD) sampling and blood sampling were performed simultaneously to measure the effectiveness of delivery. The *in vivo* portion of this study also served to evaluate passive delivery and intravenous (IV) injection administered drug, to compare both localized and systemic levels measured to those obtained by iontophoresis.

2. Materials and Methods

2.1. *Animals*

Male CD-hairless rats (Charles River, Wilmington, MA, USA) weighing 290-350 g were used. The research adhered to the "Principles of Laboratory Animal Care" (NIH publication #85-23, revised in 1985). Food and water were provided ad libitum. The average number of replicates for each study was four.

2.2. *Chemicals*

Diclofenac potassium was purchased from Exim-Pharm International (Mumbai, India). Naproxen was purchased from Sigma Aldrich (St. Louis, MO, USA), Sterile and pyrogen-free 0.9% sodium chloride USP was purchased from Baxter Healthcare Corporation (Deerfield, IL, USA). Water, acetonitrile, glacial acetic acid, and sodium acetate were purchased from Fisher Scientific (Pittsburgh, PA, USA). All solvents used were of HPLC grade.

2.3. *Cyclic voltammetry system*

A BASi Epsilon (Bioanalytical Systems, Inc., West Layfayette, IN, USA) electrochemical analyzer using a platinum working electrode, silver-silver chloride reference electrode, and titanium-wire counter electrode was used for cyclic voltammetry. Figure legends (Figures 2 and 3) contain experimental sweep conditions.

2.4. *Microdialysis system*

CMA102 microdialysis pump with CMA142 micro fraction collector (CMA/Microdialysis AB, Stockholm, Sweden) was used. CMA 20 microdialysis probes (CMA/Microdialysis AB, Stockholm, Sweden) with 10 mm polycarbonate membrane, 20 kDa molecular weight cut off were used for subcutaneous insertion.

2.5. *In vitro iontophoretic delivery of diclofenac*

Side-by-side cells ($n = 4$) were used in this study with a 1 mL donor volume, a 3 mL receiver chamber, and a 0.64 cm^2 connection area. The donor cell was filled with a diclofenac solution of varying formulation, with an immersed silver chloride cathode. The receiver cell was filled with 0.9% saline, with an immersed silver anode. As a barrier to Passive flux, a 1000 NMWL Millipore ultrafiltration membrane was used to separate donor and receiver chambers. For power, a voltage/resistance circuit was connected in series to provide approximately 1 mA of current flow. Applied charge dosage was monitored as an integration of current over time. As a control, passive studies were conducted (to measure delivery without any applied current) and tested at the same time-points as corresponding active cells. Samples were extracted from the receiver chamber, then diluted and analyzed using UV spectrophotometer at 277 nm against a standard curve.

2.6. *In vivo iontophoretic delivery of diclofenac potassium*

2.6.1. *Iontophoretic patch – principle of operation*

WEDD® patches were custom-designed to fit the animal. Each was powered by a 4-volt system, consisting of a 1-volt Zn anode and Ag/AgCl cathode connected

in series to a 3-volt lithium button cell battery. The anode absorbent pad was loaded with 500 µL normal saline solution and the cathode pad was loaded with 500 µL of 20 mg/mL diclofenac potassium. Electric current was monitored during the delivery period to ensure proper electrical connections immediately after patch application. The electrochemistry involved at the electrode interfaces:

$$Zn \rightarrow Zn^{++} + 2e^- \text{ (Anode)};$$
$$AgCl + e^- \rightarrow Ag + Cl^- \text{ (Cathode)} \qquad (1)$$
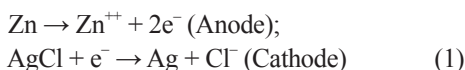
CD hairless rats weighing between 250-400 g were used in the study. Each was anesthetized by intraperitonial injection of ketamine (75 mg/kg) and xylazine (10 mg/kg). A CMA microdialysis probe (polycarbonate membrane, 10×0.5 mm, 20 kDa molecular weight cut-off) was inserted subcutaneously into the abdominal area of the rat using a guide cannula, and sutured into the skin (*16*). Drug containing reservoir of the patch was aligned exactly above the site where microdialysis probe was inserted. Microdialysis probe was perfused at a flow rate of 2 µL/min (CMA microdialysis pump) using sterile 0.9% NaCl as perfusion fluid. Samples were collected every 30 min for 6 h. For iontophoretic and passive patch testing, serum samples were collected at 0, 1, 2, 4, 6, 8, and 10 h. For IV testing, a microdialysis analysis was performed in the same abdominal region using the same time points and methodology as in the patch testing. Blood samples (300 µL) were also collected at different time intervals from the tail vein and serum was collected after clotting. Serum samples were stored at −20°C until analyzed by HPLC. At the end of each experiment, animals were sacrificed using a CO_2 chamber. The skin was cut and visually observed for the probe placement after sacrificing the animal. Passive (control) experiments were also done following the same protocol, but the patches used were without the electrodes or power.

2.6.2. *Microdialysis probe recovery*

Probe implantation is followed by 1 h recovery period prior to microdialysis probe calibration. During this time, probes were perfused with 0.9% w/v NaCl solution at 2 µL/min flow rate. Microdialysis probe recovery *in vivo* was determined by perfusing 500 ng/mL of diclofenac solution at 2 µL/min flow rate. The samples (dialysate) were collected simultaneously every 30 min. In parallel, collected dialysate was analyzed immediately for the drug content using HPLC until three steady values were obtained. Then the recovery factor (RF) was calculated by the following formula.

$$RF = (C_p - C_d)/C_p \qquad (2)$$

Where, C_p = concentration of perfusate; C_d = concentration of microdialysate.

2.6.3. *Intravenous administration of diclofenac potassium*

Animals were anesthetized as described before. Diclofenac solution was prepared using water for injection, which was injected (1.5 mg/kg dose) into the femoral vein of the animal and blood samples were collected from tail vein at different time intervals (0, 5, 10, 15, 30, 45, 60, 120, 240, 360, 480, and 600 min). Serum was collected after clotting and stored at −20°C until HPLC analysis.

2.6.4. *Analytical method*

A Waters® Alliance HPLC system with Empower® software and a Waters® 2475 fluorescence detector was used. Several methods have been reported to analyze diclofenac levels in the biological fluids (*17-25*). The operating parameters were adopted from literature and the simplified HPLC assay was validated for intra-day and inter-day variations. All *in vivo* samples were analyzed using C18, Varian microsorb-MV (250×4.6 mm, 5 µm) column with fluorescence detection at 282 nm and 365 nm as excitation and emission wavelengths, respectively. The elution was performed using mobile phase, sodium acetate (0.075 M; pH 5) and acetonitrile (55:45). Serum samples were extracted by adding 50 µL of standards to 100 µL of serum and boiled on a water bath for 10 min at 85°C followed by adding 200 µL of methanol. This was mixed by pipetting up and down. After cooling for two minutes, 50 µL of 560 ng/mL of internal standard, naproxen, was added and vortexed for few seconds. Supernatant was obtained after centrifugation at 3,500 rpm for three minutes and injected into HPLC for analysis.

2.7. *Cyclic voltammetry*

Cyclic voltammetry is a unique technique for the electrochemical study of the redox systems (*26*). The stability of diclofenac in an applied electric field was tested using cyclic voltammetry (Pt disk electrode/Ag-AgCl reference/Ti counter electrode). With this method, the voltage of an electrode immersed in a test solution is increased linearly and then decreased to its starting point, while current flow is monitored for the evidence of oxidation or reduction reactions.

2.8. *Pharmacokinetic data analysis*

Serum concentration *versus* time profiles from IV injection and iontophoretic delivery of diclofenac potassium were analyzed using non-compartmental analysis (NCA) by WinNonlin (5.0.1). Pharmacokinetic parameters such as AUC_{0-inf}, terminal elimination rate constant (λz), clearance/F, and C_{max} were calculated. Clearance obtained from IV data

was used to calculate the dose delivered during iontophoresis by the following equation, with the assumption that iontophoretic delivery provides a zero order infusion:

$$\text{F*Dose delivered} = \text{AUC}_{\text{Iontophoretic}} \times \text{Clearance}_{\text{IV}} \quad (3)$$

Rate of infusion (R_0) at steady state was calculated by the following equation:

$$R_0 = \text{F*Dose delivered/Duration of patch application} \quad (4)$$

Where, 'F' represents the fraction of dose absorbed into systemic circulation. F*Dose delivered was calculated as a single function from Equation 3.

2.9. Statistical analysis

The data is presented as mean ± SE. Pharmacokinetic parameters were calculated for individual rat, and then mean was calculated. Student's paired *t*-test with two tailed distribution was performed for comparisons at *p* = 0.05 set a priori as significant.

3. Results and Discussion

3.1. In vitro iontophoretic delivery of diclofenac

In the first portion of our *in vitro* testing, diclofenac concentration was varied in the donor cell and measured the efficiency at which diclofenac was delivered by iontophoresis. It was hypothesized that as donor concentration is increased, improved delivery efficiency would be seen owing to a more favorable ratio of drug ions relative to competing ions present (Table 1). It was concluded that there is a substantial benefit in using the potassium salt of diclofenac, with efficiency nearly two-fold higher than that found using a comparable concentration of the sodium salt (Table 1). Therefore, by employing the potassium salt form, the total dosage of the Hui *et al.* study (*8*) was possible using much less current. In the second part of the *in vitro* study, the effect of excipients added to a formulation containing 20 mg/mL diclofenac potassium was investigated. The total diclofenac delivered, following a 3 mA·hr (180 mA·min) applied

Table 1. Delivery efficiency of donor cell formulation

Donor cell formulation*	Delivery efficiency ± SD**
4 mg/mL (12.6 mM); sodium	7.1 ± 1.5
8 mg/mL (25.1 mM); sodium	10.3 ± 0.7
18 mg/mL (56.6 mM); sodium	9.2 ± 1.6
20 mg/mL (59.8 mM); potassium	17.6 ± 1.8
30 mg/mL (89.8 mM); potassium	17.5 ± 1.9
40 mg/mL (125.7 mM); sodium	9.5 ± 2.1

* Total diclofenac concentration and salt form. ** μg per mA·min applied charge, to a charge dosage between 150 and 180 mA·min.

charge dosage, was measured with different donor cell formulations (Table 2). In general, we did not find significant variation in efficiency as a function of the additives tested (Figure 1). We hypothesize that the lower efficiency noted with the PVA formulation may be due to ionic impurities.

The stability of diclofenac in an applied electric field was assessed using cyclic voltammetry (Figures 2 and 3). With this method, the voltage of an electrode immersed in a test solution is increased linearly and then decreased to its starting point, while current flow is monitored for evidence of oxidation or reduction reactions. Similarities between scans in blank buffer and diclofenac solutions indicate electroactive stability of the drug (Figures 2 and 3).

3.2. In vivo iontophoretic delivery of diclofenac potassium

The linear range of the HPLC assay for serum extractions was obtained between 10-1,000 ng/mL with extraction efficiency of greater than 90%. The mean recovery factor from microdialysis probe calibration was calculated to be 0.75. Recovery factor was later used to calculate actual concentrations surrounding the microdialysis probe.

Table 2. List of donor cell formulations

| Formulation	Content
Control	1 mL of 20 mg/mL diclofenac potassium in distilled water
A	+ 2% HPMC
B	+ 10% polyvinylalcohol
C	+ 0.2 mg/mL benzalkonium chloride
D	+ 1% butyl alcohol
E	+ 1.5 mg/mL methylparaben, 0.2 mg/mL butylparaben at pH 7.45
F	+ 1.5 mg/mL methylparaben, 0.2 mg/mL butylparaben at pH 7.68
G	+ 1.5 mg/mL methylparaben, 0.2 mg/mL butylparaben at pH 8.06
H	Control formulation delivered from flex printed electrode
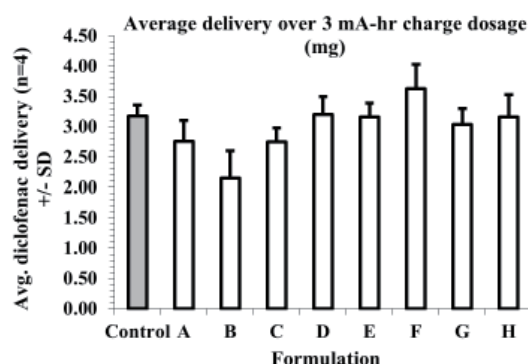
Figure 1. Effect of excipients added to 20 mg/mL diclofenac potassium donor cell formulation (*n* = 4).
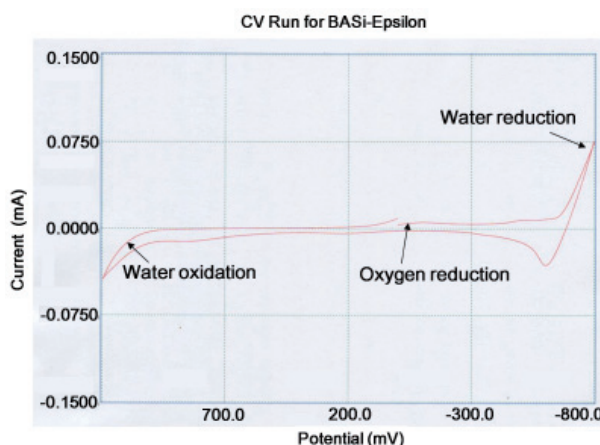
Figure 2. Cyclic voltammogram of 0.1 M TES buffer solution, pH 7.4; number of data points: 4000, current full scale: 1 mA, switching potential 1: −800 mV, switching potential 2: 1,200 mV, initial and final potential: 0 mV, scan rate: 100 mV/sec, filter: 10 Hz, sample interval: 1 mV, number of segments: 3, quiet time: 2 sec.
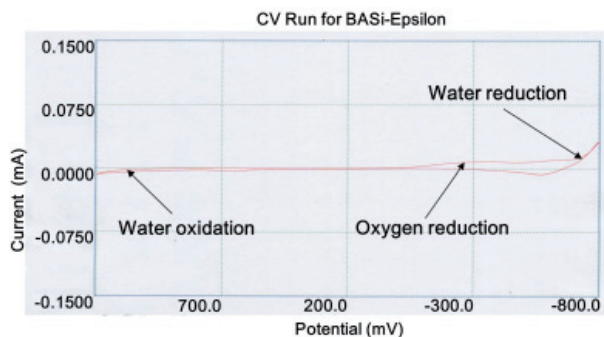
Figure 3. Cyclic voltammogram of 0.1 M TES buffer (pH 7.4) with 5 mg/mL diclofenac potassium; number of data points: 4000, current full scale: 1 mA, switching potential 1: −800 mV, switching potential 2: 1,200 mV, initial and final potential: 0 mV, scan rate: 100 mV/sec, filter: 10 Hz, sample interval: 1 mV, number of segments: 3, quiet time: 2 sec.

Figure 4. Average iontophoretic current during six hours of WEDD® patch application (*n* = 4).
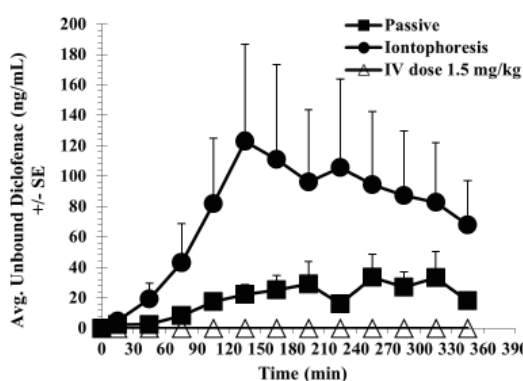
Figure 5. Average microdialysate levels in the subcutaneous tissue (*n* = 4).

The current measurements for the Active WEDD® patches are shown in Figure 4. Current levels peaked at approximately 1.0 mA at 30 min, and then fell to a steady state of approximately 0.4 mA. Both passive and WEDD® patches produced measurable levels of diclofenac in the subcutaneous region below the application site (Figure 5). In comparing WEDD® active delivery with passive, the trend indicates that active delivery produces tissue concentrations more than two-fold higher, and faster, than passive delivery (Figure 5). However, minimal levels in the subcutaneous tissue may be surprising when compared to similar studies that we have conducted with Granisetron (*16*) and another study with diclofenac (*8*). The anticipated subcutaneous concentrations of diclofenac were about 5,000-10,000 ng/mL. The difference seen is most likely a function of the drug and microdialysis measurement technique used in this study (Figure 5). Diclofenac is known to bind with proteins; as binding is approximately 99.7 % in plasma, and approximately 99.5 % in synovial fluid (*27*). The protein-bound forms of diclofenac will not diffuse through the dialysis membrane of the microdialysis probe. Since significant protein levels are found in the interstitial fluid of rats (*28*) and humans (*29*), binding effects should be anticipated. Therefore, microdialysis measurements of diclofenac penetration should be interpreted on the assumption that it is an unbound fraction of a much higher total concentration delivered.

It was noticed that an increase in the number of HPLC peaks over time at elution times slightly different from the diclofenac peak. These peaks were found in active, passive and *in vivo* calibration data sets; and therefore, it is not indicative of diclofenac degradation from an electric field. However, these peaks may be related to diclofenac that can be attributed to percentage of protein bound diclofenac, capable of entering the microdialysis probe. The stability of diclofenac in an applied electric field was further confirmed by investigation using cyclic voltammetry (Figures 2 and 3).

A high degree of variability is also noted; with approximately 100% coefficient of variation seen in both WEDD® and passive data sets. This is apparently not unusual, since variability as high as 146-215% has been noted in numerous other studies with transdermal delivery of diclofenac (*1*). Some have speculated that high variability may be due to biologic confounders such as skin thickness, local blood flow, lipid content, and the presence of hair follicles (*1*).

Table 3. Pharmacokinetic parameters after IV bolus administration (*n* = 3)

Parameter	Units	Estimate ± SE
Elim. rate const. (λz)	min^{-1}	0.01 ± 0.002
Half life	min	74.2 ± 14.9
Clearance	mL/min	0.87 ± 0.09
Vol. of dist. (Vz)	mL	97.5 ± 28.7
$AUC_{0-\alpha}$	min·µg/mL	573.4 ± 30.7

Table 4. Pharmacokinetic parameters of diclofenac

Parameter	Units	Estimate ± SE Passive	Iontophoresis
C_{max}	µg/mL	1.143 ± 0.354	1.974 ± 0.166
AUC_{0-6}	h·µg/mL	4.326 ± 1.372	8.187 ± 0.927
F*Dose delivered (6 h)	mg	0.226 ± 0.072	0.430 ± 0.048

The pharmacokinetic parameter, clearance, from IV bolus study was used to calculate F*Dose delivered as a single function from equation 3 (Table 3). Both passive and active WEDD® patches produced measurable levels of diclofenac in the serum (Table 4). In comparing WEDD® active delivery with passive, a trend very similar to our microdialysis results indicates that active delivery shows serum concentrations two-fold higher, and faster than passive delivery (Figure 6 and Table 4). Given the discussion above, it is important to recognize that the serum results are for total diclofenac. The higher concentrations seen in serum, when compared to the unbound microdialysis concentrations in the subcutaneous space, are consistent with the hypothesis of protein binding effects associated with the microdialysis measurement technique.

In a first animal administered with a 1.5 mg/kg IV dosage, a microdialysis probe was inserted into the same subcutaneous space as in the passive and active patch testing. This was performed to measure an amount reached subcutaneously *via* IV compared to the amounts reached *via* transdermal patches. The MD results after IV dosing for the animal were below the detection limits at all time points (Figure 5). The substantially higher subcutaneous levels found in the iontophoresis and passive testing supports the potential advantage of localized delivery to tissue when compared to systemic dosing.

The minimal effective concentration (MEC) of unbound diclofenac was estimated to be in the range of 0.5 to 2.5 ng/mL based on the following assumptions: estimated MEC of total diclofenac in synovial fluid is 100-500 ng/mL (*27*). Protein binding of diclofenac was measured to be 99.5% in synovial fluid (*27*). Therefore, 0.5% unbound fraction of total diclofenac (100-500 ng/mL) is 0.5-2.5 ng/mL. Thus, unbound concentration from subcutaneous microdialysis was multiplied by a factor, 200, to compare with our serum result. This factor is supported as our estimated total subcutaneous
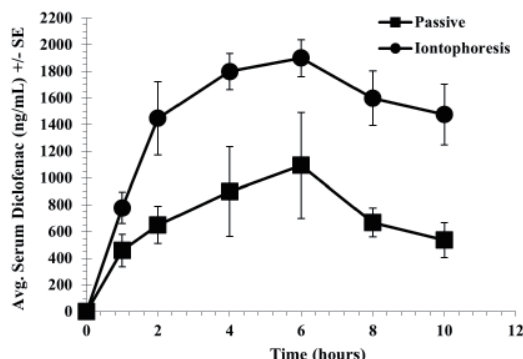
Figure 6. Average serum diclofenac levels after passive and iontophoretic delivery (*n* = 4).

concentration of 18,840 ng/mL is comparable to a previous study with direct measurement of ~11,000 ng/mL subcutaneous diclofenac after iontophoresis (*8*).

In spite of their potential use as anti-inflammatory agents, NSAIDs exhibit undesirable side effects when administered by oral route. Topical application provides an attractive choice to target deeper tissue beneath the skin for various clinical conditions that calls for NSAIDS. However, conventional formulations are not able to target deeper tissue while minimizing the systemic exposure. Passive delivery of diclofenac to the deeper tissue was shown to be highly variable (*1,8*). There have been contradictory findings reported in the literature related to direct deeper tissue penetration of diclofenac (*8*). In our study, subcutaneous levels by iontophoresis have also shown variability possibly due to the variability associated with microdialysis probe recovery of higher tissue concentrations (iontophoresis) compared to lower tissue concentrations (passive). In contrast, pharmacokinetic parameters of serum samples from passive delivery shown to be highly variable when compared to WEDD® application in hairless rats (Table 4). This can be attributed partly to different diclofenac transport pathways in the skin during iontophoresis and passive delivery.

4. Conclusion

The results of this study suggest that a user-friendly, disposable WEDD® patch may be used to deliver diclofenac in amounts and rates that can exceed passive delivery. Further, evidence is presented that suggests the delivered amounts may be efficacious on a localized basis at a subcutaneous tissue depth. Microdialysis has been confirmed to be a useful measurement for localized concentrations, although with limitations hypothesized to be associated with protein binding.

Conflict of interest

There is no conflict of interest but Dr. Banga has served as a consultant to Travanti in the past.

References

1. Dehghanyar P, Mayer BX, Namiranian K, Mascher H, Muller M, Brunner M. Topical skin penetration of diclofenac after single- and multiple-dose application. Int J Clin Pharmacol Ther. 2004; 42:353-359.
2. Peters DCFoster RH. Diclofenac/hyaluronic acid. Drugs Aging. 1999; 14:313-319.
3. Merk HF. Topical diclofenac in the treatment of actinic keratoses. Int J Dermatol. 2007; 46:12-18.
4. Boinpally RR, Zhou SL, Poondru S, Devraj G, Jasti BR. Lecithin vesicles for topical delivery of diclofenac. Eur J Pharm Biopharm. 2003; 56:389-392.
5. Raz I, Hussein Z, Samara E, Ben David J. Comparative pharmacokinetic analysis of a novel sustained-release dosage form of diclofenac sodium in healthy subjects. Int J Clin Pharmacol Ther Toxicol. 1988; 26:246-248.
6. Fini A, Fazio G, Gonzalez-Rodriguez M, Cavallari C, Passerini N, Rodriguez L. Formation of ion-pairs in aqueous solutions of diclofenac salts. Int J Pharm. 1999; 187:163-173.
7. Ajay K.Banga. Therapeutic Peptides and Proteins: Formulation, Processing and Delivery Systems. CRC Press/Taylor & Francis, Boca Raton, FL, USA, 2006.
8. Hui X, Anigbogu A, Singh P, Xiong G, Poblete N, Liu P, Maibach HI. Pharmacokinetic and local tissue disposition of [14C]sodium diclofenac following iontophoresis and systemic administration in rabbits. J Pharm Sci. 2001; 90:1269-1276.
9. Stagni GShukla C. Pharmacokinetics of methotrexate in rabbit skin and plasma after iv-bolus and iontophoretic administrations. J Control Release. 2003; 93:283-292.
10. Stagni G, Ali ME, Weng D. Pharmacokinetics of acyclovir in rabbit skin after i.v.-bolus, ointment, and iontophoretic administrations. Int J Pharm. 2004; 274:201-211.
11. Fang JY, Sung KC, Lin HH, Fang CL. Transdermal iontophoretic delivery of diclofenac sodium from various polymer formulations: *In vitro* and *in vivo* studies. Int J Pharm. 1999; 178:83-92.
12. Fang JY, Hsu LR, Huang YB, Tsai YH. Evaluation of transdermal iontophoresis of enoxacin from polymer formulations: *In vitro* skin permeation and *in vivo* microdialysis using Wistar rat as an animal model. Int J Pharm. 1999; 180:137-149.
13. Graumlich JF, McLaughlin RG, Birkhahn D, Shah N, Burk A, Jobe PC, Dailey JW. Subcutaneous microdialysis in rats correlates with carbamazepine concentrations in plasma and brain. Epilepsy Res. 2000; 40:25-32.
14. Groth L, Jorgensen A, Serup J. Cutaneous microdialysis in the rat: Insertion trauma studied by ultrasound imaging. Acta Derm Venereol. 1998; 78:10-14.
15. Groth LSerup J. Cutaneous microdialysis in man: Effects of needle insertion trauma and anaesthesia on skin perfusion, erythema and skin thickness. Acta Derm Venereol. 1998; 78:5-9.
16. Chaturvedula A, Joshi DP, Anderson C, Morris R, Sembrowich WL, Banga AK. Dermal, subdermal, and systemic concentrations of granisetron by iontophoretic delivery. Pharm Res. 2005; 22:1313-1319.
17. Avgerinos A, Karidas T, Malamataris S. Extractionless high-performance liquid chromatographic method for the determination of diclofenac in human plasma and urine. J Chromatogr. 1993; 619:324-329.
18. Blagbrough IS, Daykin MM, Doherty M, Pattrick M, Shaw PN. High-performance liquid chromatographic determination of naproxen, ibuprofen and diclofenac in plasma and synovial fluid in man. J Chromatogr. 1992; 578:251-257.
19. Godbillon J, Gauron S, Metayer JP. High-performance liquid chromatographic determination of diclofenac and its monohydroxylated metabolites in biological fluids. J Chromatogr. 1985; 338:151-159.
20. Lee HS, Kim EJ, Zee OP, Lee YJ. High performance liquid chromatographic determination of diclofenac sodium in plasma using column-switching technique for sample clean-up. Arch Pharm (Weinheim). 1989; 322:801-806.
21. Millership JS, Hare LG, Farry M, Collier PS, McElnay JC, Shields MD, Carson DJ. The use of hydrophilic lipophilic balanced (HLB) copolymer SPE cartridges for the extraction of diclofenac from small volume paediatric plasma samples. J Pharm Biomed Anal. 2001; 25:871-879.
22. Moncrieff J. Extractionless determination of diclofenac sodium in serum using reversed-phase high-performance liquid chromatography with fluorimetric detection. J Chromatogr. 1992; 577:185-189.
23. Rbeida O, Christiaens B, Hubert P, Lubda D, Boos KS, Crommen J, Chiap P. Evaluation of a novel anion-exchange restricted-access sorbent for on-line sample clean-up prior to the determination of acidic compounds in plasma by liquid chromatography. J Chromatogr A. 2004; 1030:95-102.
24. Riegel MEllis PP. High-performance liquid chromatographic assay for antiinflammatory agents diclofenac and flurbiprofen in ocular fluids. J Chromatogr B Biomed Appl. 1994; 654:140-145.
25. Roskar RKmetec V. Liquid chromatographic determination of diclofenac in human synovial fluid. J Chromatogr B Analyt Technol Biomed Life Sci. 2003; 788:57-64.
26. Huang T, Gao P, Hageman MJ. Rapid screening of antioxidants in pharmaceutical formulation development using cyclic voltammetry--potential and limitations. Curr Drug Discov Technol. 2004; 1:173-179.
27. Radermacher J, Jentsch D, Scholl MA, Lustinetz T, Frolich JC. Diclofenac concentrations in synovial fluid and plasma after cutaneous application in inflammatory and degenerative joint disease. Br J Clin Pharmacol. 1991; 31:537-541.
28. Wiig H, Reed RK, Tenstad O. Interstitial fluid pressure, composition of interstitium, and interstitial exclusion of albumin in hypothyroid rats. Am J Physiol Heart Circ Physiol. 2000; 278:H1627-H1639.
29. Fogh-Andersen N, Altura BM, Altura BT, Siggaard-Andersen O. Composition of interstitial fluid. Clin Chem. 1995; 41:1522-1525.

Selection of generic preparations of famotidine orally disintegrating tablets for use in unit-dose packages

Noriko Yamazaki[1], Rie Iizuka[1], Shinsuke Miyazawa[1], Yuko Wada[2], Ken-ichi Shimokawa[2], Fumiyoshi Ishii[2,*]

[1] *Department of Health Care and Sciences, Meiji Pharmaceutical University, Tokyo, Japan;*
[2] *Department of Pharmaceutical Sciences, Meiji Pharmaceutical University, Tokyo, Japan.*

ABSTRACT: Changes in the hardness, dissolution, and the disintegration time of brand name and generic preparations (6 preparations) of famotidine orally disintegrating tablets were investigated. Tablets had been stored in a thermo-hygrostat-controlled environment set to simulate the home conditions of patients up to 8 weeks after unit-dose packaging. Among the tablets in unit-dose packaging prepared immediately after blister packs (BP) were opened, one generic had decreased hardness to less than 2.0 kg after 1 week, 55.1% of its initial hardness value, and a shorter disintegration time of about 1/5 of its initial disintegration time. Generics met the standard for dissolution 8 weeks after unit-dose packaging. The decrease in hardness after unit-dose packaging is presumed to be associated with additives, and particularly the types and amounts of binding agents, but evidence of this association was lacking. The hardness noted in drug interview forms (IFs) and the state of sales of bulk tablet packages must be determined to facilitate the selection of generics that remain hard even after unit-dose packaging.

Keywords: Unit-dose packaging, generics, tablet hardness, famotidine orally disintegrating tablet

1. Introduction

The "2008 Patient Survey" by the Ministry of Health, Labor, and Welfare listed "estimated numbers of patients receiving medical treatment for major diseases"; of these, about 520,000 persons were found to be receiving medical treatment for gastric or duodenal ulcers (*1*). Drug treatment for these conditions mainly involves histamine H_2 receptor antagonists (H_2RAs), which

inhibit gastric acid secretion, and proton pump inhibitors (PPIs) (*2*). Orally disintegrating tablets of these drugs are also widely used by elderly patients and patients with difficulty swallowing.

A neighboring medical institution consulted the current authors about orally disintegrating tablets of famotidine as an H_2RA to determine if generics were as susceptible to disintegration after unit-dose packaging as their brand name counterparts. Otori *et al*. studied brand name and 4 generic preparations of famotidine orally disintegrating tablets subjected to Accelerated Testing as described in the Stability Testing Guidelines, and they reported differences in stability and sensory evaluations over the long term (*3*).

Harada *et al*. evaluated disintegration properties using a newly proposed disintegration test featuring a rotating shaft and rotation speed, and they reported that this test helped to estimate the actual disintegration time in humans (*4*). Tokuyama *et al*. measured dissolution of brand name and generic preparations and compared their degree of bitterness; they reported that there were large variances in the intensity of bitterness; they found that some generics were significantly more bitter than their brand name counterparts (*5*). As mentioned earlier, many studies of famotidine orally disintegrating tablets have been conducted. However, no studies compared changes in the hardness, dissolution, and disintegration time of brand name and generic tablets after unit-dose packaging. Therefore, the current study compared the hardness, dissolution, and disintegration time up to 8 weeks after unit-dose packaging of brand name and generic preparations. This study also evaluated the criteria for famotidine orally disintegrating tablets for use in unit-dose packaging.

2. Materials and Methods

2.1. *Materials*

A brand name preparation (Gaster® D tablet 10 mg: Astellas Pharma Inc.) and 6 generic preparations (A-F) of famotidine orally disintegrating tablets were used. Of the 10 generics that were commercially available at the

*Address correspondence to:
Dr. Fumiyoshi Ishii, Department of Pharmaceutical Sciences, Meiji Pharmaceutical University, 2-522-1, Noshio, Kiyose, Tokyo 204-8588, Japan.
E-mail: fishii@my-pharm.ac.jp

start of this study (September 2011), 6 were selected because they came in smaller packages, facilitating purchase by medical institutions, and because they had different combinations of binding agents as additives (*6-8*). Differences in the additives in brand name tablets and the 6 generics are shown in Table 1. The paper used for unit-dose packaging was E Ueda Cello-Poly (polyethylene laminated cellophane; thickness, 0.04 mm; transparent packaging paper: MEG Co.).

2.2. *Measurement of hardness*

The hardness of famotidine orally integrating tablets was measured immediately after blister packs (BPs) were opened. The tablet hardness in unopened BPs was also measured 2, 4, and 8 weeks after storage in BPs in a thermo-hygrostat (Emviros: Tokyo, at a temperature of 27°C (± 0.5°C) with a humidity of 55% (± 3%)). Unit-dose packaging took place immediately after BPs were opened, and tablets were stored in a thermo-hygrostat at the same temperature with the same humidity, and hardness was measured after 1, 2, 4, and 8 weeks of storage. The hardness of 10 tablets of each preparation was measured under the same conditions at each measurement point using a Monsanto hardness tester (Tablet Hardness Meter Type A, 15 kg: Fuji Rikakogyo Co., Ltd.), and the mean was determined. The temperature (27°C) and humidity (55%) used for the thermo-hygrostat in this study were determined based on measurements from the homes of 10 teachers and students of the University. The temperature and humidity of places where drugs were stored in the home were measured 3 times a day over 3 days from September 1 to 10, 2008. The mean temperature and humidity were used, as shown in Table 2.

Table 1. List of additives in famotidine orally disintegrating tablets

Additive	Original brand product	Generic products A	B	C	D	E	F
Cornstarch	binder			○	○		
Crystalline cellulose	binder		○	○			
Dextrin	binder				○		
Ethyl acrylate, methyl methacrylate polymer	binder	○					
Ethylcellulose	binder	○		○			○
Hydroxypropyl cellulose	binder						○
Hydroxypropyl starch	binder		○				
Hydroxyproryl methylcellulose 2910	binder	○					
D-Mannitol	binder	○	○	○		○	○
Methylcellulose	binder	○					
Povidone	binder		○				
Aspartame	○	○	○	○	○	○	○
Anhydrous silicic acid					○		
Calcium silicate						○	
Calium stearate	○						
Cetyl alcohol	○			○			○
Cyclodextrin	○						
β-Cyclodextrin		○					
Ethyl vanillin							○
Fragrance	○	○		○	○	○	○
Glucono-σ-lactone		○					
Gum arabic					○		
Lactose hydrate			○		○		
Light anhydrous silicic acid				○			
Magnesium stearate		○	○	○	○	○	
Magnesium aluminometasilicate		○					
Maltitol starch syrup							○
L-Menthol		○	○	○	○	○	
Polyoxyethylene nonylphenyl ether		○					
X-Povidone		○	○	○		○	
Powder candy	○						
Sodium lauryl sulfate	○			○			○
Sodium stearyl fumarate							○
Starch syrup		○					
Synthesis aluminum silicate			○				
Talc		○			○		○
Triacetin	○			○			○
Vanillin							○
Be non-sealed tablet	○	○		○	○	○	○
Be hardness in IF		○	○		○	○	○

Data are shown as the combination of binding agents as additives in brand name tablets and 6 generic (A-F) tablets.

Table 2. The mean temperature and humidity of the place where drugs were stored in the homes of 10 volunteers

Cooperator	A	B	C	D	E	F	G	H	I	J	Mean
Temperature max. (°C)	28	27	28	27	28	28	29	28	29	29	
Temperature min. (°C)	24	24	24	25	24	24	26	26	26	26	
Temperature mean (°C)	26	26	26	26	26	26	28	27	28	28	26.5
Humidity max. (%)	68	65	76	62	64	75	61	60	60	55	
Humidity min. (%)	42	44	49	48	41	57	47	44	45	45	
Humidity mean (%)	55	55	63	55	53	66	54	52	53	50	55.4

2.3. *Measurement of the dissolution rate*

The dissolution rate of famotidine orally disintegrating tablets was measured immediately after BPs were opened and 1, 2, 4, and 8 weeks after storage in unit-dose packages in a thermo-hygrostat at the same temperature and humidity as noted earlier. Dissolution was measured according to Japanese Pharmaceutical Codex, Part III using the second method of the dissolution test (the paddle method) with a medium volume of 900 mL, temperature of 37 ± 0.5°C, and paddle rotation rate of 50 rpm. The medium was 0.05 mol/L acetic acid/sodium acetate buffer, measurement was performed at each measurement time using 5 tablets, and the mean value was used. Samples (5 mL) were collected 1, 2, 5, 10, 20, and 40 min after measurement started and analyzed using an ultraviolet and visible spectrophotometer (JASCO V-650 Spectrophotometer: JASCO Co., Tokyo, Japan) at a wavelength of 266 nm.

2.4. *Measurement of disintegration time*

Famotidine orally disintegrating tablets were stored under the same conditions as in the hardness and dissolution rate experiments, and the disintegration time was measured after 1, 2, 4, and 8 weeks. In accordance with the Disintegration Test of the Japanese Pharmacopoeia used to measure the disintegration time of brand name drugs, water was used as a medium, and a disintegration tester (NT-1HM Toyama Disintegration Tester: Toyama Sangyo Co., Ltd. Osaka, Japan) was operated at 37 ± 2°C. Measurement was performed at each measurement time using 6 tablets, and the mean was determined.

3. Results

3.1. *Hardness*

All generics except generic B were harder than the brand name tablets immediately after BPs were opened. The hardness of brand name and generic tablets stored in unopened BPs in a thermo-hygrostat at a temperature of 27°C ± 0.5°C with a humidity of 55% ± 3% for 8 weeks is shown in Figure 1, and the hardness of tablets stored in unit-dose packages prepared immediately after BPs were opened in a thermo-hygrostat at the same temperature with the same humidity for 8 weeks is shown in Figure 2. Figure 1 indicates that the hardness

of brand name tablets decreased by 13.4%. Similarly, the hardness of other preparations decreased less than 20%. As shown in Figure 2, the hardness of brand name tablets decreased by 5.4% while that of generic B decreased by 55.1% (hardness < 2 kg) after 1 week. After 2, 4, and 8 weeks, generic B was softer than brand name tablets, and some tablets of generic B had disintegrated during measurement.

3.2. *Dissolution rate*

The dissolution rate for brand name and generic tablets 1, 2, 5, 10, 20, and 40 min after measurement started is shown in Figure 3. Figure 3 indicates that the dissolution rate of all tablets reached nearly 100% 10 min after measurement started. The dissolution rate was evaluated within 10 min after measurement started. The dissolution rate for brand name and generic tablets after storage for 2, 4, and 8 weeks following unit-dose packaging is shown in Figures 4-6, respectively. These figures indicate that generic E had the slowest dissolution. Generics B and C had faster dissolution than other tablets.

3.3. *Disintegration time*

The disintegration time of tablets stored in unopened BPs and in unit-dose packages throughout the 8-week storage period compared to when measurement started is shown in Figures 7 and 8, respectively. These figures indicate that the disintegration time of most tablets stored in unit-dose packages began to decrease after one week. Disintegration time decreased to about 1/5 after one week for generic B in particular in comparison to when BPs were opened.

4. Discussion

As noted earlier, this study was initiated because a neighboring medical institution consulted the current authors regarding "the susceptibility to disintegration of generic preparations of famotidine orally disintegrating tablets after unit-dose packaging in comparison to brand name preparations". The hardness of brand name tablets and 6 generic preparations (A-F) was measured immediately after unit-dose packaging and also 8 weeks later. One week after the storage of tablets at a temperature of 27°C ± 0.5°C with a humidity of 55% ± 3% following unit-dose packaging,
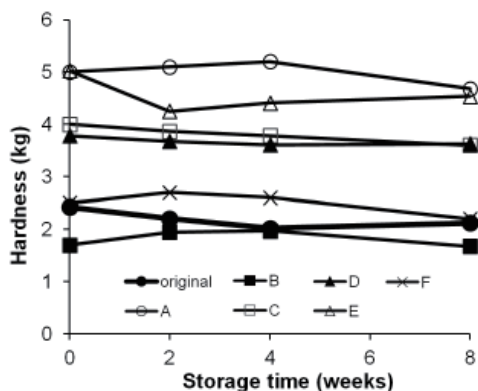
Figure 1. Hardness of famotidine orally disintegrating tablets stored in BPs. Data are shown as the mean for 10 tablets measured at each measurement point using a Monsanto hardness tester. Brand name, ●; generic A, ○; generic B, ■; generic C, □; generic D, ▲; generic E, △; generic F, ×.
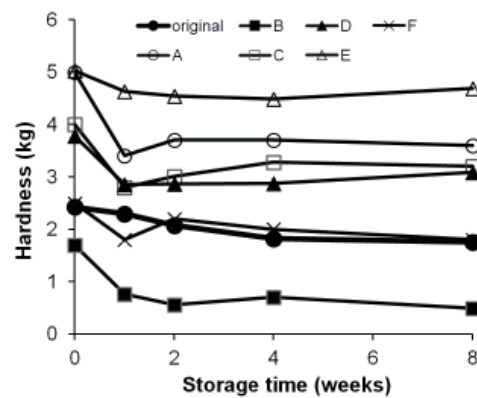
Figure 2. Hardness of famotidine orally disintegrating tablets stored in unit-dose packages. Data are shown as the mean for 10 tablets measured at each measurement point using a Monsanto hardness tester. Brand name, ●; generic A, ○; generic B, ■; generic C, □; generic D, ▲; generic E, △; generic F, ×.
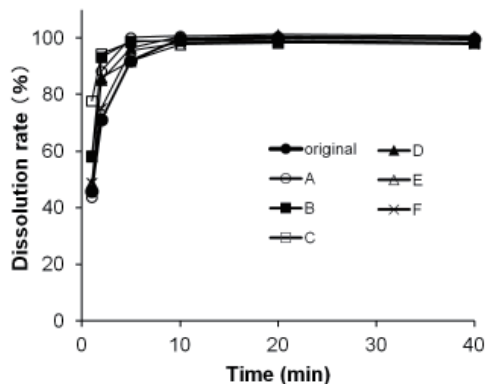
Figure 3. Dissolution rate of famotidine orally disintegrating tablets immediately after BPs were opened (0-40 min). Data are shown as the mean for 5 tablets measured at each measurement point using an ultraviolet and visible spectrophotometer. Brand name, ●; generic A, ○; generic B, ■; generic C, □; generic D, ▲; generic E, △; generic F, ×.
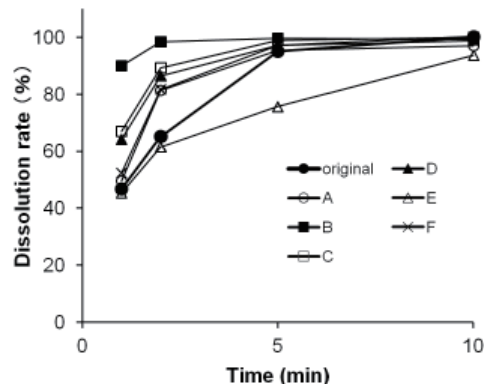
Figure 4. Dissolution rate of famotidine orally disintegrating tablets after storage for 2 weeks following unit-dose packaging (0-10 min). Data are shown as the mean for 5 tablets measured at each measurement point using an ultraviolet and visible spectrophotometer. Brand name, ●; generic A, ○; generic B, ■; generic C, □; generic D, ▲; generic E, △; generic F, ×.
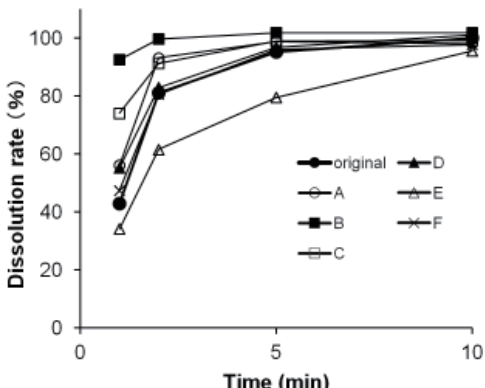
Figure 5. Dissolution rate of famotidine orally disintegrating tablets after storage for 4 weeks following unit-dose packaging (0 - 10 min). Data are shown as the mean for 5 tablets measured at each measurement point using an ultraviolet and visible spectrophotometer. Brand name, ●; generic A, ○; generic B, ■; generic C, □; generic D, ▲; generic E, △; generic F, ×.
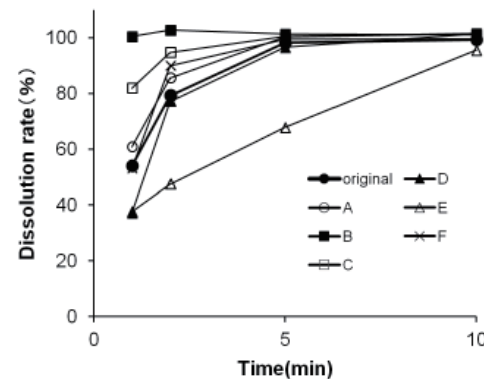
Figure 6. Dissolution rate of famotidine orally disintegrating tablets after storage for 8 weeks following unit-dose packaging (0-10 min). Data are shown as the mean for 5 tablets measured at each measurement point using an ultraviolet and visible spectrophotometer. Brand name, ●; generic A, ○; generic B, ■; generic C, □; generic D, ▲; generic E, △; generic F, ×.
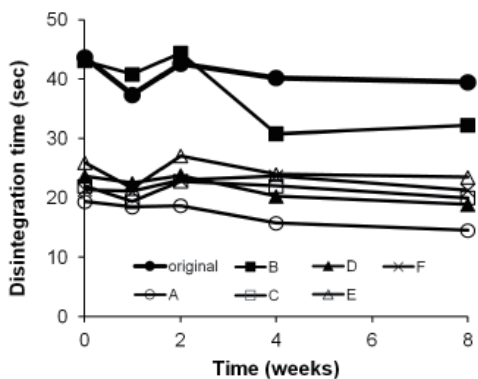
Figure 7. Disintegration time of famotidine orally disintegrating tablets 8 weeks after storage in BPs. Data are shown as the mean for 6 tablets measured at each measurement point using a disintegration tester. Brand name, ●; generic A, ○; generic B, ■; generic C, □; generic D, ▲; generic E, △; generic F, ×.
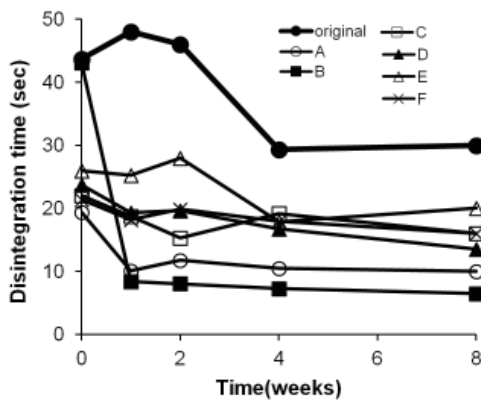
Figure 8. Disintegration time of famotidine orally disintegrating tablets 8 weeks after storage in unit-dose package. Data are shown as the mean for 6 tablets measured at each measurement point using a disintegration tester. Brand name, ●; generic A, ○; generic B, ■; generic C, □; generic D, ▲; generic E, △; generic F, ×.

brand name tablets and generic E had a 5.4 and 7.8% decrease in hardness, respectively, but generic B had a 55.1% decrease. The "stability date for uncovered tablets and capsules" proposed by the Japanese Society of Hospital Pharmacists (standard criteria in August 20, 1999) defines the "presence of a change (nonstandard)" in hardness as a change of 30% or more in hardness or a hardness value < 2.0 kg. The results of this study show that generic B was nonstandard when unit-dose packaging was done under the conditions noted earlier. Unless pharmacists give patients instructions regarding the most appropriate method of drug storage to prevent moisture absorption by tablets stored in unit-dose packages (*9*), the hardness of generic B may decrease and the potential for its disintegration may increase, resulting in a decrease in patient compliance. The decrease in the hardness of generic B may have been due to increased moisture absorption after BPs were opened. Although bulk tablet packages of generic B are not commercially available, caution is necessary since unit-dose packages are often prepared in clinical practice. The environmental conditions for storage in this study were a temperature of 27°C and a humidity of 55% given the general conditions at patients' homes. However, tablet hardness may further decrease with seasonal changes in the storage environment or changes in the storage location in the home. Therefore, patients need to be given instructions regarding methods of drug storage.

In the dissolution test, the dissolution of brand name and generic tablets differed during the first 10 min. When tablets were stored in unit-dose packages, the dissolution rates of generics B and C tended to increase compared to other preparations after 2-8 weeks, but the dissolution rate of generic E tended to decrease. However, all tablets had dissolution of 85% or more within 15 min, so there may be no dissolution problems even after unit-dose packaging according to the criteria of the Guidelines for Bioequivalence Studies of Generics (*10*).

In recent years, the dissolution test has been performed prior to the disintegration test (*11*). In the current study, disintegration tests were performed to ensure drug quality. In Japan, there are no established public criteria for the disintegration time of oral fast-disintegrating tablets. In the U.S., the U.S. Pharmacopoeia (USP) recommends 30 sec or less as the disintegration time in the disintegration test (*12*). In the current study, some took slightly more than 30 sec to disintegrate. However, the disintegration time of generic B stored in unit-dose packages decreased to about 1/5 after 1 week, affecting storage.

Based on these results, unit-dose packaging of brand name or generic (A-F) orally disintegrating tablets of famotidine causes no bioequivalence problems in terms of dissolution. The hardness of one of the generics became nonstandard and its disintegration time decreased to about 1/5, which may cause "susceptibility to disintegration" in a clinical setting. Since factors for the evaluation of the bioequivalence of brand name preparations do not include hardness or the disintegration time, generics that are susceptible to disintegration over time are on the market. When generics are used, pharmacists should be fully aware of their characteristics.

Preparations used in the current study were chosen assuming that additives, and particularly binding agents, affect hardness and are associated with disintegration. However, brand name and generic B tablets had few similarities. The generic was softer and its disintegration time decreased to about 1/5 when stored in unit-dose packages. Brand name tablets contained ethylcellulose and D-mannitol as binders while generic B contained three different binders: crystalline cellulose, hydroxypropyl starch, and povidone. Generic E (which had only a slight decrease in hardness when stored in unit-dose packages) did not contain ethylcellulose. No association between binders

and hardness was noted because binder intensity will vary from preparation to preparation depending on the amount, type, and number of binders. However, package inserts and drug interview forms (IFs) provide no information on the additives contained. As shown in Table 1, brand name and generic tablets differed substantially in terms of the additives they contained, so their formulations may differ. When selecting generics in a clinical setting, a drug's susceptibility to disintegration may thus be difficult to assess based only on a description of its additives.

In this study, the hardness of every preparation decreased 1 week after unit-dose packaging when tablets were stored at a temperature and humidity simulating those at a patient's home. Therefore, other types of tablets should be selected for patients who do not need orally disintegrating tablets. Changes in the hardness of all of the tablets in this study were within 20% when they were stored in unopened BPs, presenting no problems. The description of hardness should be confirmed in the IF when these preparations are used after unit-dose packaging, and tablets should not have decreased hardness to ≤ 2.0 kg or $\geq 30\%$ change in hardness compared to when the BP is opened. Table 1 suggests that a lack of commercially available bulk tablet packages may result in use of preparations with softer tablets. This aspect can be considered when selecting generics in a clinical setting.

The discussion in this study is based on the latest IFs from September 2011. This study was planned in August 2008, but additives in generics A and F changed. Bulk tablets of generic F also became available commercially. Pharmacists must obtain the latest drug information and utilize that information when selecting generics.

References

1. Ministry of Health, Labor, and Welfare. Ministry of Health, Labor, and Welfare Report: 2008 Patient Survey. *http://www.mhlw.go.jp/toukei/saikin/hw/kanja/08/index.html* (accessed December 3, 2009).

2. Study Group to Assess and Adapt Guidelines for Treatment of Gastric Ulcers. Evidence-based guidelines for gastric ulcer treatment. 2nd ed, Jiho K.K., Tokyo, Japan, 2007; pp. 31-54.

3. Otori K, Nishino T, Taguchi Y, Kaji E, Yago K. Evaluation of the long-term stability and sensory properties of orodispersible famotidine tablets. J Jpn Soc Hosp Pharm. 2008; 44:1259-1263.

4. Harada T, Narazaki R, Nagira S, Ohwaki T, Aoki S, Iwamato K. Evaluation of the disintegration properties of commercial famotidine 20 mg orally disintegrating tablets using a simple new test and human sensory test. Chem Pharm Bull. 2006; 54:1072-1075.

5. Tokuyama E, Matsunaga C, Yoshida K, Mifsud J, Irie T, Yoshida M, Uchida T. Famotidine orally disintegrating tablets: Bitterness comparison of original and generic products. Chem Pharm Bull. 2009; 57:382-387.

6. Ministry of Health, Labor, and Welfare. The Japanese Pharmacopoeia, 16th edition. Hirokawa Shoten Co., Tokyo, Japan, 2011; pp. 687-4137.

7. Japan Pharmaceutical Excipients Council. Handbook of Pharmaceutical Excipients, 5th edition. Yakuji Nippo Limited, Tokyo, Japan, 2007; pp. 123-128, 490-492, 700-705, 898-909.

8. Japanese Pharmaceutical Excipients Directory 2000. Yakuji Nippo Limited, Tokyo, Japan, 2000; pp. 268.

9. Yamazaki N, Taya K, Shimokawa K, Ishii F. The most appropriate storage method in unit-dose package and correlation between color change and decomposition rate of aspirin tablets. Int J Pharm. 2010; 396:105-110.

10. National Institute of Health Sciences. Guidelines for bioequivalence studies of generics. *http://www.nihs.go.jp/drug/DrugDiv-J.html* (accessed February 29, 2012).

11. Ministry of Health, Labor, and Welfare. The Japanese Pharmacopoeia, 16th edition. Hirokawa Shoten Co., Tokyo, Japan, 2011; pp. 284-287.

12. U.S. Department of Health and Human Services, Food and Drug Administration Center for Drug Evaluation and Research. Guidance for Industry Orally Disintegrating Tablets. *http://www.fda.gov/downloads/Drugs/GuidanceComplianceRegulatoryInformation/Guidances/UCM070578.pdf* (accessed November, 2008).

Development of an osmotic pump system for controlled delivery of diclofenac sodium

Laila Hassanein Emara[1],*, Nesrin Fouad Taha[1], Rania Mohamed Badr[1], Nadia Mohamed Mursi[2]

[1] *Industrial Pharmacy Laboratory, Division of Pharmaceutical Industries, National Research Centre, Dokki, Giza, Egypt;*
[2] *Department of Pharmaceutics, Faculty of Pharmacy, Cairo University, Cairo, Egypt.*

ABSTRACT: Based on an elementary osmotic pump, controlled release systems of diclofenac sodium (DS) were designed to deliver the drug in a zero-order release pattern. Osmotic pump tablets containing 100 mg DS were prepared and coated with either semipermeable (SPM) or microporous (PM) membranes. The tablet coats were composed of hydrophobic triacetin (TA) or hydrophilic polyethylene glycol 400 (PEG 400) incorporated in cellulose acetate (CA) solution, for SPM and PM, respectively. Variable tablet core compositions such as swelling polymers (PEO and HPMC) and osmotic agents (lactose, NaCl, and KCl) were studied. An optimized, sensitive and well controlled *in vitro* release design, based on the flow-through cell (FTC), was utilized to discriminate between preparations. The results revealed that the presence of PEG 400 in the coating membrane accelerated the drug release rate, while TA suppressed the release rate of DS. In the case of SPM, the amount of DS released was inversely proportional to the membrane thickness, where 5% (w/w) weight gain gave a higher DS release rate than 10% (w/w). Results of different tablet core compositions revealed that the release rate of DS decreased as PEO molecular weight increased. HPMC K15M showed the lowest DS release rate. The presence of lactose, KCl, or NaCl pronouncedly affected DS release rate depending on polymer type in the core. Scanning electron microscopy (SEM) confirmed formation of pores in the membrane that accounts for faster DS release rate. These results revealed that DS could be formulated as an osmotic pump system with a prolonged, zero-order release pattern.

Keywords: Cellulose acetate, polyethylene glycol 400 (PEG 400), controlled release, flow-through cell

---

*Address correspondence to:
Dr. Laila Emara, Industrial Pharmacy Lab, National Research Centre, El-Tahrir Street, Dokki, Giza 12622, Egypt.
E-mail: lhhemara@yahoo.com

1. Introduction

Controlled release (CR) drug delivery systems have received considerable attention in the past two decades with numerous technologically sophisticated products in the marketplace. The major benefits of CR products lie in the optimization of drug input rate into the systemic circulation in order to achieve an appropriate pharmacodynamic response. This in turn should add to product safety and reduce the extent and incidence of major adverse drug reactions due to more strict control of blood levels. Furthermore, with less frequent dosing, it is speculated that this should improve patient compliance and possibly maximize drug product efficacy in therapeutics (*1*). A number of designs are available to control or modulate drug release from dosage forms. The majority of per oral CR dosage forms falls in the category of matrix, reservoir, or osmotic systems (*2*).

Osmotic drug delivery systems utilize osmotic pressure as the driving force for delivery of drugs. The pH, presence of food, and other physiological factors may affect drug release from conventional CR systems (matrices and reservoirs), whereas drug release from per oral osmotic systems is independent of these factors to a large extent (*3-5*). Thus, an appropriately designed osmotically controlled oral drug delivery system can be a major advance towards overcoming some problems associated with traditional CR systems. Osmotic pump systems have many advantages including reducing risk of adverse reactions, improving compliance of patients, and could exhibit comparable *in vitro/in vivo* drug release (*6*). In 1955, Rose and Nelson utilized the principle of osmotic pressure in drug delivery for the first time (*7*). In 1975, Theeuwees (*6*) further simplified the Rose-Nelson pump and developed a system known as the "Elementary Osmotic Pump" (EOP). In the EOP system, an active agent, having suitable osmotic pressure, is compressed in the form of a tablet, and then coated with a semipermeable membrane (SPM), and a small orifice is created in the membrane. In operation, the osmotic agent draws water through the SPM because

of the osmotic pressure gradient and forms a saturated solution. As the membrane is non extensible, the increase in volume caused by imbibition of water leads to the development of hydrostatic pressure inside the tablet. This pressure is relieved by the flow of saturated solution out of the device through the delivery orifice. The EOP is simple to design and is well suited for drugs with intermediate water solubility (*2,3,8,9*). For delivery of poorly or highly soluble drugs, several modifications of the EOP were done, with the introduction of different systems based on principles of osmotic pressure such as the sandwiched osmotic tablet system (SOTS) (*3*), the push-pull osmotic pump (PPOP) (*2,3,10*), controlled porosity osmotic pumps (CPOP) (*2,5,11,12*), asymmetric membrane osmotic pumps (*13-15*), and the single composition osmotic tablet, SCOT (*16*).

Diclofenac sodium (DS) is a non steroidal anti-inflammatory analgesic with potent cyclooxygenese inhibition activity and is commonly used for pain control and the treatment of rheumatic diseases. DS has biological half life of 2 h and is absorbed throughout the intestinal tract. The drug shows linear pharmacokinetics. DS is considered a good candidate for CR preparations due to its relatively short biological half life, also it would be advantageous to slow down its release in the gastrointestinal (GI) tract not only to prolong its therapeutic action but also to minimize possible side effects encountered with frequent administration (*17*).

Some efforts have been made to prepare osmotically controlled release DS tablets (*18-22*). These studies used polymers such as HPMC K4M and microcrystalline cellulose (*19,21,22*) in the tablet core with other additives such as sodium lauryl sulfate and talc (*18-21*). Different osmotic agents were incorporated in the tablet core such as potassium chloride (*18-21*), potassium bicarbonate (*18,19*), potassium carbonate (*21*), sodium chloride (*21,22*) and sodium carbonate (*21*). The tablet core was coated with a cellulose acetate (CA) membrane containing either castor oil (*19-21*), triacetin (TA) (*18*) or polyethylene glycol (PEG 400) (*18-22*) as plasticizers. It is worthy to mention that the *in vitro* evaluation of the prepared DS osmotic tablets have been carried-out using the conventional USP dissolution apparatus I (*22*) or USP II (*18-21*).

A previous *in vitro* release study to evaluate DS sustained release tablets of Voltaren Retard (Novartis – Swizerland) and Voltaren SR (Novartis – Egypt), using the more advanced flow-through cell (FTC) dissolution apparatus (USP IV), was carried out (*23*). This study describes an optimum condition for the FTC that is sensitive and capable of discriminating between different products and detecting variations in DS dissolution rate due to change of the manufacturing site of the product.

Thus, the objective of the present study was development of osmotically controlled release tablets of DS with different polymers in the tablet core such

as HPMC K15M and polyethylene oxide (PEO) in the presence of lactose, potassium chloride, or sodium chloride as osmotic agents. Also, variations in coat thickness and membrane composition were studied. The *in vitro* evaluation of the prepared DS osmotic tablets were carried-out using our previously optimized FTC dissolution apparatus (*23*).

2. Materials and Methods

2.1. *Materials*

DS powder, polyethylene oxide (PEO) [M.W. 300,000, 900,000], hydroxypropylmethyl cellulose HPMC K15M (the viscosity of 2% water solution is 15,000 cps), and cellulose acetate (M.W. 30,000, 39.8% acetyl content) were purchased from Sigma-Aldrich, St. Louis, MO, USA. Polyvinylpyrolidone K-30 (PVP K-30) (M.W. 40,000), sodium chloride (NaCl), potassium chloride (KCl), sodium hydroxide pellets, potassium dihydrogen orthophosphate, mannitol, and polyethylene glycol 400 (PEG 400) were purchased from Rasayan Laboratories, Gujarat, India. Lactose was purchased from BDH, Poole, UK. Triacetin (TA) was purchased from Fluka, Buchs, Switzerland. Distilled water (Milli RO plus 10, Millipore, Billerica, MA, USA) was used. All other ingredients were of analytical grade.

2.2. *Development of diclofenac sodium osmotic pump system*

2.2.1. *Tableting*

DS powder was weighed, granulated with an alcoholic solution of PVP K-30, and then sieved through a 355 μm standard sieve (mesh number 42, US standard sieves, Fisher- Brand, USA). Granules were dried for 4 h at 50ºC (drying oven, Heraeus, USA). All other ingredients were weighed to their specified amounts (composition of core tablets are listed in Table 1), sieved through a 710 μm standard sieve (mesh number 24, US standard sieves, Fisher-Scientific, Pittsburgh, PA, USA), then mixed with dried granules of DS. Blending of all ingredients was carried out simultaneously, after which, the blends were compressed into concave tablets (Single Punch Press Model 511-7-A, Strokes-Merrill, Bristol, PA, USA) with a round die (13 mm diameter) and a concave-face punch. The average tablet weight was adjusted to 400 mg, with each containing 100 mg DS.

2.2.2. *Tablet coating and orifice formation*

Coating solutions were prepared by dissolving cellulose acetate (CA) in acetone solution containing known levels of plasticizers (10% (w/v) total solids in acetone). The types and amounts of plasticizers for different formulations are listed in Table 1.

Table 1. The compositions of osmotic pump tablets of diclofenac sodium (100 mg/tablet)

Formulation codes	Core composition (mg)					Membrane composition (%, w/w)			Membrane weight (%)
	Polymer	Osmotic agent				CA: Plasticizer			
		NaCl	KCl	Lactose	Mannitol	CA	PEG 400	TA	
F1	300[a]					2		1.5	10% (2 Orifices)
F2	300[a]					2		3.0	10% (2 Orifices)
F3	300[a]					2	1.5		10%
F4	100[a]			200		2	1.5		10%
F5	100[a]	200				2	1.5		10%
F6	200[a]		100			2	1.5		10%
F7	40[a]				260	2		1.5	5% (1 Orifices)
F8	40[a]				260	2		1.5	5% (2 Orifices)
F9	40[a]				260	2		1.5	10% (1 Orifice)
F10	40[a]				260	2		1.5	10% (2 Orifices)
F11	100[b]	200				2	1.5		10%
F12	200[b]		100			2	1.5		10%
F13	200[b]		100			2	3.0		10%
F14	100[c]	200				2	1.5		10%
F15	200[c]		100			2	1.5		10%

[a] PEO 300 000; [b] PEO 900 000; [c] HPMC K15M; NaCl (sodium chloride); KCl (potassium chloride); CA (cellulose acetate); TA (triacetin); PEG (polyethylene glycol 400).

Core tablets were coated with either a semipermeable membrane (SPM) using TA as a hydrophobic plasticizer or with a microporous membrane (PM) consisting of hydrophilic PEG 400 incorporated in CA. The coating was done using the dip-coating technique as described in other studies (*13,24,25*). Coating was continued several times until the desired weight gain was obtained (5 or 10% weight gain). For removal of the residual solvent, the coated osmotic tablets were allowed to dry in a drying oven at 50ºC overnight. For SPM, an orifice was drilled manually on one side or both sides of the tablet with a sharp needle (*3,8,26-28*). The size of the delivery orifice was kept in the range of 550-600 μm diameter.

The prepared osmotic tablets were evaluated by visual inspection of the film smoothness, uniformity of coating, edge coverage, and luster. Thickness and diameter of tablets were measured before and after coating with a standard screw gauge (Shimadzu, Kytoto, Japan).

2.3. *In vitro release study*

The release rates of DS from the prepared osmotic tablets were determined, in triplicate, by employing the open system of the flow-through cell (FTC) dissolution tester (USP Apparatus IV, Dissotest CE-6 equipped with piston pump CY 7-50, Sotax, Basel, Switzerland) (*23*). Each tablet was placed in the 22.6 mm diameter cell according to the design described in Figure 1. A built-in filtration system (0.7 μm Whatman GF/F and GF/D glass micro-fiber, and glass wool) was used throughout the study. Temperature of the dissolution medium was kept at 37 ± 0.5ºC. The
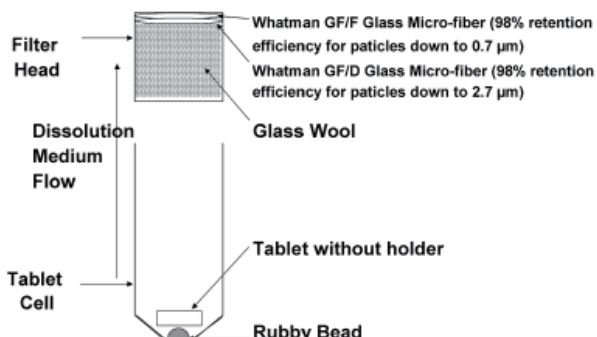
Figure 1. Schematic diagram showing the flow-through cell dissolution design.

latter design of the FTC was previously designed and validated to carry-out the release rate studies because it was found to achieve optimal drug release *i.e.* large dissolution cell, free tablet position with turbulent flow conditions, 8 mL/min flow rate of dissolution medium. Dissolution medium consisting of phosphate buffer pH 6.8 was filtered (0.45 μm), degassed, and used throughout the study. Volume fractions were collected every half-hour for 6 h and analyzed spectrophotometrically (UV-Visible spectrophotometer DU-650, Beckman-Coulter, Brea, CA, USA) for DS content by measuring the absorbance at λ_{max} 275 nm against phosphate buffer pH 6.8 as a blank.

2.4. *Kinetic study of drug release data:*

In order to describe the kinetics of drug release from DS osmotic tablets, various mathematical equations were applied such as:

Zero-order equation: $dQ/dt = K_0$ (*29*)

First-order equation: $dQ/dt = K_1 Q$ (*29*)

Higuchi release model: $Q_t = k_H t^{1/2}$ (*30,31*)

Where, Q is fraction of drug release at time *t*; k_0, k_1, and k_H are release rate constants for zero-order, first-order, and Higuchi square root of time model, respectively.

2.5. *Scanning electron microscopy (SEM) studies*

A scanning electron microscope (JXA-840A, JEOL, Tokyo, Japan) was employed to observe the cross section of the semipermeable and the microporous membranes of the tablets before and after the release study. Each sample was sputter coated with gold using gold Sputter (S150A, Edwards, West Sussex, UK) before the SEM observation.

3. Results and Discussion

The release of drug from the oral osmotic system (OROS) is governed by *i*) total solubility and osmotic pressure of the core, *ii*) the hydraulic permeability of the membrane, *iii*) thickness and surface area of the membrane, and *iv*) the internal pressure (*18*). Osmotically CR systems require only osmotic pressure to be effective and are essentially independent of its environment. Thus, in light of the rather harsh and inconsistent conditions of pH and mixing in the digestive tract, this appears to be a good CR system for oral dosage forms (*32*). In this study, we investigated the effect of certain formulation variables on the release rate of DS from OROS including type and composition of coating membrane, the number of delivery orifices as well as variation of tablet core components.

3.1. *Influence of membrane variables*

The choice of the membrane components is an important aspect in the development of OROS. The membranes used for osmotic systems are categorized as: *i*) *Semipermeable membrane* (*SPM*) which allows the osmotic passage of water but do not allow solute molecules to pass to any appreciable extent. *ii*) *Microporous membrane* (*PM*) which allows free flow of water but offers a diffusion barrier to solutes. The release from these membranes is controlled by: *i*) the concentration difference and/or osmotic pressure difference across the membrane, *ii*) the permeability of the membrane to water and drug, and *iii*) the thickness of the membrane. Plasticizers can change visco-elastic behavior of polymers significantly; they can turn a hard and brittle polymer into a softer, more pliable material, and possibly make it more resistant to mechanical stress. These changes can affect the permeability of polymer films (*33*). The effect of type and amount of plasticizers as well as different membrane

weight gain (membrane thickness) on the release of DS from OROS were studied.

The optimization of dissolution design might greatly affect the release rate results. Differentiating between formulations depends on the optimum choice of the criteria of the dissolution conditions (*23*). In this study, the selection of the dissolution design was chosen depending on a previous study describing the effect of different FTC designs on the release of DS sustained release tablets (*23*). The results revealed that turbulent flow of the dissolution medium pumped at a flow rate of 8 mL/min using either the large or small tablet cells was the ideal design for sustained release DS products. This design was capable of properly discriminating between products among other designs tested.

3.1.1. *Effect of type of plasticizers*

In this study SPM and PM were prepared and studied. For SPM, TA was incorporated in CA solution, two orifices were drilled (orifice size ~600 μm) on the side surfaces of the tablet using a sharp needle. For PM, PEG 400 was incorporated in CA solution. The total weight gain was adjusted to 10% (w/w).

Figure 2 compares the release profiles of DS from PEO 300,000 tablets with no osmotic agent, either coated with SPM or PM (F1 and F3, respectively). The figure shows that the amount of DS released was 16.23% *versus* 26.29% in the case of SPM (F1) and PM (F3), respectively. Thus, incorporation of PEG 400 into the coating solution gave a faster release rate of DS compared to TA, which might be due to the difference in hydrophilicity and hydrophobicity of the two plasticizers. Because PEG 400 is a hydrophilic plasticizer, it could be leached out easily leading to the formation of pores within the membrane, which increases the membrane permeability, thus, enhance drug release rate. In contrast, because TA is a hydrophobic plasticizer, with a low solubility of 1 part in 14 parts of water, and thus it would resist water
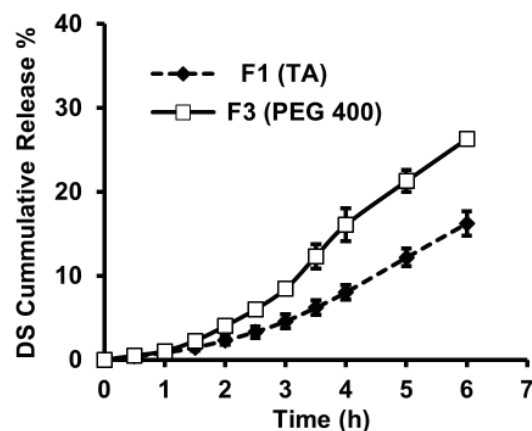

Figure 2. Effect of type of plasticizer on DS release rate from osmotic pump tablets containing PEO 300,000; F1 (TA); F3 (PEG 400). Bars represent ± SD (*n* = 3).

diffusion and, as a consequence, the drug release was less (*33*). This result was confirmed in a previous study done by Rani and Mishra (*18*), who reported that a higher rate and extent of DS release rate was observed from osmotic matrix tablets (containing HPMC K4M in the core) using PEG 400 compared to TA as plasticizers (porosigenic agents). Liu *et al.* (*26*) studied the influence of nature and amount of plasticizers on the release rate of nifidepine from osmotic pump tablets. Their results showed that films plasticized using PEG developed a completely porous structure after 24 h leaching, whereas films plasticized with TA retained their dense structure. Therefore, in our study a porous membrane was suggested to give a higher DS release rate than the non-porous semipermeable membrane.

Figure 3 compares the release profiles of DS from F1 and F2 containing PEO 300,000 with no osmotic agent, using two different ratios of CA:TA (2.0:1.5 and 2.0:3.0, respectively) (Table 1). The results reveal that increasing the amount of TA to CA led to a decrease in DS release rate, where the amount of DS released was 16.23% *versus* 4.45% upon increasing the amount of TA. These results might be due to a decrease of the water permeability of SPM when increasing the amount of hydrophobic plasticizers (*e.g.* TA). Increasing the hydrophobic plasticizer led to a decrease in the molecular mobility of CA (*2*), thus, a decrease in the penetration of water into the system, and as a consequence, a lower osmotic pressure gradient and slower drug release was observed.

On the other hand, Figure 4 shows the release profiles of DS from F12 and F13 containing PEO 900,000 and KCl as an osmotic agent, using two different ratios of CA:PEG 400 (2.0:1.5 and 2.0:3.0, respectively). The results show that increasing the amount of PEG 400 in CA led to a simultaneous increase in the release rate, where the amount of DS released was doubled (*viz.* 25.68% *versus* 57.41%

for F12 and F13, respectively) when the amount of PEG 400 was doubled. A previous study by Mishra *et al.* (*21*) was carried-out to evaluate the effect of membrane types on DS release from osmotic tablets using semipermeable (CA containing castor oil) and microporous (CA containing PEG 400) membranes. Drug release results showed that the microporous membrane coated batches gave more drug release. In addition, the PEG 400 (20%) containing batch gave a much higher drug release than the PEG 10% containing batch (*21*). The same results were obtained by Lu *et al.* (*34*), who studied the influence of the amount of PEG 400 incorporated in the coating membrane on the release of water insoluble naproxen. Their results showed that increasing the PEG 400 level, led to increased drug release rate, as the more PEG 400 incorporated in the coating solution, the more void space formed after leaching and, as a result, higher membrane permeability and higher release rate. However, the study clarified that a high percentage of PEG 400 (50%) in CA would make the membrane fragile, which was not observed in our study, where the two ratios of CA:PEG 400 (2.0:1.5 and 2.0:3.0) produced a relatively strong membrane. These membranes were capable of keeping their shape and integrity during the 6 h release study without any observed deformation or rupture of the membranes.

In general, in case of SPM, the membrane becomes stronger on addition of a high level of TA, and thus, slower drug release will be observed. On the contrary, in the case of PM, the membrane becomes more porous on addition of PEG, which in turn accounts for a faster release rate. These findings could be considered as important key factors and should be taken into account during manufacture of osmotic devices, as the osmotic device should release drug quickly and at the same time give a sufficiently high burst strength to prevent premature rupture and the attendant dose dumping in the GI tract (*35*).
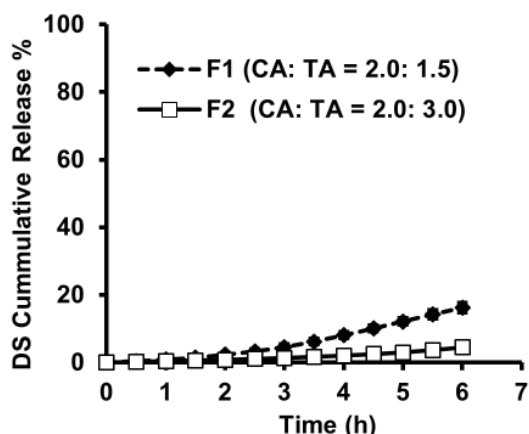
Figure 3. Effect of the amount of hydrophobic plasticizer (TA) in CA membranes on DS release rate from osmotic pump tablets containing PEO 300,000; F1 and F2 (CA:TA = 2.0:1.5 and 2.0:3.0, respectively). Bars represent ± SD (*n* = 3).
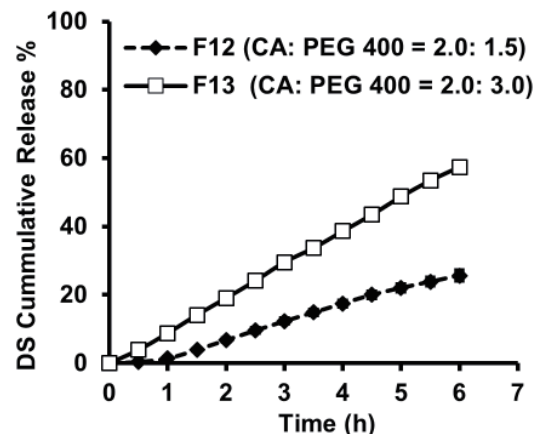
Figure 4. Effect of the amount of hydrophilic plasticizer (PEG 400) in CA membranes on DS release rate from osmotic pump tablets containing PEO 900,000; F12 and F13 (CA:PEG 400 = 2.0:1.5 and 2.0:3.0, respectively). Bars represent ± SD (*n* = 3).

3.1.2. *Effect of membrane weight gain and number of delivery orifices*

The osmotic delivery systems should contain at least one delivery orifice in the membrane for drug delivery, which should be optimized in order to control drug release from osmotic systems. Delivery orifices in osmotic systems can be created with the help of a mechanical drill (*33*), but for a commercial production scale, tablets need to be produced using a continuous process, and therefore, laser drilling is considered to be one of the mostvaluable techniques to create delivery orifices in osmotic tablets. However, due to the expense of using a laser-drilling machine, its use is limited to large-scale production, whereas, for research scale, reports have studied the use of other techniques, *e.g.* systems with passage ways formed *in situ*, use of modified punches, and indentation of the core which is not covered during coating (*8,28,33*).

To study the effect of membrane weight gain (membrane thickness) on DS release rate, tablets containing PEO 300,000 as a swelling polymer and mannitol as an osmotic agent, were coated with SPM to obtain tablets with two different weight gains (*viz.* 5% and 10% (w/w), F7-F10, respectively) (Table 1). The release profiles of DS from these formulations are shown in Figures 5A and 5B. It was clearly evident

that the drug release rate decreased upon increasing the membrane weight gain. This result was observed in the presence of one or two delivery orifices (Figures 5A and 5B, respectively). On the other hand, it was found that increasing the number of delivery orifices increases DS release rate, which was clearly observed only in the case of tablets having 5% weight gain. The increase in membrane weight resulted in the increase of resistance of the membrane to water diffusion and a decrease in the rate of water imbibition, therefore, a simultaneous decrease in the rate of drug liquefaction, and as a result, drug release decreased (*33*). Similar results were obtained in previous studies (*19,21*), where a DS release rate from osmotic tablets was decreased with an increase in coating thickness of the semipermeable membrane. Therefore, tablet coat thickness might be a critical property of osmotic pump preparations and should be optimized to safeguard both the integrity of the system, during its trip through the GI tract, and the required release rate of the drug. However, the presence of two orifices was preferred, in case one orifice gets blocked. Also, Figure 5 showed a shorter lag time period in the presence of two orifices especially for tablets with a 5% weight gain (F9, Figure 5B).

3.2. *Influence of tablet core components*

Tablets with various core compositions were prepared and coated with a microporous membrane consisting of PEG 400 dissolved in CA solution. Total tablet weight gain, representing membrane thickness, was kept at 10% (w/w). For the microporous membrane, once the tablet comes in contact with the aqueous environment, the water soluble component (PEG 400) dissolves, and therefore, drug release from these systems occurs from the surface rather than from a single orifice (*33*). Different core variables were studied as follows.

3.2.1. *Effect of hydrophilic swellable polymers*

Figures 6A and 6B show the effect of PEO (MW 300,000 and 900,000) and HPMC K15M, on the release rate of DS in the presence of either NaCl (F5, F11, and F14) or KCl (F6, F12, and F15) as osmotic agents, respectively (Table 1). The results revealed that the release rate of DS decreased as PEO molecular weight increased while HPMC K15M showed the slowest release rate. Figure 6A shows that for DS osmotic tablets containing NaCl, the amount of DS released was 58.4%, 55.45%, and 9.27% using PEO MW 300,000 (F5), 900,000 (F11), and HPMC K15M (F14), respectively. While, with DS osmotic tablets containing KCl, the amount of DS released were 55.5%, 25.6%, and 4.04% for F6, F12, and F15, respectively. The presence of KCl, as an osmotic agent, compared to NaCl, generally slowed the release rate of DS to a certain extent depending on the kind and
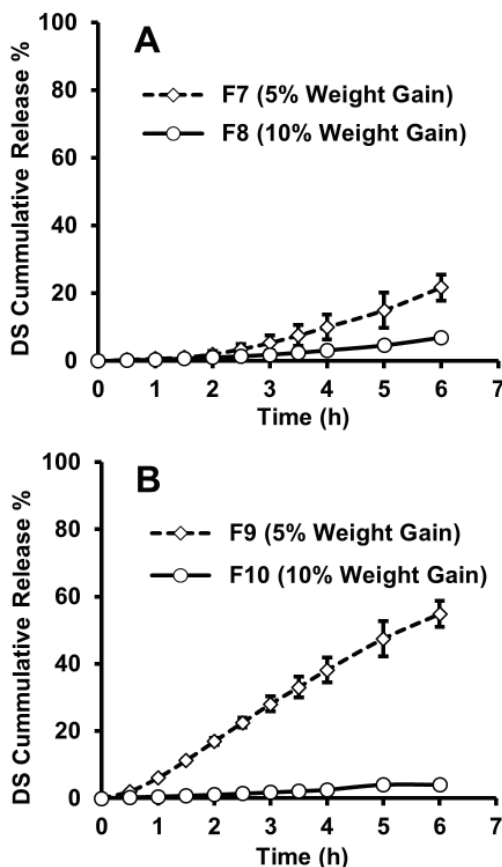

Figure 5. Effect of membrane weight gain on DS release rate from osmotic pump tablets; (A) One delivery orifice; (B) Two delivery orifices. Bars represent ± SD (*n* = 3).
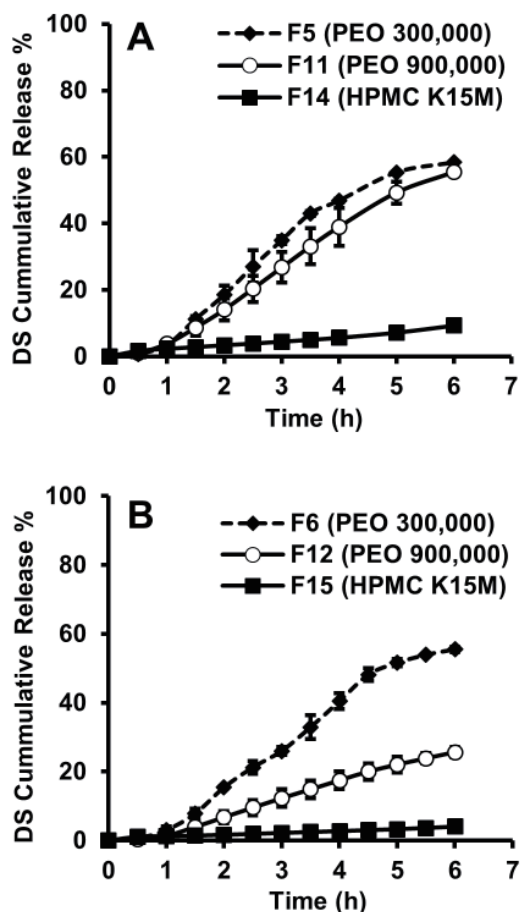
Figure 6. Effect of different hydrophilic polymers on DS release rate from CPOP tablets containing (A) NaCl and (B) KCl. Bars represent ± SD (*n* = 3).


Figure 7. Effect of different osmotic agents on DS release rate from CPOP tablets containing PEO 300,000; F3 (absence of osmotic agent); F4 (lactose); F5 (NaCl). Bars represent ± SD (*n* = 3).

type of swelling polymer used. When replacing NaCl with KCl, the amounts of DS released were decreased very slightly by 5% in the case of PEO 300,000. This could be comparable to a study carried-out by Mishra *et al.* (*21*), where they replaced NaCl with KCl in osmotic tablets containing MCC in a tablet core, and a slight decrease in the rate and extent of DS release was observed. On the other hand, when replacing NaCl with KCl in osmotic tablets, the amounts of DS decreased considerably by 55% and 56% using PEO 900,000 and HPMC K15M, respectively. The previous study of Mishra *et al.* (*21*) as well as the current study drew attention to the importance of the proper selection of polymer/osmogent combination to give the desired release characteristics for DS osmotic tablets.

3.2.2. *Effect of osmotic agents*

The osmotic pressure gradient between the inner core compartment and the external environment should be studied and optimized case by case. The simplest way to achieve a constant osmotic pressure is to maintain a saturated solution of osmotic agent in the core compartment (*33*). Figure 7 compares the release profiles of DS from PEO 300,000 CPOP tablets,

containing either lactose (F4) or NaCl (F5) compared to F3 which contains no osmotic agents. Figure 7 shows an initial lag time of about 1 h in all formulations which is the time taken by the system to hydrate and solubilize the contents of the core before generating sufficient osmotic pressure to start drug release (*36*). The study revealed that the presence of osmotic agents increased the release rate of DS from 26.29% to 39.41% and 58.40% in the absence of osmotic agent, presence of lactose and NaCl (F3, F4, and F5, respectively). The higher release rate of DS obtained in the case of NaCl could be attributed to the fact that NaCl possesses a higher osmotic pressure (356 atm) compared to lactose (150 atm pressure), upon imbibition of water, both solutes absorb water and dissolve, but NaCl produces a more distinct osmotic gradient, which in turn allows faster release of drug (*32*).

It is noteworthy to mention that the two osmotic agents, *i.e.* NaCl (F5) and KCl (F6), gave almost the same release rate for DS from the two formulations (58.04% and 55.50%, respectively), which in turn concluded that addition of NaCl or KCl [osmotic pressure 356 and 245 atm, respectively (*33*)] gave the same release rate. These results might be important, and should be considered when proposing a formulation of an osmotic system containing DS, especially for hypertensive patients, where it is not recommended to incorporate sodium salts in their regimen.

3.3. *SEM studies*

Figure 8 compares the cross-sectional SEM micrographs of both SPM containing TA as well as PM containing PEG 400. Before dissolution, both coating membranes appeared to be integral and smooth with no visible imperfections (Figures 8A and 8C), also the PM showed no evidence of pore formation. After dissolution (Figures 8B and 8D), the coating membranes lost their integrity, and the pores were
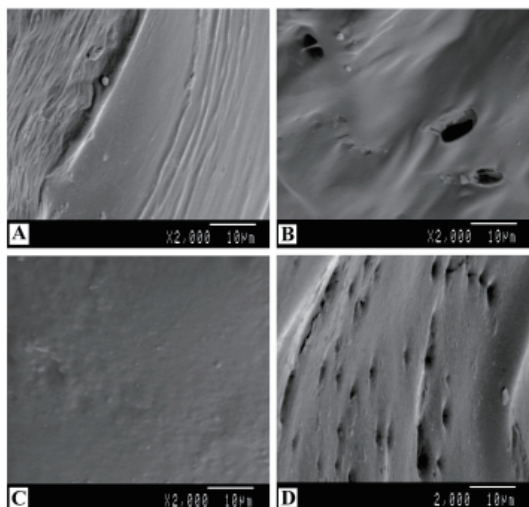
Figure 8. Scanning electron micrographs of cross section of (A) semipermeable membrane (SPM) before dissolution; (B) SPM after dissolution; (C) microporous membrane (PM) before dissolution; (D) PM after dissolution.

clearly evident. More pores were observed in PM with PEG 400 as compared to SPM with TA, which was possibly a result of the more hydrophilic nature of PEG 400 compared to TA. The obtained micrographs of the SEM correlated well with DS release rate results, which proved that the formation of pores in the membrane controled DS release rate from the proposed osmotic systems.

3.4. *Kinetic analysis of the data*

By applying the linear regression method, and subjecting the release rate data of the CPOP tablets to different release kinetics and mechanisms (zero-order, first-order, and Higuchi diffusion model), all the controlled porosity osmotic pump formulations were found to follow the zero-order release model.

4. Conclusion

DS can be formulated in an osmotic pump system. The optimum choice of polymer type, osmotic agent, type and amount of plasticizer as well as membrane thickness could provide a prolonged, zero-order release pattern and it can be expected that the osmotic pump system will perform therapeutically better with improved patient compliance. However, an elaborate in *vivo* study, in human subjects, of these systems is required.

References

1. Pillay V, Fassihi R. Electrolyte-induced compositional heterogeneity: A novel approach for rate-controlled oral drug delivery. J Pharm Sci. 1999; 88:1140-1148.
2. Verma RK, Krishna DM, Garg S. Formulation aspects in the development of osmotically controlled oral drug delivery systems. J Control Rel. 2002; 79:7-27.
3. Liu L, Ku J, Khang G, Lee B, Rhee JM, Lee HB. Nifedipine controlled delivery by sandwiched osmotic tablet system. J Control Rel. 2000; 68:145-156.
4. Verma RK, Kaushal AM, Garg S. Development and evaluation of extended release formulations of isosorbide mononitrate based on osmotic technology. Int J Pharm. 2003; 263:9-24.
5. Makhija SN, Vavia PR. Controlled porosity osmotic pump-based controlled release system of pseudoephedrine. J Control Rel. 2003; 89:5-18.
6. Theeuwes F. Elementary osmotic pump. J Pharm Sci. 1975; 64:1987-1991.
7. Rose S, Nelson JF. A continuous long-term injector. Aus J Exp Biol Med Sci. 1955; 33:415-419.
8. Santus G, Baker RW. Osmotic drug delivery: A review of the patent literature. J Control Rel. 1995; 35:1-21.
9. Prabakaran D, Singh P, Kanaujia P, Vyas SP. Effects of hydrophilic polymers on the release of diltiazem hydrochloride from elementary osmotic pumps. Int J Pharm. 2003; 259:173-179.
10. Theeuwes F. Osmotic system for delivering selected beneficial agents having varying degrees of solubility, 1978; US Patent No. 4,111, 201.
11. Thombre AG, Zentner GM, Himmelstein KJ. Mechanism of water transport in controlled porosity osmotic devices. J Membr Sci. 1989; 40:279-310.
12. Zentner GM, MeClelland GA, Sutton SC. Controlled porosity solubility and resin-modulated osmotic drug delivery systems for release of diltiazem hydrochloride. J Control Rel. 1991; 16:237-244.
13. Herbig SM, Cardinal JR, Korsmeyer RW, Smith KL. Asymmetric-membrane tablet coatings for osmotic drug delivery. J Control Rel. 1995; 35:127-136.
14. Thombre AG, Cardinal JR, DeNoto AR, Herbig SM, Smith KL. Asymmetric membrane capsules for osmotic drug delivery. J Control Rel. 1999; 57:55-73.
15. Thombre AG, Appel LE, Chidlaw MB, Daugherity PD, Dumont F, Evans LAF, Sutton SC. Osmotic drug delivery using swellable-core technology. J Control Rel. 2004; 94:75-89.
16. Speers M, Bonnano C. Economic aspects of controlled drug delivery. Encyclopedia of Controlled Drug Delivery, Wiley, New York, USA, 1999; pp.341-347.
17. Gohel MC, Amin AF. Formulation optimization of controlled release diclofenac sodium microspheres using factorial design. J Control Rel. 1998; 51:115-122.
18. Rani M, Mishra B. Comparative *in vitro* and *in vivo* evaluation of matrix, osmotic matrix, and osmotic pump tablets for controlled delivery of diclofenac sodium. AAPS PharmSciTech. 2004; 5:71.
19. Rani M, Surana R, Sankar C, Mishra B. Development and biopharmaceutical evaluation of osmotic pump tablets for controlled delivery of diclofenac sodium. Acta Pharm. 2003; 53:263-273.
20. Rani M, Surana R, Sankar C, Mishra B. Formulation and biopharmaceutical evaluation of osmotic matrix tablets of diclofenac sodium. Drug Deliv. 2004; 11:263-270.

21. Mishra B, Sankar C, Dilip C, Pravitha V, Arun Raj, Anwar Sadique T. Osmotically controlled diclofenac sodium tablets: Membrane and osmogens effects. Der Pharmacia letter. 2010; 2:21-27.

22. Edavalath S, Shivanand K, Prakasam K, Rao B, Divakar G. Formulation developement and optimization of controlled porosity osmotic pump tablets of diclofenac sodium. Int J of Pharm and Pharm Sci. 2011; 3:80-87.

23. Emara LH, Taha NF, Mursi NM. Investigation of the effect of different flow-through cell designs on the release of diclofenac sodium SR tablets. Dissolution Technol. 2009; 23-31.

24. Samani SM, Adrangui RJ, Siahi-Shadbad MR, Nokhodchi A. An approach to controlled-release dosage form of propranolol hydrochloride. Drug Dev Ind Pharm. 2000; 26:91-94.

25. Altinkaya SA, Yenal H. *In vitro* drug release rates from asymmetric-membrane tablet coatings: Prediction of phase-inversion dynamics. Biochem Engin J. 2006; 28:131-139.

26. Liu L, Khang G, Rhee JM, Lee HB. Monolithic osmotic tablet system for nifedipine delivery. J Control Release. 2000; 67:309-322.

27. Lee DH, Khang G, Rhee JM, Lee HB. Preparation of a new-osmotic tablet system for oral drug deliveryof nifedipine. Controlled Release Society 29th Annual Meeting Proceedings. 2002; 525:992-993.

28. Liu L, Che B, 2006. Preparation of monolithic osmotic pump system by coating the indented core tablet. Eur J Pharm Biopharm. 2006; 64:180-184.

29. Martin A, Swarbrick J, Cammara A. In: Physical Pharmacy, Chapter 14. 3rd ed., Lee & Febiger, Philadelphia, 1983; pp. 352-398.

30. Higuchi T. Mechnism of sustained-action medication. Theoretical analysis of rate of release of solid drugs dispersed in solid matrices. J Pharm Sci. 1963; 52:1145-1149.

31. Karasulu E, Yesim Karasulu H, Ertan G, Kirilmaz L, Guneri T. Extended release lipophilic indomethacin microspheres: Formulation factors and mathematical equations fitted drug release rates. Eur J Pharm Sci. 2003; 19:99-104.

32. Razaghi AM, Schwartz JB. Investigation of cyclobenzaprine hydrochloride from oral osmotic delivery systems containing a water-soluble polymer. Drug Dev Ind Pharm. 2002; 28:631-639.

33. Verma RK, Mishra B, Garg S. Osmotically controlled oral drug delivery. Drug Dev Ind Pharm. 2000; 26:695-708.

34. Lu E, Jiang Z, Zhang Q, Jiang X. A water-insoluble drug monolithic osmotic tablet system utilizing gum arabic as an osmotic, suspending and expanding agent. J Control Rel. 2003; 92:375-382.

35. Appel LE, Clair JH, Zentner GM. Formulation and optimization of a modified microporous cellulose acetate latex coating for osmotic pumps. Pharm Res. 1992; 9: 1664-1667.

36. Ramakrishna N, Mishra B. Design and evaluation of osmotic pump tablets of naproxen sodium. Pharmazie 2001; 56:958-962.

Aortopulmonary fistula caused by an infected thoracic aortic false aneurysm rupturing after endovascular stent placement

Suguru Yamashita*, Tomotaka Dohi, Yuichiro Shimizu, Shin-ichi Momomura

Cardiovascular Center, Toranomon Hospital, Tokyo, Japan.

ABSTRACT: We report a case of 74-year-old man presenting with a rupture of a thoracic aortic false aneurysm after undergoing conventional total arch replacement for aortic arch aneurysm (62 mm) and endovascular stent placement for descending aortic aneurysm (70 mm). His chief complaints at the present admission were fever and sensation of dyspnea and we put him on a course of antibiotics for stent graft infection. However he died of massive hemoptysis. From a standpoint of autopsy findings, a thoracic aortic false aneurysm formed at the just proximal landing zone owing to type Ia endoleak, and simultaneously stent graft infection lead to make fistula formation between the false aneurysm and the lung. We examined ourselves that stent graft infection and aortopulmonary fistula caused by an infected thoracic aortic false aneurysm rupturing into the lung should be promptly treated such as complete removal of the stent and another revascularization in a reasonable period of time except if there are complications such as comorbid1ities or withholding of consent. We experienced and reported one rare case associated with a rupture of thoracic aortic false aneurysm caused by stent graft infection and the fistulization between the lung and the stent graft.

Keywords: Rupture, thoracic aortic false aneurysm, endovascular stent placement, graft infection, type Ia endoleak

1. Introduction

The initial experiences with endovascular treatment of thoracic aortic pathologies are promising, showing acceptable mortality and paraplegia rates (*1*). The

indications for thoracic aortic endovascular repair include thoracic aortic aneurysms (TAA), acute and chronic expanding type B dissection, traumatic aortic rupture, and penetrating aortic ulcer (*2*). Although the number of thoracic endovascular aortic repair (TEVAR) is increasing rapidly, less is known about complications after TEVAR in contrast to abdominal endovascular aortic repair (AEVAR). Depending on the different aortic pathologies, procedure-related complications frequently occur. Serious complications include primary or secondary type I endoleak, retrograde type A dissection, stent collapse, and rupture with subsequent death. Series involving stent grafting of TAAs have shown that endoleaks occur in 3-29% (*3-7*), and about 50% of these are life threatening type I endoleaks with unchanged pressurized aneurysm sack. Meanwhile, Ducasse *et al*. demonstrated that the frequency of aortoiliac stent graft, which had been located by endovascular technique, infection in their study, *i.e.*, 0.43%, seems low and would indicate that stent grafts have a lower infection rate than that of prosthetic grafts used for conventional open repair (range 0.5-3%) (*8,9*). Although coexistence of these complications after TEVAR is rare, such pathological condition is fatal and the prompt therapeutic strategy for each individual case should be cautiously determined.

2. Case presentation

The case was a 74-year-old man whose chief complaints at the admission were fever and sensation of dyspnea. He had had hypertension for longer than 10 years and given β-blocker at the department of internal medicine of the hospital. In 1995, he presented with chest and abdominal pain. Chest computed tomography (CT) revealed an aneurysm of aortic arch of 52 mm in diameter. At first, medical conservative treatment to control blood pressure was chosen due to patient's wishes but it expanded to a diameter of 62 mm 5 years later, in 2000. The department of cardiovascular surgery of the hospital determined that it was an indication for surgery and performed a total aortic arch replacement. Postoperatively, another hospital found an aneurysm of descending aorta of up to 70 mm in diameter and carried out an endovascular stent placement in 2003.

*Address correspondence to:
Dr. Suguru Yamashita, Department of Surgery, Kanto Medical Center NTT EC, Higashi-Gotanda 5-9-22, Shinagawa-ku, Tokyo 141-8625, Japan.
E-mail: origin0304@yahoo.co.jp

Since then, he had been followed up at our hospital and entered twice to treat hypertensive heart failure in 2004. He frequently underwent insertion and placement of a central venous catheter during these admissions. As of obstructive sleep apnoea syndrome which he developed in this period, continuous positive airway pressure was introduced and his systolic blood pressure was kept at around 140 mmHg by four antihypertensive medications, angiotensin II receptor blocker, angiotensin converting enzyme inhibitor, calcium channel blocker, and β-blocker. In March 2005, cold-like symptoms appeared and inflammation reaction continued high in spite of internal use of levofloxacin. Based on the left-sided accumulation of pleural effusion and expansion of the aortic aneurysm around the stent graft shown by chest X-ray (Figure 1), we considered that the patient had stent graft infection and hospitalized him for further investigation and treatment in April 2005. Examinations at admission revealed intensified inflammatory response, undernutrition, decreased renal function, and anemia associated with chronic inflammation (Table 1). Venous blood culture was positive for *Staphylococcus aureus*. As for the post-hospitalization progress, vancomycin hydrochloride and meropenem hydrate were given against stent infection probably caused by a previous central venous catheter placement, which reduced the patient's temperature and mitigated inflammatory response. However, on the 21st hospital day, his hemoglobin level suddenly dropped accompanying hematemesis and another onset of fever. In response to this, thoracic plain CT was performed on the 22nd hospital day, and it revealed the enlargement of the aortic aneurysm around the stent graft compared to that on the 12th hospital day (Figure 2). On the 22nd hospital day, large amounts of black watery stool

appeared. Gastroscopy identified blood only in the trachea (Figure 3), which indicated hemoptysis, not gastrointestinal bleeding. The patient then developed aspiration pneumonia and received antibiotic treatment. On the 34th hospital day, the second massive hemoptysis appeared and caused airway obstruction and cardiac arrest. After receiving cardiopulmonary resuscitation, he was put under mechanical ventilator and given proper blood transfusion. On the 36th hospital day, he died of the third massive hemoptysis. Reoperation was not performed on request of the family during the admission. As for the result of autopsy, the aorta showed saccular dilatation macroscopically (Figure 4). Thinning of wall and massive infiltration of neutrophils were identified especially in the area where the stent was placed. Therefore, it was considered that the massive hemoptysis which was the immediate cause of death was led by a ruptured false aneurysm with a fistula opened to the lung parenchyma. The false aneurysm was located between the graft which was placed at the total aortic arch replacement and the stent which was later placed at TEVAR, and was formed probably through type Ia endoleak at the just proximal end of the stent. It seemed more likely that the proximal edge of the stent graft made contacts to the native aorta and subsequently endoleak occurred. Inflammation and infection at the site then caused formation of the fistula. Fistulization was microscopically confirmed in the adhesive area between the false aneurysm and the lung (Figure 5).

3. Discussion

Endovascular stent grafts are evolutionary medical devices that blend the vessel wall fixation properties of
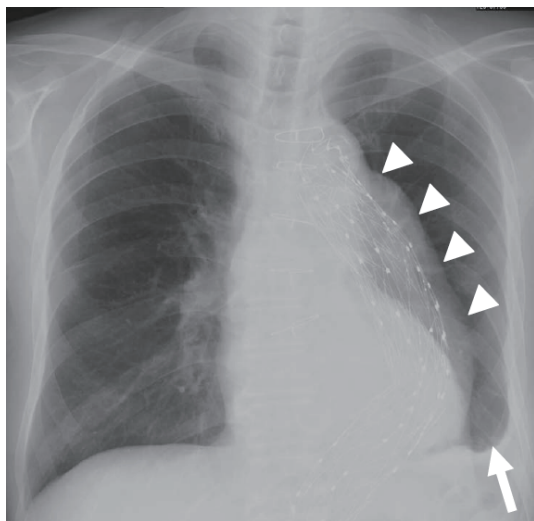
Figure 1. Chest X-ray on admission. Chest X-ray showed left-sided accumulation of pleural effusion (white arrow) and expansion of the aortic aneurysm around the stent graft (white arrowhead).

Table 1. Blood test findings on the present admission

Index	Measured value (Reference value)
Alb	2.2 g/dL (3.9-4.9 g/dL)
T-bil	0.3 mg/dL (0.2-1.0 mg/dL)
AST	27 IU/L (10-40 IU/L)
ALT	20 IU/L (5-45 IU/L)
BUN	36 mg/dL (7.2-20.0 mg/dL)
Cre	1.7 mg/dL (0.5-1.1 mg/dL)
Na	137 mmol/L (136-145 mmol/L)
K	3.6 mmol/L (3.6-4.8 mmol/L)
Cl	104 mmol/L (99-109 mmol/L)
LDH	122 IU/L (120-245 IU/L)
ALP	359 IU/L (104-338 IU/L)
γ-GTP	90 IU/L (16-73 IU/L)
CRP	16.4 mg/dL (< 0.3 mg/dL)
WBC	14,000 μL (3,100-9,500 μL)
Hb	9.4 g/dL (13.5-16.9 g/dL)
Plt	29.6×10^4 /μL (15.1-34.9/μL)
Fe	13 μg/dL (64-187 μg/dL)
Ferritin	404 mg/dL (27-320 ng/mL)
PT	76.9% (70-130%)
APTT	38.0 sec (24-38 sec)

Values in parentheses are normal ranges in our institution.
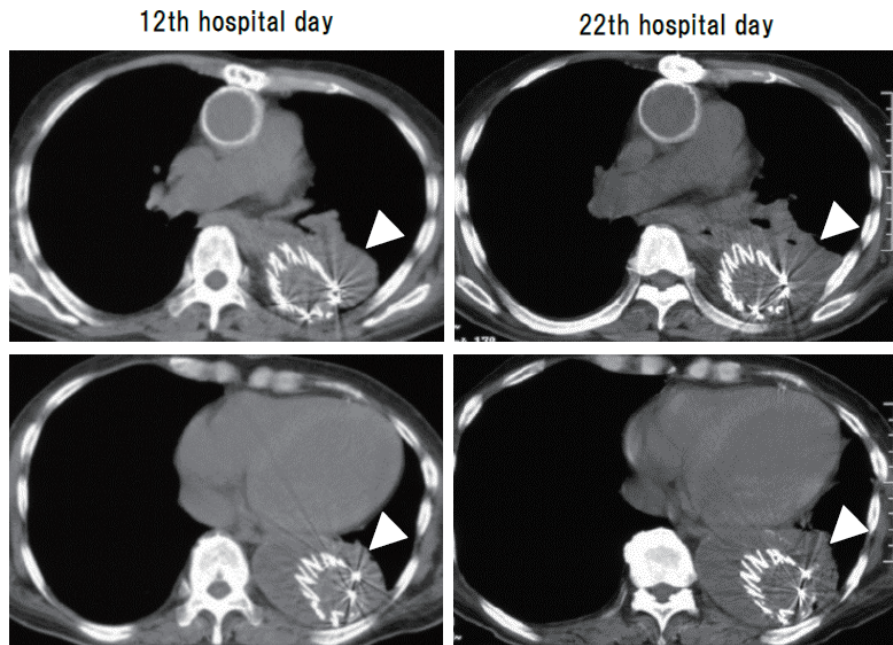
Figure 2. Changes of the thoracic CT findings during admission. The comparison between the findings of plain thoracic CT at 12th (left sided) and 22th hospital day (right sided) revealed that the aortic aneurysm around the stent graft had enlarged with time (white arrow head).
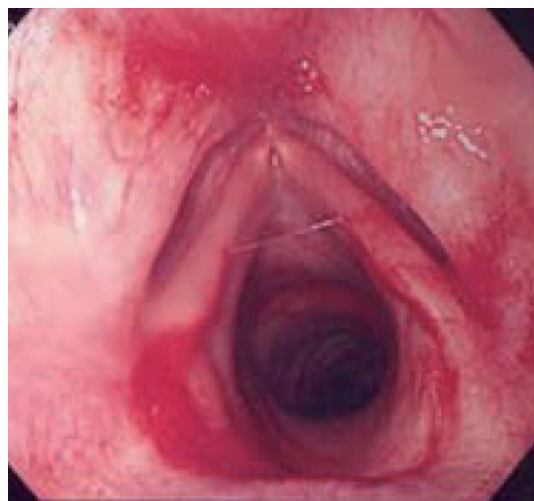
Figure 3. Gastroscopy findings at first hemoptysis. Gastroscopy revealed hemorrhage from the respiratory tract.
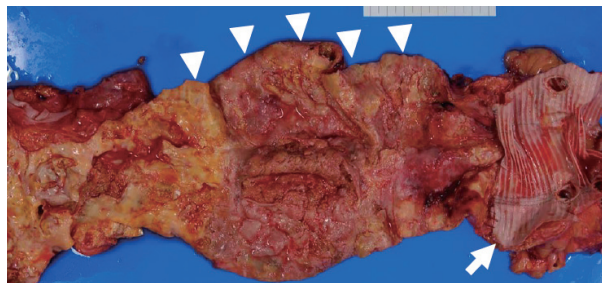
Figure 4. Macroscopic finding of descending aorta at autopsy. The autopsy specimen of the descending aorta, in which the stent graft placed at TEVAR had already been removed, showed saccular dilatation and thinning of the wall (white arrow head) at the distal side to the graft (white arrow), which had placed at the total aortic arch replacement. Right, cranial; left, caudal.
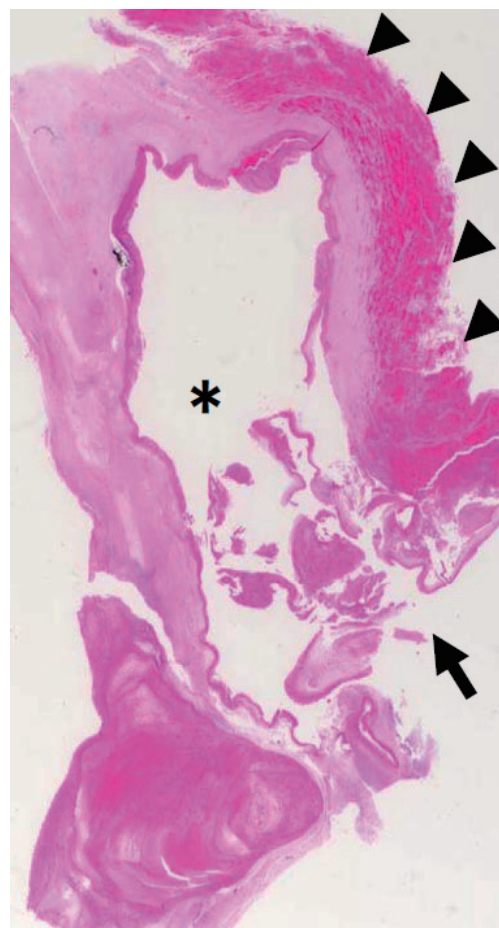
Figure 5. Microscopic finding of fistula detected between pulmonary parenchyma and aortic false aneurysm. Histological findings revealed the fistulization (black arrow) between the aortic false aneurysm (asterisk) and pulmonary parenchyma (black arrow head). H&E, ×100.

metallic intravascular stents with the arterial conduit properties of prosthetic vascular grafts. Endovascular stent placement has various advantages compared to surgical treatment, such as being noninvasive and low risks of spinal cord ischemia and bleeding. One of the first proposals for a minimally invasive intraluminal bypass was included with the initial clinical developments of catheter-based vascular intervention in the early 1960s (*10,11*). The landmark work by Dotter *et al*. using arterial angioplasty and vascular stents suggested the application of these newly developed devices to the treatment of traumatic arterial injuries and aneurysms (*12*). Marin *et al*. described that the overall technical success rate, which demonstrated free from major complications or major reinterventions, of TEVAR and AEVAR for TAA and abdominal aortic aneurysm was 85.1% in total of 817 patients over 10 years experience at one institution (*13*). However, immediately following TEVAR, 15% of patients had type I or III endoleaks and 10% had type II endoleaks (*13*). Additionally Alimi *et al*. emphasized the need for lifelong surveillance because the possibility for developing a late failure with type I endoleak of a previously excluded aneurysm was not negligible (*14*). Accurate detection and classification is essential for the proper management since the method of endoleak treatment is determined by the different source. High-pressure leaks (type I and type III) require urgent management because of the relatively high short-term risk of sac rupture. Once detected, endoleaks warranting correction are usually treated by endovascular route for poor surgical patients (*15*). A variety of techniques including extension endografts or cuff, balloon angioplasty, bare stents, and a combination of transvascular and direct sac puncture embolization techniques has allowed to treat the vast majority of these endoleaks without conversion to open surgical repair.

On the other hand, aortic stent graft infection is an uncommon complication and little is known about the general features and potential risk factors for aortic stent-graft infection, thus treatment is administered on a case-by-case basis with no consensus guidelines. Ducasse *et al*. demonstrated that more than half of patients (35/56, 62.5%) revealed stent graft infection at > 4 months after endovascular stent placement (*8*). They also showed that the offending microorganism was identified in 67.7% (44/65) and especially *Staphylococcus aureus* occupied the majority of patients (24/44, 54.5%) (*8*), in analogy with the present case. The treatments of stent graft infection could be grouped into conservative treatment, including using antimicrobial therapy and effusion drainage, and surgical treatment involving stent graft excision followed by aortic reconstruction. Ducasse *et al*. described that mortality of stent graft infection was 18% (11/61) overall, 36.4% (4/11) after conservative treatment, and 14% (7/50) after surgical treatment (*p* = 0.086). Despite a low infection rate, the associated mortality rates are extremely high

and the morbidity rate, even with aggressive surgical interventions, is also high (*16*). Nevertheless, when stent infection occurred, complete removal of the stent graft and another revascularization should be advisable if feasible.

In the present case, it was certain that an aortopulmonary fistula occurred by an infected thoracic aortic false aneurysm rupturing into the lung. However, the trigger of enlargement of the thoracic aortic false aneurysm might be not only stent graft infection but also type Ia endoleak from the result of autopsy. The type Ia endoleak and the stent graft infection simultaneously might occur about 2 years after from TEVAR. Acctually etiologies of the aortic false aneurysms were reported to include leakage from surgical or endovascular placed graft, penetrating atherosclerotic ulcer, pneumonia, perforated esophageal ulcer, and mycotic aneurysm (*17*).

Aortopulmonary fistula caused by an infected thoracic aortic false aneurysm rupturing after endovascular stent placement has rarely been reported and we should bear in mind that it is possible and unusually-serious. Although his family did not prefer the invasive treatment such as reoperation and reintervention, effective treatment should be promptly administered on a case-by-case basis. Further accumulation and elucidation of clinical cases including these complications are significantly required so as to overcome them in the future.

References

1. Leurs LJ, Bell R, Degrieck Y, Hobo R, Lundbom J; EUROSTAR; UK Thoracic Endograft Registry collaborators. Endovascular treatment of thoracic aortic diseases: Combined experience from the EUROSTAR and United Kingdom Thoracic Endograft registries. J Vasc Surg. 2004; 40:670-679.
2. Leurs LJ, Harris PL, Buth J. Secondary interventions after elective endovascular repair of degenerative thoracic aortic aneurysms: Results of the European collaborators registry (EUROSTAR). J Vasc Interv Radiol. 2007; 18:491-495.
3. Grabenwoger M, Fleck T, Ehrlich M, Czerny M, Hutschala D, Schoder M, Lammer J, Wolner E. Secondary surgical interventions after endovascular stent-grafting of the thoracic aorta. Eur J Cardiothorac Surg. 2004; 26:608-613.
4. Parmer SS, Carpenter JP, Stavropoulos SW, Fairman RM, Pochettino A, Woo EY, Moser GW, Bavaria JE. Endoleaks after endovascular repair of thoracic aortic aneurysms. J Vasc Surg. 2006; 44:447-452.
5. Ueda T, Fleischmann D, Dake MD, Rubin GD, Sze DY. Incomplete endograft apposition to the aortic arch: Bird-beak configuration increases risk of endoleak formation after thoracic endovascular aortic repair. Radiology. 2010; 255:645-652.
6. Grisafi JL, Boiteau G, Detschelt E, Potts J, Kiproff P, Muluk SC. Endoluminal treatment of type IA endoleak with Onyx. J Vasc Surg. 2010; 52:1346-1349.
7. Shah AA, Barfield ME, Andersen ND, Williams JB, Shah JA, Hanna JM, McCann RL, Hughes GC. Results of thoracic endovascular aortic repair 6 years after United

States Food and Drug Administration Approval. Ann Thorac Surg. 2012; 94:1394-1399.

8. Ducasse E, Calisti A, Speziale F, Rizzo L, Misuraca M, Fiorani P. Aortoiliac stent graft infection: Current problems and management. Ann Vasc Surg. 2004; 18:521-526.

9. Jackson MR, Clagett GP. Aortic graft infection. In: Decision Making in Vascular Surgery (Cronenwett JL, Rutherford RB, eds.). WB Saunders, Philadelphia, USA, 2001; pp. 186-191.

10. Fogarty T, Cranley J, Krause R, Strasser ES, Hafner CD. A method for extraction of arterial emboli and thrombi. Surg Gynecol Obstet. 1963; 116:241-244.

11. Dotter CT, Judkins MP. Transluminal treatment of arteriosclerotic obstruction. Description of a new technic and a preliminary report of its application. Circulation. 1964; 30:654-670.

12. Dotter CT. Transluminally-placed coil-spring endarterial tube grafts. Long-term patency in canine popliteal artery. Invest Radiol. 1969; 4:329-332.

13. Marin ML, Hollier LH, Ellozy SH, Spielvogel D, Mitty H, Griepp R, Lookstein RA, Carroccio A, Morrissey NJ, Teodorescu VJ, Jacobs TS, Minor ME, Sheahan CM, Chae K, Oak J, Cha A. Endovascular stent graft repair of abdominal and thoracic aortic aneurysms: A ten-year experience with 817 patients. Ann Surg. 2003; 238:586-595.

14. Alimi YS, Chakfe N, Rivoal E, Slimane KK, Valerio N, Riepe G, Kretz JG, Juhan C. Rupture of an abdominal aortic aneurysm after endovascular graft placement and aneurysm size reduction. J Vasc Surg. 1998; 28:178-183.

15. Cao P, De Rango P, Verzini F, Parlani G. Endoleak after endovascular aortic repair: Classification, diagnosis and management following endovascular thoracic and abdominal aortic repair. J Cardiovasc Surg (Torino). 2010; 51:53-69.

16. Numan F, Gulsen F, Solak S, Cantasdemir M. Management of endograft infections. J Cardiovasc Surg (Torino). 2011; 52:205-223.

17. Maruyama K, Ishiguchi T, Kato K, Naganawa S, Itoh S, Sakurai T, Ishigaki T. Stent-graft placement for pseudoaneurysm of the aorta. Radiat Med. 2000; 18:177-185.

A comment on: *Research progress in the radioprotective effect of superoxide dismutase*

Prasan R. Bhandari*

Department of Pharmacology, S.D.M. College of Medical Sciences and Hospital, Karnataka, India.

I thank and commend the authors Xiaojing Huang *et al.* of the article titled *"Research progress in the radioprotective effect of superoxide dismutase"* for having brought a comprehensive review of the molecular, cellular, tissue, and organ level mechanism of radioprotection by superoxide dismutase (SOD) (*1*). The authors in the article have made the following statements:

- *"Thus, to seek the radiation modifiers with selective protection for normal tissues has been a realm of intense investigation."*

- *"Therefore, the search for other radioprotectors with high potency and low toxicity should be the primary subject of further research."*

Supporting the authors, it is acknowledged that the exposure to radiation would chiefly produce intracellular reactive oxygen species (ROS, *viz.*, superoxide and hydroxyl radicals), causing DNA strand breaks and conformational alterations of biomolecules. This will certainly cause damage to surrounding normal cells. Consequently, certain compounds/formulations could be envisaged to competently scavenge the free radicals and thus protect the adjacent normal cells from radiation induced injury.

It might be proposed that the use of radioprotective compounds, like antioxidants, which selectively safeguard normal tissues against radiation injury, will also permit use of higher doses of radiation to obtain better control of cancers.

Traditionally, the critical findings on the radio-protective capacity of naturally occurring amino-metabolites like cysteine and cysteamine encouraged the quest for other thiolamines which would defend patients from the acute effects of radiation. Thus, amifostine ([S-2-[3-aminopropylamino] ethylphosphorothioic acid) was developed as a prospective radioprotector molecule (*2-4*).

However, until now no ideal radioprotectors are available because most synthetic compounds, including the Food and Drug Administration (FDA), USA, approved aminothiol, *S*-2-(3-aminopropyl-amino) ethyl phosphorothioic acid, [WR-2721, amifostine, ethiophos (USA), or gammaphos (former USSR)], are toxic at their optimal concentrations. Obviously, there has been limited success using these agents in clinics (*5*).

This drawback might possibly be overcome by the use of herbal drugs or dietary modifications which offer a substitute for the synthetic compounds as they are considered either non-toxic or less toxic than their synthetic counterparts. Plants and their phytochemicals, especially with free radical scavenging, antioxidant properties, and immunostimulatory effects have been evaluated for their radioprotective effects. Preclinical studies in the past two decades have shown that some commonly used medicinal plants and their phytochemicals possess radioprotective effects. Additionally, screening and testing of compounds from natural sources have been carried out over the last few decades in order to find effective radioprotectors capable of inhibiting radiation damage not only during radiotherapy of cancer patients, but also to healthy individuals subjected to occupational and accidental exposure to radiation.

Substantial evidence from pre-clinical studies advocates the usefulness of mint (peppermint) in averting the toxic effects of ionizing radiation at non-toxic concentrations. Similarly, *Ocimum sanctum*, *Panax ginseng*, *Podophyllum hexandrum*, *Emblica officinalis*, *Tinospora cordifoila*, *Syzygium cumini*, *Zingiber officinale*, *Ageratum conyzoides*, *Aegle marmelos*, and *Aphanamixis polystachya* have also demonstrated radioprotective effects (*5*).

Aloe arborescens, *Azadirachta indica*, *Biophytum sensitivum*, *Boerhaavia diffusa*, *Citrus sinensis*, *Grewia asiatica*, *Moringa oleifera*, and *Punica granatum* has been reviewed by Hazra B *et al.* for their prospective role in radioprotection (*6*).

Whereas most studies of plants and their phytochemicals have been with animals, clinical applicability to humans necessitates further exploration. Furthermore, *in vitro* studies with pertinent propagatory cell lines and primary cultures will benefit in

Address correspondence to:
Dr. Prasan R. Bhandari, Department of Pharmacology, S.D.M. College of Medical Sciences and Hospital, Sattur, Dharwad, Karnataka 580009, India.
E-mail: prasangeeta2012@gmail.com

understanding the molecular mode of action responsible for the radioprotection. Additional studies defining the radioprotective activity of plants and their active components should be with tumor-bearing animals of diverse histological and metastatic potentialities, essentially to observe for normal tissue protection. Since most published radioprotective studies have been with γ-radiation and Swiss albino mice, it is vital that analogous experiments are performed with other sources of ionizing radiation, particularly high linear energy transfer (LET) sources and with additional species of experimental animals because only then will the radioprotective spectrum be understood.

Therefore, there is an imperative requisite for investigators to clinically explore such remedies to be used in conjunction with chemo- and radio-therapy of cancer in order to curtail adverse effects, and to augment the overall curative outcome in patients.

Likewise, plants and their components with pharmacological activities that may be pertinent to amelioration of radiation-mediated damage, including antiemetic, antiinflammatory, antioxidant, cell proliferative, wound healing, and hemopoietic stimulatories should also be investigated.

If these medicinal plants/dietary constituents are effective in enhancing the radioprotective effects of low doses or decrease the systemic toxicity and delay cytogenetic damage (polyploidy and chromatid breaks), it will be an immense help in clinics and will also reduce treatment cost.

The eventual objective is to cultivate multi-disciplinary proficiency and therapeutic synergy between conventional and complementary therapies. Owing to its abundance, cost-effectiveness, and safety in consumption, these herbal/dietary radioprotectors have remarkable prospects and numerous opportunities for further investigation. This has the possibility to produce a non-toxic radioprotective agent, however, only when gaps in the prevailing understanding are linked.

References

1. Huang XJ, Song CX, Zhong CQ, Wang FS. Research progress in the radioprotective effect of superoxide dismutase. Drug Discov Ther. 2012; 6:169-77.
2. Weiss JF, Landauer MR. Radioprotection by antioxidants. Ann N Y Acad Sci. 2000; 899:44-60.
3. Grdina DJ, Murley JS, Kataoka Y. Radioprotectants: Current status and new directions. Oncology. 2002; 63:2-10.
4. Bensadoun RJ, Schubert MM, Lalla RV, Keefe D. Amifostine in the management of radiation-induced and chemo-induced mucositis. Support Care Cancer. 2006; 14:566-72.
5. Baliga MS, Rao S. Radioprotective potential of mint: A brief review. J Can Res Ther. 2010; 6:255-62.
6. Hazra B, Ghosh S, Kumar A, Pandey BN. The Prospective Role of Plant Products in Radiotherapy of Cancer: A Current Overview. Front Pharmacol. 2011; 2:94.

(Received October 12, 2012)

DD&T
Drug Discoveries & Therapeutics

Guide for Authors

1. Scope of Articles

Drug Discoveries & Therapeutics welcomes contributions in all fields of pharmaceutical and therapeutic research such as medicinal chemistry, pharmacology, pharmaceutical analysis, pharmaceutics, pharmaceutical administration, and experimental and clinical studies of effects, mechanisms, or uses of various treatments. Studies in drug-related fields such as biology, biochemistry, physiology, microbiology, and immunology are also within the scope of this journal.

2. Submission Types

Original Articles should be well-documented, novel, and significant to the field as a whole. An Original Article should be arranged into the following sections: Title page, Abstract, Introduction, Materials and Methods, Results, Discussion, Acknowledgments, and References. Original articles should not exceed 5,000 words in length (excluding references) and should be limited to a maximum of 50 references. Articles may contain a maximum of 10 figures and/or tables.

Brief Reports definitively documenting either experimental results or informative clinical observations will be considered for publication in this category. Brief Reports are not intended for publication of incomplete or preliminary findings. Brief Reports should not exceed 3,000 words in length (excluding references) and should be limited to a maximum of 4 figures and/or tables and 30 references. A Brief Report contains the same sections as an Original Article, but the Results and Discussion sections should be combined.

Reviews should present a full and up-to-date account of recent developments within an area of research. Normally, reviews should not exceed 8,000 words in length (excluding references) and should be limited to a maximum of 100 references. Mini reviews are also accepted.

Policy Forum articles discuss research and policy issues in areas related to life science such as public health, the medical care system, and social science and may address governmental issues at district, national, and international levels of discourse. Policy Forum articles should not exceed 2,000 words in length (excluding references).

Case Reports should be detailed reports of the symptoms, signs, diagnosis, treatment, and follow-up of an individual patient. Case reports may contain a demographic profile of the patient but usually describe an unusual or novel occurrence. Unreported or unusual side effects or adverse interactions involving medications will also be considered. Case

Reports should not exceed 3,000 words in length (excluding references).

News articles should report the latest events in health sciences and medical research from around the world. News should not exceed 500 words in length.

Letters should present considered opinions in response to articles published in Drug Discoveries & Therapeutics in the last 6 months or issues of general interest. Letters should not exceed 800 words in length and may contain a maximum of 10 references.

3. Editorial Policies

Ethics: Drug Discoveries & Therapeutics requires that authors of reports of investigations in humans or animals indicate that those studies were formally approved by a relevant ethics committee or review board.

Conflict of Interest: All authors are required to disclose any actual or potential conflict of interest including financial interests or relationships with other people or organizations that might raise questions of bias in the work reported. If no conflict of interest exists for each author, please state "There is no conflict of interest to disclose".

Submission Declaration: When a manuscript is considered for submission to Drug Discoveries & Therapeutics, the authors should confirm that 1) no part of this manuscript is currently under consideration for publication elsewhere; 2) this manuscript does not contain the same information in whole or in part as manuscripts that have been published, accepted, or are under review elsewhere, except in the form of an abstract, a letter to the editor, or part of a published lecture or academic thesis; 3) authorization for publication has been obtained from the authors' employer or institution; and 4) all contributing authors have agreed to submit this manuscript.

Cover Letter: The manuscript must be accompanied by a cover letter signed by the corresponding author on behalf of all authors. The letter should indicate the basic findings of the work and their significance. The letter should also include a statement affirming that all authors concur with the submission and that the material submitted for publication has not been published previously or is not under consideration for publication elsewhere. The cover letter should be submitted in PDF format. For example of Cover Letter, please visit http://www.ddtjournal.com/downcentre.php (Download Centre).

Copyright: A signed JOURNAL PUBLISHING AGREEMENT (JPA) must be provided by post, fax, or as a scanned file before acceptance of the article. Only forms with a hand-written signature are accepted. This copyright will ensure the widest possible dissemination of information. A form facilitating transfer of copyright can be downloaded by clicking the appropriate link and can be returned to the e-mail address or fax number noted on the form (Please visit

Download Centre). Please note that your manuscript will not proceed to the next step in publication until the JPA form is received. In addition, if excerpts from other copyrighted works are included, the author(s) must obtain written permission from the copyright owners and credit the source(s) in the article.

Suggested Reviewers: A list of up to 3 reviewers who are qualified to assess the scientific merit of the study is welcomed. Reviewer information including names, affiliations, addresses, and e-mail should be provided at the same time the manuscript is submitted online. Please do not suggest reviewers with known conflicts of interest, including participants or anyone with a stake in the proposed research; anyone from the same institution; former students, advisors, or research collaborators (within the last three years); or close personal contacts. Please note that the Editor-in-Chief may accept one or more of the proposed reviewers or may request a review by other qualified persons.

Language Editing: Manuscripts prepared by authors whose native language is not English should have their work proofread by a native English speaker before submission. If not, this might delay the publication of your manuscript in Drug Discoveries & Therapeutics.

The Editing Support Organization can provide English proofreading, Japanese-English translation, and Chinese-English translation services to authors who want to publish in Drug Discoveries & Therapeutics and need assistance before submitting a manuscript. Authors can visit this organization directly at http://www.iacmhr.com/iac-eso/support.php?lang=en. IAC-ESO was established to facilitate manuscript preparation by researchers whose native language is not English and to help edit works intended for international academic journals.

4. Manuscript Preparation

Manuscripts should be written in clear, grammatically correct English and submitted as a Microsoft Word file in a single-column format. Manuscripts must be paginated and typed in 12-point Times New Roman font with 24-point line spacing. Please do not embed figures in the text. Abbreviations should be used as little as possible and should be explained at first mention unless the term is a well-known abbreviation (*e.g.* DNA). Single words should not be abbreviated.

Title page: The title page must include 1) the title of the paper (Please note the title should be short, informative, and contain the major key words); 2) full name(s) and affiliation(s) of the author(s), 3) abbreviated names of the author(s), 4) full name, mailing address, telephone/fax numbers, and e-mail address of the corresponding author; and 5) conflicts of interest (if you have an actual or potential conflict of interest to disclose, it must be included as a footnote on the title page of the manuscript; if no conflict of interest exists for each author, please state "There is no conflict of interest to disclose"). Please visit Download Centre and refer to the title page of the manuscript sample.

Abstract: A one-paragraph abstract consisting of no more than 250 words must be included. The abstract should briefly state the purpose of the study, methods, main findings, and conclusions. Abbreviations must be kept to a minimum and non-standard abbreviations explained in brackets at first mention. References should be avoided in the abstract. Key words or phrases that do not occur in the title should be included in the Abstract page.

Introduction: The introduction should be a concise statement of the basis for the study and its scientific context.

Materials and Methods: The description should be brief but with sufficient detail to enable others to reproduce the experiments. Procedures that have been published previously should not be described in detail but appropriate references should simply be cited. Only new and significant modifications of previously published procedures require complete description. Names of products and manufacturers with their locations (city and state/country) should be given and sources of animals and cell lines should always be indicated. All clinical investigations must have been conducted in accordance with Declaration of Helsinki principles. All human and animal studies must have been approved by the appropriate institutional review board(s) and a specific declaration of approval must be made within this section.

Results: The description of the experimental results should be succinct but in sufficient detail to allow the experiments to be analyzed and interpreted by an independent reader. If necessary, subheadings may be used for an orderly presentation. All figures and tables must be referred to in the text.

Discussion: The data should be interpreted concisely without repeating material already presented in the Results section. Speculation is permissible, but it must be well-founded, and discussion of the wider implications of the findings is encouraged. Conclusions derived from the study should be included in this section.

Acknowledgments: All funding sources should be credited in the Acknowledgments section. In addition, people who contributed to the work but who do not meet the criteria for authors should be listed along with their contributions.

References: References should be numbered in the order in which they appear in the text. Citing of unpublished results, personal communications, conference abstracts, and theses in the reference list is not recommended but these sources may be mentioned in the text. In the reference list, cite the names of all authors when there are fifteen or fewer authors; if there are sixteen or more authors, list the first three followed by *et al*. Names of journals should be abbreviated in the style used in PubMed. Authors are responsible for the accuracy of the references. Examples are given below:

Example 1 (Sample journal reference):
Nakata M, Tang W. Japan-China Joint Medical Workshop on Drug Discoveries and Therapeutics 2008: The need of Asian pharmaceutical researchers' cooperation. Drug Discov Ther. 2008; 2:262-263.

Example 2 (Sample journal reference with more than 15 authors):
Darby S, Hill D, Auvinen A, *et al*. Radon in homes and risk of lung cancer: Collaborative analysis of individual data from 13 European case-control studies. BMJ. 2005; 330:223.

Example 3 (Sample book reference):
Shalev AY. Post-traumatic stress disorder: Diagnosis, history and life course. In: Post-traumatic Stress Disorder, Diagnosis, Management and Treatment (Nutt DJ, Davidson JR, Zohar J, eds.). Martin Dunitz, London, UK, 2000; pp. 1-15.

Example 4 (Sample web page reference):
World Health Organization. The World Health Report 2008 – primary health care: Now more than ever. *http://www.who.int/whr/2008/whr08_en.pdf* (accessed September 23, 2010).

Tables: All tables should be prepared in Microsoft Word or Excel and should be arranged at the end of the manuscript after the References section. Please note that tables should not in image format. All tables should have a concise title and should be numbered consecutively with Arabic numerals. If necessary, additional information should be given below the table.

Figure Legend: The figure legend should be typed on a separate page of the main manuscript and should include a short title and explanation. The legend should be concise but comprehensive and should be understood without referring to the text. Symbols used in figures must be explained.

Figure Preparation: All figures should be clear and cited in numerical order in the text. Figures must fit a one- or two-column format on the journal page: 8.3 cm (3.3 in.) wide for a single column, 17.3 cm (6.8 in.) wide for a double column; maximum height: 24.0 cm (9.5 in.). Please make sure that artwork files are in an acceptable format (TIFF or JPEG) at minimum resolution (600 dpi for illustrations, graphs, and annotated artwork, and 300 dpi for micrographs and photographs). Please provide all figures as separate files. Please note that low-resolution images are one of the leading causes of article resubmission and schedule delays. All color figures will be reproduced in full color in the online edition of the journal at no cost to authors.

Units and Symbols: Units and symbols conforming to the International System of Units (SI) should be used for physicochemical quantities. Solidus notation (*e.g.* mg/kg, mg/mL, mol/mm^2/min) should be used. Please refer to the SI Guide www.bipm.org/en/si/ for standard units.

Supplemental data: Supplemental data might be useful for supporting and enhancing your scientific research and Drug Discoveries & Therapeutics accepts the submission of these materials which will be only published online alongside the electronic version of your article. Supplemental files (figures, tables, and other text materials) should be prepared according to the above guidelines, numbered in Arabic numerals (*e.g.*, Figure S1, Figure S2, and Table S1, Table S2) and referred to in the text. All figures and tables should have titles and legends. All figure legends, tables and supplemental text materials should be placed at the end of the paper. Please note all of these supplemental data should be provided at the time of initial submission and note that the editors reserve the right to limit the size and length of Supplemental Data.

5. Submission Checklist

The Submission Checklist will be useful during the final checking of a manuscript prior to sending it to Drug Discoveries & Therapeutics for review. Please visit Download Centre and download the Submission Checklist file.

6. Online submission

Manuscripts should be submitted to Drug Discoveries & Therapeutics online at http://www.ddtjournal.com. The manuscript file should be smaller than 5 MB in size. If for any reason you are unable to submit a file online, please contact the Editorial Office by e-mail at office@ddtjournal.com

7. Accepted manuscripts

Proofs: Galley proofs in PDF format will be sent to the corresponding author *via* e-mail. Corrections must be returned to the editor (proof-editing@ddtjournal.com) within 3 working days.

Offprints: Authors will be provided with electronic offprints of their article. Paper offprints can be ordered at prices quoted on the order form that accompanies the proofs.

Page Charge: A page charge of $140 will be assessed for each printed page of an accepted manuscript. The charge for printing color figures is $340 for each page. Under exceptional circumstances, the author(s) may apply to the editorial office for a waiver of the publication charges at the time of submission.

(Revised October 2011)

Editorial and Head Office:

Pearl City Koishikawa 603
2-4-5 Kasuga, Bunkyo-ku
Tokyo 112-0003
Japan
Tel: +81-3-5840-9697
Fax: +81-3-5840-9698
E-mail: office@ddtjournal.com

JOURNAL PUBLISHING AGREEMENT (JPA)

Manuscript No.:

Title:

Corresponding author:

The International Advancement Center for Medicine & Health Research Co., Ltd. (IACMHR Co., Ltd.) is pleased to accept the above article for publication in Drug Discoveries & Therapeutics. The International Research and Cooperation Association for Bio & Socio-Sciences Advancement (IRCA-BSSA) reserves all rights to the published article. Your written acceptance of this JOURNAL PUBLISHING AGREEMENT is required before the article can be published. Please read this form carefully and sign it if you agree to its terms. The signed JOURNAL PUBLISHING AGREEMENT should be sent to the Drug Discoveries & Therapeutics office (Pearl City Koishikawa 603, 2-4-5 Kasuga, Bunkyo-ku, Tokyo 112-0003, Japan; E-mail: office@ddtjournal.com; Tel: +81-3-5840-9697; Fax: +81-3-5840-9698).

1. Authorship Criteria

As the corresponding author, I certify on behalf of all of the authors that:

1) The article is an original work and does not involve fraud, fabrication, or plagiarism.

2) The article has not been published previously and is not currently under consideration for publication elsewhere. If accepted by Drug Discoveries & Therapeutics, the article will not be submitted for publication to any other journal.

3) The article contains no libelous or other unlawful statements and does not contain any materials that infringes upon individual privacy or proprietary rights or any statutory copyright.

4) I have obtained written permission from copyright owners for any excerpts from copyrighted works that are included and have credited the sources in my article.

5) All authors have made significant contributions to the study including the conception and design of this work, the analysis of the data, and the writing of the manuscript.

6) All authors have reviewed this manuscript and take responsibility for its content and approve its publication.

7) I have informed all of the authors of the terms of this publishing agreement and I am signing on their behalf as their agent.

2. Copyright Transfer Agreement

I hereby assign and transfer to IACMHR Co., Ltd. all exclusive rights of copyright ownership to the above work in the journal Drug Discoveries & Therapeutics, including but not limited to the right 1) to publish, republish, derivate, distribute, transmit, sell, and otherwise use the work and other related material worldwide, in whole or in part, in all languages, in electronic, printed, or any other forms of media now known or hereafter developed and the right 2) to authorize or license third parties to do any of the above.

I understand that these exclusive rights will become the property of IACMHR Co., Ltd., from the date the article is accepted for publication in the journal Drug Discoveries & Therapeutics. I also understand that IACMHR Co., Ltd. as a copyright owner has sole authority to license and permit reproductions of the article.

I understand that except for copyright, other proprietary rights related to the Work (*e.g.* patent or other rights to any process or procedure) shall be retained by the authors. To reproduce any text, figures, tables, or illustrations from this Work in future works of their own, the authors must obtain written permission from IACMHR Co., Ltd.; such permission cannot be unreasonably withheld by IACMHR Co., Ltd.

3. Conflict of Interest Disclosure

I confirm that all funding sources supporting the work and all institutions or people who contributed to the work but who do not meet the criteria for authors are acknowledged. I also confirm that all commercial affiliations, stock ownership, equity interests, or patent-licensing arrangements that could be considered to pose a financial conflict of interest in connection with the article have been disclosed.

Corresponding Author's Name (Signature):

Date:

Drug Discoveries & Therapeutics (www.ddtjournal.com)

Pearl City Koishikawa 603, 2-4-5 Kasuga, Bunkyo-ku, Tokyo 112-0003, Japan; E-mail: office@ddtjournal.com; Tel: +81-3-5840-9697; Fax: +81-3-5840-9698